이학박사 학위논문

Mechanisms of neuropathic pain associated with metabotropic glutamate receptor 5 in the brain

신경병성 통증에 관한

뇌내 대사성 글루타메이트 수용체 5 관련 기전 연구

2018 년 2 월

서울대학교 대학원

뇌인지과학과

정 지 훈

신경병성 통증에 관한

뇌내 대사성 글루타메이트 수용체 5 관련 기전 연구

지도교수 김상정

이 논문을 이학박사 학위논문으로 제출함

2017 년 11 월

서울대학교 대학원

뇌인지과학과 뇌인지과학 전공

정 지 훈

Mechanisms of neuropathic pain associated with metabotropic glutamate receptor 5 in the brain

A Dissertation Submitted to the Faculty of the
Department of Brain and Cognitive Sciences
at
Seoul National University

by

Geehoon Chung

in Partial Fulfillment of the
Requirements for the Degree of

Doctor of Philosophy

Advisor: Sang Jeong Kim

November 2017

Approved by Thesis Committee:

December 2017

Abstract

Mechanisms of neuropathic pain associated with metabotropic glutamate receptor 5 in the brain

Neuropathic pain is a pathological pain caused by damage to the peripheral or central nervous system. As symptoms of neuropathic pain are often intractable, patients suffer from long-lasting severe pain and easily develop abnormal mental problems such as depression and anxiety. However, underlying mechanisms are not fully understood.

I investigated the brain-level mechanisms of neuropathic pain in an animal model of spinal nerve ligation, using brain imaging techniques of positron emission tomography (PET), electrophysiological recording, pharmacological and genetic manipulation and animal behavior analysis. Metabotropic glutamate receptor 5 (mGluR5) was a particular target, as this molecule plays a pivotal role in the plastic change of the neurons.

This thesis consists of three research parts and a review part. In chapter 1, it is shown that the mGluR5 level in the medial prefrontal cortex (mPFC) is increased in neuropathic pain state, and this upregulation is responsible for the amplified aversive perception and negative moods. Chapter 2 deals with brain patterns of the mGluR5 levels which encode the degree of neuropathic pain behavior. A method I developed for the objective evaluation of neuropathic pain using the patterns in the PET image is introduced. In chapter 3, mGluR5 activity in the periaqueductal gray (PAG) region

is focused. I found that the mGluR5 within the PAG is persistently active in normal state, and a conditional inactivation of it drives chronic pain. Chapter 4 discusses molecular mechanisms underlying the sustained activation of mGluR5.

As a whole, this thesis illustrates how the pain becomes chronic and why it is not treated well. The alteration of the brain in neuropathic pain state and underlying mechanisms are revealed, focusing on the mGluR5. Based on the mechanisms, this thesis identifies mGluR5 in the brain regions as therapeutic targets for the treatment of chronic neuropathic pain. In addition, a method for decoding the status of the individual neuropathic pain subject is demonstrated. This method evaluates the pain status objectively using the information of mGluR5 patterns in the brain, and thus is applicable for a diagnostic purpose in the clinic. This thesis provides new insight into the brain signature of neuropathic pain, and offers a novel perspective on the status of mGluR5 in physiological and pathological conditions.

Keywords : Neuropathic pain, Metabotropic glutamate receptor 5, Medial prefrontal cortex, Periaqueductal gray

Contents

Chapter 1.

Upregulation of prefrontal metabotropic glutamate receptor 5 mediates neuropathic pain and negative mood symptoms after spinal nerve injury in rats

Summary

Patients with chronic pain easily accompany the negative mood symptoms such as depression and anxiety, and these disturbances, in turn, affect the aversive perception of pain. However, the underlying mechanisms are largely unknown. I hypothesized that the alteration of metabotropic glutamate receptor 5 (mGluR5) level in the brain region underlies such a comorbidity of aversive states. I scanned the brain of chronic neuropathic pain model rats using positron emission tomography (PET) technique with an mGluR5-selective radiotracer [11C] ABP688 and found various brain regions with higher or lower level of mGluR5 compared to control rats. Among the brain areas, a prominent upregulation of mGluR5 was shown in the prelimbic region (PrL) of the medial prefrontal cortex (mPFC) of chronic neuropathic pain animals. A pharmacological blockade of upregulated mGluR5 in the PrL ameliorated the negative symptoms including tactile hypersensitivity and depressive-like behavior, which relieved the subjects from the unpleasant state of chronic neuropathic pain condition. Conversely, lentiviral overexpression of the mGluR5 in the PrL of naïve rats successfully induced comorbid pain and negative moods. These data provide deeper insight into the shared mechanism of pain perception and negative emotions, identifying a therapeutic target for the treatment of chronic pain and mood disorders.

Introduction

Neuropathic pain persists even after the healing phase following an injury, and patients suffer from symptoms including allodynia, hyperalgesia, and spontaneous pain. Central sensitization mechanisms of the pain system including the spinal cord and the brain are considered to be the main reason of such an unrelenting chronic pain.

As the pain becomes chronic, supraspinal brain centers become crucial for how the patients perceive pain. Previous studies have demonstrated that the long-term pain arising from peripheral nerve injury induces maladaptive changes in the various cortical structures (Maihöfner et al., 2005; Metz et al., 2009; Seifert and Maihöfner, 2009; Seminowicz et al., 2009; Thompson et al., 2014; Zhuo, 2008) including the prefrontal cortex (PFC) which are also involved in the affective and emotional processing of the brain. Chronic neuropathic pain easily accompanies the abnormal mental states such as depression or anxiety (Gupta et al., 2007; Radat et al., 2013; Turk et al., 2010), and these emotional mood symptoms in return affect the manifestation of the sensory pain symptoms (Leite-Almeida et al., 2015; Li, 2015; Shi et al., 2010; Suzuki et al., 2007). This indicates that the shared supraspinal brain mechanisms play a critical role in the pathologically amplified negative perception in chronic pain condition.

One possible candidate is the alteration of metabotropic glutamate receptor 5 (mGluR5) in the brain. The mGluR5 is a G protein-coupled receptor which plays an important role in the modulation of neuronal excitability and is involved in the pathophysiology of various neurological and psychiatric disorders. The changes of mGluR5 expression in the brain regions and their functional impact have been reported from studies of chronic pain (Kim et al., 2016; Kolber, 2015; Matos et al., 2015) and negative mood disorders (Bannerman et al., 2014; Duman et al., 2016;

Marsden, 2013). Both of pain processing and mental disorders are modulated by mGluR5 actions, implicating change of this receptor in the brain circuit as their common mechanism. In the processing of pain and negative mood, the affective and cognitive interactions actively participate in the perception, and the maladaptive sensitization of this system in chronic pain condition amplifies negative appraisal and aversive sensations (Baliki et al., 2006; Bushnell et al., 2013; Yalcin et al., 2014). My primary hypothesis is that the persistent unavoidable pain would trigger the alteration of mGluR5 in the brain area related to the negative appraisal such as the PFC, and this alteration, in turn, mediates pain facilitation and precipitates negative mood.

I sought to identify the brain alteration underlying the comorbidity of chronic pain and negative mood disorders. I used the mGluR5 as a target molecule, as this molecule is known to be involved in the pathophysiology of pain as well as negative moods. The common brain circuit was pursued by investigating the altered mGluR5 in the chronic pain state and was verified by effects of the local mGluR5 manipulation on the pain and mood behaviors. To assess the regional expression of mGluR5 among brains of chronic neuropathic pain rats and control rats, positron emission tomography (PET) technique was used with [11C] ABP688, a highly selective radiotracer of mGluR5. After this step, I went on further tests with pharmacological modulation and viral manipulation of mGluR5 in the identified brain area to investigate the specific role of the local mGluR5 alteration in the pain-related and mood-related behaviors.

Results

Altered mGluR5 level in the brain following nerve injury-induced neuropathic pain

Right L5 spinal nerve ligation (SNL) surgery-performed rats were used for chronic neuropathic pain group (Kim and Chung, 1992) and sham surgery-performed rats were used for the control group. After surgery, paw withdrawal threshold was measured using von Frey test. SNL rats showed a consistent reduction of paw withdrawal threshold, which represents altered behavioral response due to nerve injury-induced mechanical allodynia (Fig. 1A). To identify the regional difference of brain mGluR5 in the chronic pain condition, [11C] ABP688-PET scans were performed to SNL and sham group animal 15-24 days after surgery (Fig. 1B). The non-displaceable binding potential (BP_{ND}) of [11C] ABP688 were calculated from each brain image with cerebellum as a reference region to assess the level of mGluR5 (Fig. 1C and 1D) and compared between groups on a voxel-by-voxel basis. The BP_{ND} of mGluR5 was found to be significantly different between SNL and sham rats in multiple pain-related brain regions (Fig. 2A and 2B, Table 1 and Table 2). SNL rats showed a significantly higher level of mGluR5 in the bilateral medial prefrontal cortex (mPFC) including caudal part prelimbic area (PrL), dysgranular zone of the primary somatosensory cortex (contralateral to nerve injury), the somatosensory cortices and caudate putamen (ipsilateral to nerve injury), retrosplenial cortex, and the medial septum (Fig. 2A). Conversely, the insular cortex (contralateral to nerve injury), the rostral pole of nucleus accumbens (ipsilateral to nerve injury), the endopiriform nucleus (ipsilateral to nerve injury), small areas of corpus callosum which contact to caudate putamen (ipsilateral to nerve injury), and piriform cortices and olfactory tubercle (contralateral to nerve injury) showed lower level of mGluR5 in the SNL group (Fig. 2B).

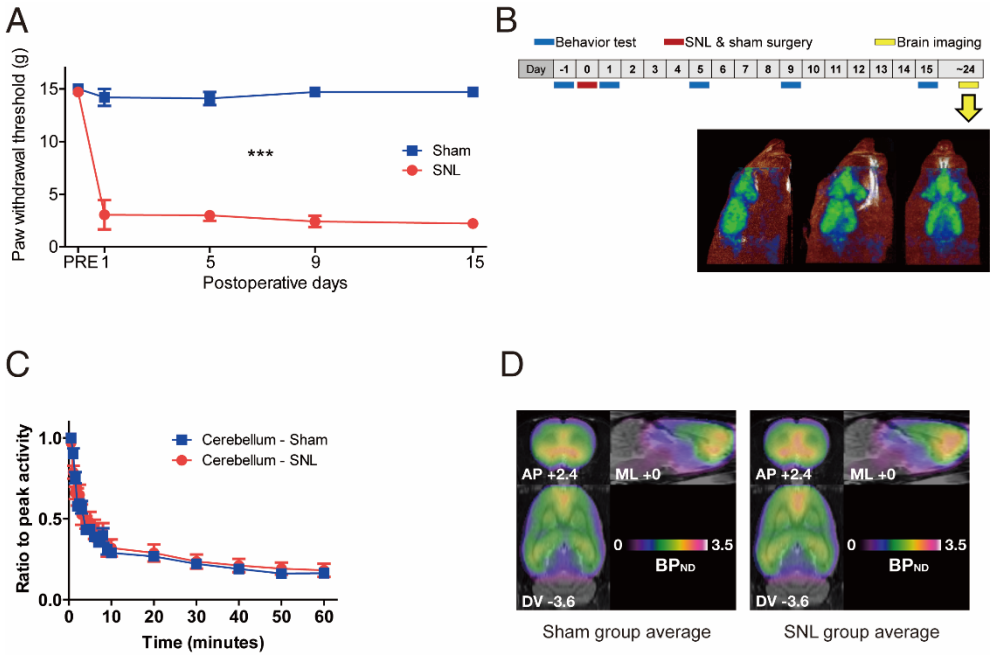

Figure 1. Experimental design and assessment of mGluR5 level in the brain

A. After the surgery, SNL group animals showed reduced hindpaw withdrawal threshold compared to control group (n=10 per each group, ***p <0.001, Two-way repeated measures ANOVA with Bonferroni test).

B. Experimental design of [11C] ABP688 PET scan and sample image. PET scan was performed to animal 15-24 days after the SNL or sham surgery.

C. Time-activity curve of [11C] ABP688 in the cerebellum. The cerebellum was used as a reference region for the quantification of the mGluR5, as this region is devoid of the mGluR5

D. Averaged [11C] ABP688 images from each group. The images without proportional scaling were used. The anterior-posterior (AP), mediolateral (ML), dorsoventral (DV) coordinates in the representative plane images are the distance from the bregma (mm).

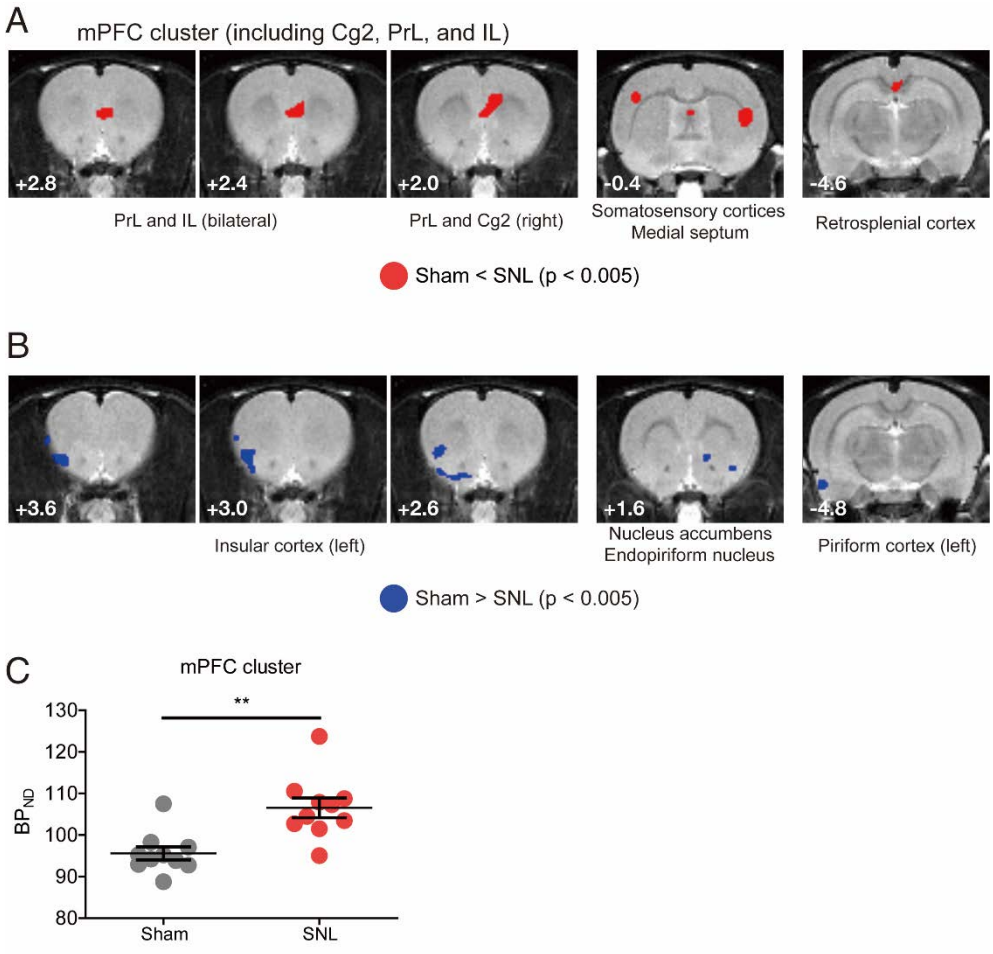

Figure 2. Comparison of mGluR5 level between SNL group and sham group animals

A. Brain regions of which the mGluR5 level was higher in the SNL group compared to the sham control group. The PrL region of the SNL group showed the prominently higher level of mGluR5.

B. Brain regions with the lower mGluR5 level in the SNL group.

C. The mGluR5 level was higher in the mPFC cluster of SNL group animals (**p=0.0011 with two-sample t-test. Data of the cluster were extracted from proportionally scaled images).

Upregulation of mGluR5 in the mPFC of chronic neuropathic pain animals

I sought to identify a brain region with an altered mGluR5 level which affects to the amplified aversiveness in the chronic pain condition. Among the brain regions which showed prominent alteration of the mGluR5 level in neuropathic pain group, I focused on the mPFC cluster because of its suggested major roles in the mood disorders and affective perception (Alexander and Brown, 2012; Baliki et al., 2006; Etkin et al., 2011; Lemogne et al., 2012; McEwen et al., 2012; Treadway et al., 2015). According to previous studies, mGluR5 in the mPFC mediates depressive-like behavior (Lee et al., 2015), and depressive and anxious symptoms following chronic pain are mediated by PrL subregions of the mPFC (Wang et al., 2015a; Zhang et al., 2015). Brain images from the PET experiment showed that the mGluR5 level of the mPFC is increased in the neuropathic pain group (Fig. 2A). I conducted additional region-of-interest (ROI) analysis using BP_{ND} extracted from the mPFC cluster of each animal, which confirmed the significant increase of the mGluR5 level in the mPFC of SNL rats (Fig. 2C). I found that the significant cluster of the mPFC extracted from the analysis mainly consists of cingulate area 2 (Cg2) and caudal part PrL, and includes a small dorsal portion of the infralimbic cortex (IL). In the posterior part (anterior-posterior range (AP) +1.4~2.4 mm from bregma) of the cluster, significant voxels were located in the Cg2 and the PrL, and the voxels of the deep layer ipsilateral to nerve injury were mainly included to the significant cluster. In the anterior part of the cluster (AP +2.4~3.0 mm from bregma), significant voxels were located bilaterally in the ventral part of the PrL and dorsal part of the IL. The dorsoventral (DV) range of significant voxels in the mPFC cluster was -3.2~-5.2 mm from bregma.

Pharmacological inactivation of mGluR5 in the caudal PrL ameliorates neuropathic mechanical allodynia

I wondered whether the increased mGluR5 in the mPFC affects the neuropathic pain behaviors. To identify its action on the peripheral nerve injury-induced tactile hypersensitivity, I injected mGluR5 antagonist 2-methyl-6-(phenylethynyl)pyridine (MPEP) into the bilateral mPFC (caudal part of the PrL) 20 days after SNL surgery via pre-implanted cannula and measured change of the paw withdrawal threshold (Fig. 3A). Administration of MPEP (PrL-MPEP treatment) evoked potent analgesic effect and significantly increased the paw withdrawal threshold. Consequently, mechanical allodynia was disappeared and paw withdrawal threshold returned to the pre-SNL level within 30 minutes following MPEP injection (Fig. 3B).

Interestingly, the analgesic effect induced by PrL-MPEP treatment did not completely disappear with the time in a subset of SNL rats. Although mechanical allodynia was rebounded, paw withdrawal thresholds of SNL rats were slightly ameliorated at 24 hours after PrL-MPEP treatment compared to the pre-MPEP level. To further investigate this long-lasting effect, I repeated PrL-MPEP treatment for 3 consecutive days and measured paw withdrawal thresholds at 24 hours after the last injection (Fig. 3C). The paw withdrawal thresholds of SNL rats measured at 24 hours after the repeated PrL-MPEP treatment were significantly increased compared to the pre-MPEP level, which confirms the residual effect of the treatment (Fig. 3D).

To exclude the possibility that the effects I observed from MPEP injection were caused by the diffusion of the drug, I injected MPEP into the off-target sites and measured paw withdrawal threshold (Fig. 3E and 3F). The injection of the MPEP into the off-target sites failed to increase the paw withdrawal threshold of neuropathic pain animals. Administration of another mGluR5 antagonist MTEP also evoked similar analgesic effect (Fig. 3G). Taken together, these data clearly

demonstrate that mGluR5 in the specific mPFC region plays a significant role in the pain processing. The effective mPFC subregion corresponds to the caudal part of the PrL.

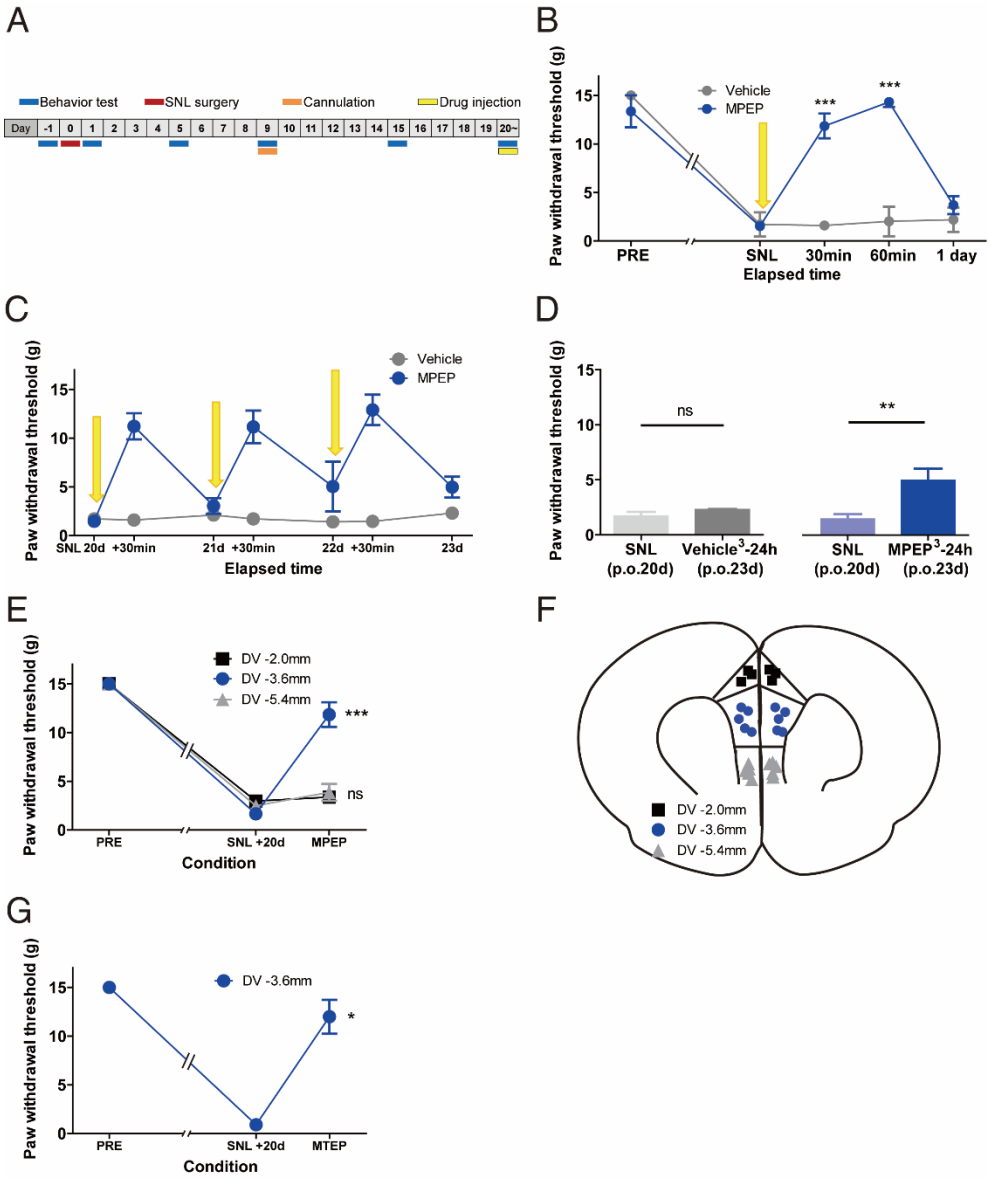
A
Behavior test
SNL surgery
Cannulation
Drug injection
Day -1 0 1 2 3 4 5 6 7 8 9 10 11 12 13 14 15 16 17 18 19 20~
B
Vehicle
MPEP
***
***
Paw withdrawal threshold (g)
PRE
SNL
30min
60min
1 day
Elapsed time
C
Vehicle
MPEP
Paw withdrawal threshold (g)
SNL 20d +30min
21d +30min
22d +30min
23d
Elapsed time
D
Paw withdrawal threshold (g)
ns
**
SNL (p.o.20d)
Vehicle3-24h (p.o.23d)
SNL (p.o.20d)
MPEP3-24h (p.o.23d)
E
DV -2.0mm
DV -3.6mm
DV -5.4mm
***
ns
Paw withdrawal threshold (g)
PRE
SNL +20d
MPEP
Condition
F
DV -2.0mm
DV -3.6mm
DV -5.4mm
G
DV -3.6mm
*
Paw withdrawal threshold (g)
PRE
SNL +20d
MTEP
Condition

Figure 3. Blockade of mGluR5 within the PrL subregion of mPFC induces analgesic effect

A. Experimental design. The MPEP injection and behavioral tests were performed at least 20 days after the SNL surgery.

B. Effect of MPEP injection into the mPFC on SNL-induced tactile hypersensitivity. PrL-MPEP treatment ameliorated SNL-induced mechanical allodynia symptom (n=4~6 per each group, ***p<0.001, Two-way repeated measures ANOVA with Bonferroni test).

C. Consecutive injection of MPEP into the PrL of SNL animals. The arrow indicates injection to the PrL.

D. The residual analgesic effect was shown 24 hours after the repeated PrL-MPEP treatment (n=4~5 per each group, **p=0.0066 with a paired t-test, ns=not significant).

E. Off-target injection of MPEP failed to induce analgesic effect, which confirms that the effect of mPFC-MPEP injection on mechanical allodynia is PrL-specific (n=3~7 per each group, ***p=0.0003, paired t-test)

F. Confirmation of injection sites.

G. The injection of another mGluR5 antagonist MTEP into the PrL also successfully induced analgesic effect (n=3, *p=0.0273, paired t-test).

Blockade of increased mGluR5 in the PrL relieves neuropathic pain-induced depressive-like behavior

Comorbid chronic pain and mood disorder have been reported from animal models of neuropathic pain (Leite-Almeida et al., 2015; Li, 2015) as well as patients with various chronic pain diseases (Gupta et al., 2007; Radat et al., 2013). To study whether the upregulation of the mGluR5 in the PrL contributes to the comorbidity, I assessed the effect of the PrL-MPEP injection on the depressive-like behavior using forced swimming test (FST) paradigm. Consistent with previous reports (Leite-Almeida et al., 2015; Li, 2015), neuropathic pain animals showed increased immobility time in the FST chamber compared to sham control (Fig. 4A). I next tested the effect of MPEP injection into the bilateral PrL using separate groups of model animals. I found that the single-time PrL-MPEP treatment evokes rapid antidepressant effect on neuropathic pain animals. MPEP-treated SNL rats showed significantly reduced immobility time in FST compared to vehicle-treated SNL rats. Consequently, the immobility time of MPEP-treated SNL rats returned to the control level (Fig. 4A). Notably, the PrL-MPEP treatment was effective only in SNL animals, as the immobility time of MPEP-treated sham group rats was comparable with that of the vehicle-treated sham group. Regarding the upregulation of mGluR5 shown from PET imaging analysis, these data suggest that the increased mGluR5 action in the caudal PrL plays an important role in the pain-induced depressive-like behavior. To rule out the possibility that the reduction of immobility time of SNL rats in the FST was mediated by an effect on the basal activeness of the animals rather than anti-depressive effect, I measured the activity level of the rats in the open field test. Indeed, the PrL-MPEP treatment could not alter the activity level of the animals in the open field in both SNL and sham groups (Fig. 4B). Interestingly, the PrL-MPEP treatment significantly increased center zone visiting duration only in SNL group animals, suggesting its relieving effect from unpleasantness also leads to induction

of a powerful anxiolytic effect (Fig. 4C).

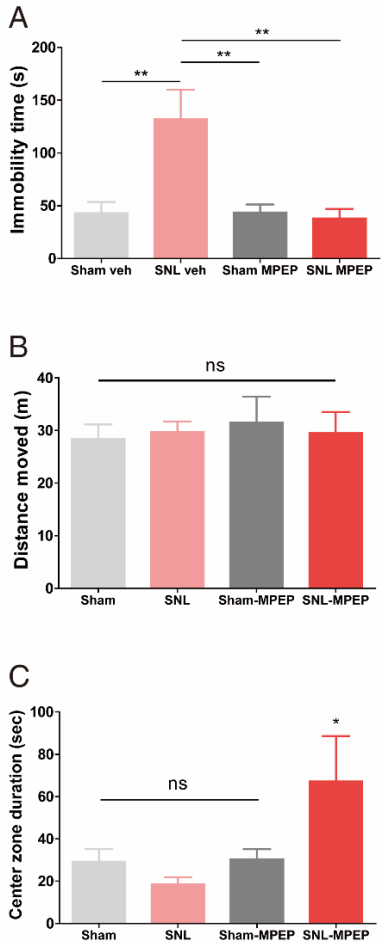

Figure 4. PrL-MPEP treatment induces antidepressive and anxiolytic effect only in SNL group

A. SNL-induced increase of immobility time in FST was rescued by PrL-MPEP treatment (n=8-10 per each group, **p<0.01, Bonferroni test in one-way ANOVA)

B. Neither SNL nor PrL-MPEP treatment altered total distance traveled in 5 min open field test (ns: not significant).

C. Treatment of PrL-MPEP increased center zone duration only in SNL group (n=4-7 per each group, *p<0.05, Newman-Keuls test in one-way ANOVA)

The antagonism of the mGluR5 in the PrL attenuates the aversive state of neuropathic pain condition

The mPFC has previously been shown to play an important role in the goal-directed behavior via processing of motivation coding and decision making. Thus, one might argue that the effects of the PrL-MPEP on the withdrawal behavior and immobility behavior I observed above might be caused by disturbance of these executive functions rather than intervention to the affective perception of the aversive state. To verify this issue, I assessed the effect of the PrL-MPEP on the formation of preference memory using conditional place preference (CPP) test. Before drug conditioning process of SNL animals, time spent in each chamber was identical between each chamber (Fig. 5A). After conditioning process, SNL animals spent significantly more time in the chamber in which they were conditioned with MPEP treatment into the PrL (Fig 5B). As the place preference is formed by reinforcement memory related to the treatment, this result indicates that the SNL animals perceived the PrL-MPEP treatment as a reward (relief from the aversive state). In contrast, animals of sham surgery group showed no preference to the chamber conditioned with the PrL-MPEP treatment (Fig. 5C and 5D). I interpret that the animals without chronic pain perceived the PrL-MPEP treatment as neither reward nor punishment, as the time spent in each chamber was not altered compared to the pre-conditioning level in the sham group. The chamber preference appeared only in SNL group (Fig. 5E). A number of midline crossings to other chambers was not significantly different between groups during the test period (Fig. 5F), which confirms that the effect of the intervention on the basal activeness of the animals was not different between groups (Zhang et al., 2015). These results imply that the chamber preference formed by the PrL-MPEP in SNL group is caused by the relief from pain and/or pain-induced depression, and supports that the PrL-MPEP effect on the withdrawal behavior and immobility time is also mediated by the reduction of unpleasant affection. Taken

together, these data demonstrate the effect of the mGluR5 blockade in the PrL on relieving the aversive state of the chronic pain condition.

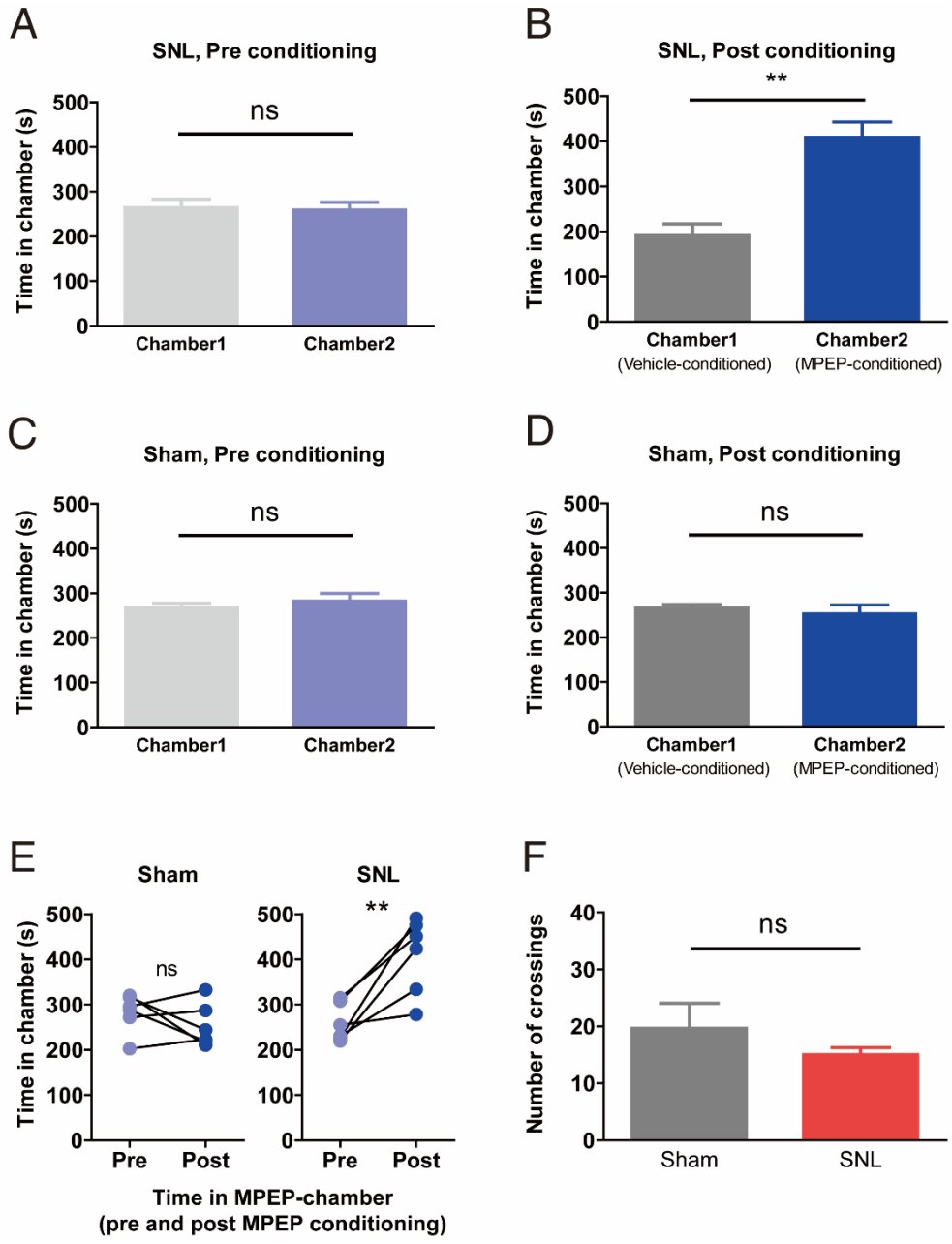
A
SNL, Pre conditioning
ns
Time in chamber (s)
500
400
300
200
100
0
Chamber1
Chamber2
B
SNL, Post conditioning
**
Time in chamber (s)
Chamber1
(Vehicle-conditioned)
Chamber2
(MPEP-conditioned)
C
Sham, Pre conditioning
ns
Time in chamber (s)
Chamber1
Chamber2
D
Sham, Post conditioning
ns
Time in chamber (s)
Chamber1
(Vehicle-conditioned)
Chamber2
(MPEP-conditioned)
E
Sham
SNL
ns
**
Time in chamber (s)
Pre
Post
Pre
Post
Time in MPEP-chamber
(pre and post MPEP conditioning)
F
ns
Number of crossings
40
30
20
10
0
Sham
SNL

Figure 5. Neuropathic pain animals show preference to the PrL-MPEP treatment.

A. The absence of chamber preference before the conditioning, SNL group (ns: not significant).

B. SNL group animals showed preference to the MPEP-conditioned chamber (n=6, **p=0.0043, Mann-Whitney test).

C. The absence of chamber preference before the conditioning, sham group.

D. The preference to MPEP-conditioned chamber was not produced in sham group animals (n=6).

E. The difference of the time spent in the MPEP-chamber before and after the conditioning. The time spent in the MPEP-conditioned chamber was significantly increased only in SNL group animals (**p=0.007, paired t-test between pre- and post-conditioning data).

F. The number of crossings to the other chamber was not different between groups during the post-conditioning test period.

mGluR5 overexpression in the PrL induces mechanical allodynia, depressive-like behavior, and anxiety-like behavior.

I asked whether the upregulation of mGluR5 in the PrL is sufficient to cause both of pain behavior and depressive-like behavior. To confirm the causal relationship between the molecular change and the behavior, I injected lentivirus expressing mGluR5 (mGluR5 LV) into the bilateral PrL of naïve animals and observed the behavioral change (Fig. 6A and 6B). Lentivirus expressing ZsGreen1 (ZsGreen LV) was used as a control. In the behavior experiments, I observed that the rats subjected to the lentiviral overexpression of mGluR5 in the PrL showed reduced paw withdrawal threshold in the von Frey test (Fig. 6C) even though the SNL surgery was absent in these animals. In consequence, tactile hypersensitivity comparable to nerve injury-induced mechanical allodynia was manifested. Furthermore, subjects developed depressive-like behavior shown by increased immobility time in the FST (Fig. 6D). Basal activity level in the open field was not altered (Fig. 6E). In addition to the higher level of the despair behavior, animals showed the decreased center-zone duration (Fig. 6F) in the open field test. This implicates that the anxiety-like state was also developed in the subjects. These data demonstrate that the overexpression of mGluR5 in the PrL altered the behavioral coping strategy to aversive events without alteration of basal activeness, and implies that this treatment made animals more vulnerable to depression and anxiety.

These findings indicate the elevated mGluR5 in the PrL induce both pain and mood disorders, showing the causal relationship between upregulation of the PrL-mGluR5 in the chronic pain state and behavioral alterations.

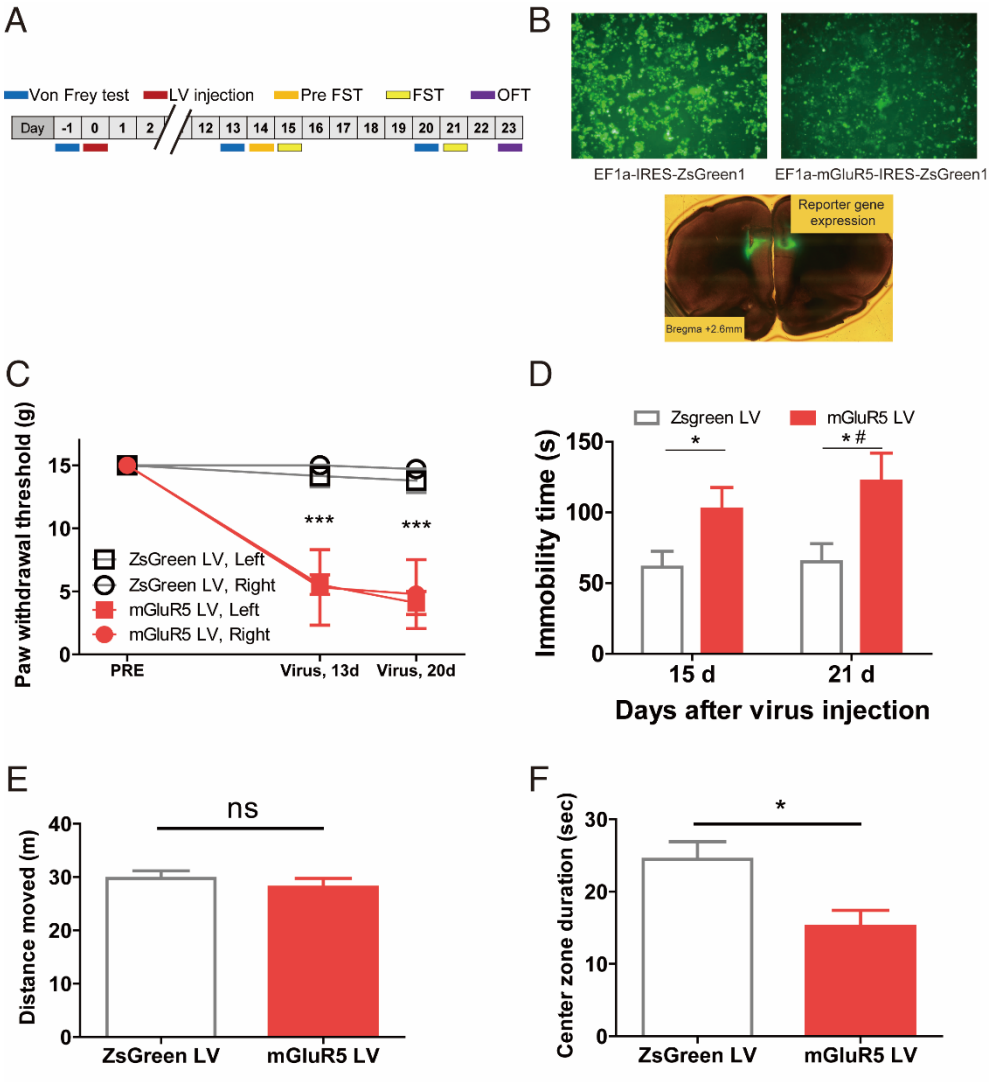
A
Von Frey test
LV injection
Pre FST
FST
OFT
Day
-1
0
1
2
12
13
14
15
16
17
18
19
20
21
22
23
B
EF1a-IRES-ZsGreen1
EF1a-mGluR5-IRES-ZsGreen1
Reporter gene expression
Bregma +2.6mm
C
Paw withdrawal threshold (g)
15
10
5
0
***
***
ZsGreen LV, Left
ZsGreen LV, Right
mGluR5 LV, Left
mGluR5 LV, Right
PRE
Virus, 13d
Virus, 20d
D
Zsgreen LV
mGluR5 LV
*
* #
Immobility time (s)
150
100
50
0
15 d
21 d
Days after virus injection
E
ns
Distance moved (m)
40
30
20
10
0
ZsGreen LV
mGluR5 LV
F
*
Center zone duration (sec)
30
20
10
0
ZsGreen LV
mGluR5 LV

Figure 6. Lentiviral overexpression of mGluR5 in the mPFC induces comorbid pain and mood disorder

A. Experimental design of lentiviral overexpression of mGluR5 and behavioral tests.

B. Confirmation of reporter gene expression in vitro (HEK293 cells) and in vivo (the PrL).

C. The injection of mGluR5 LV into the mPFC of naïve rats resulted in a reduction of the hindpaw withdrawal threshold (n=10 per each group, *** $p<0.001$, Bonferroni test in two-way repeated measures ANOVA). Consequently, tactile hypersensitivity comparable to SNL-induced mechanical allodynia was manifested.

D. The animals with mGluR5 LV injection showed higher immobility time in the FST (n=10 per each group, *$p<0.05$ with two sample t-test, #$p<0.05$ with Bonferroni test in two-way repeated measures ANOVA). The higher level of this despair behavior implies that the animals with mGluR5 LV treatment were more vulnerable to depression compared to control.

E. Total distance traveled in the OFT was not altered by mGluR5 overexpression (n=10 per each group), which confirms that the basal activeness was not affected.

F. The center zone duration in the OFT was decreased by the mGluR5 overexpression (n=10 per each group, *$p=0.0118$ with two sample t-test), which could be interpreted as increased anxiety level.

Discussion

As a modulator of the glutamatergic transmission, mGluR5 is involved in the neuronal alteration observed from various neurological disorders (Bordi and Ugolini, 1999). The mGluR5 not only mediates plastic change of the nervous system but also shows expressional plasticity of itself in physiological and pathological conditions. In this study, I found that the mGluR5 level in the brain shows a plastic change in chronic pain condition and this alteration is a crucial mechanism of pain facilitation and negative mood behaviors.

I identified brain regions with the altered mGluR5 level in chronic neuropathic pain state and sought for specific brain region of which the alteration is responsible for comorbid chronic pain and depression. My findings provide evidence which shows that the upregulation of mGluR5 level in the mPFC region is critical for the chronic neuropathic pain. I further showed that the upregulated mPFC-mGluR5 also plays a significant role in the manifestation of depressive-like behavior as well as pain behavior. Indeed, pharmacological blockade of mPFC-mGluR5 in the chronic neuropathic pain model animal was sufficient to relieve the both of the nerve injury-induced pain and the depression symptoms which are experimentally assessed by paw withdrawal threshold in von Frey test and immobility time in FST respectively. Conversely, lentiviral overexpression of mGluR5 in the mPFC of naïve animals resulted in the manifestation of tactile hypersensitivity and depressive-like behavior, further supporting the causal role of the increased mGluR5 in the mPFC.

A significant role of the mPFC has been implicated from both research fields of pain and depression performed with human and animal subjects. The rodent mPFC consists of subregions of ACC, PrL, and IL and each subregion show distinct actions on the pain as well as mood symptoms. The PrL was mainly focused on the pharmacological experiments of the current study, as I found that the mPFC cluster

with a higher level of mGluR5 mainly consisted of caudal part PrL. The neurons located in the region are known to project to pain-related brain areas including ACC, insular cortex, periaqueductal gray, caudate putamen, amygdala, somatosensory cortex, thalamus and nucleus accumbens (Cheriyan et al., 2016; Gorelova and Yang, 1996; Hoppa et al., 2015; Sesack et al., 1989; Vertes, 2004). Interestingly, several target brain areas overlap with the brain regions in which the mGluR5 level was significantly altered in pain state in my PET analyses. Regarding the known role of these brain regions in the multiple aspects of pain and relevant emotional affection, the pain-induced alteration of the mGluR5 level in these regions would be also involved in the processing pathological and/or physiological aversiveness.

Although I focused on the higher level of mGluR5 level in the PrL subregion of the mPFC in the current study, mGluR5 in other brain regions should be the target of further studies to elucidate the mechanisms of encoding aversion and depression. Of interest, the lower level of mGluR5 was shown in the brain regions of insular cortex and nucleus accumbens of neuropathic pain group in my PET analyses. Given that these brain areas are involved in the altered sensory processing, abnormal perception related to unpleasantness, and decreased motivation in chronic pain state (Benarroch, 2016; Chang et al., 2014; Kaneko et al., 2017; Schreckenberger et al., 2005; Schwartz et al., 2014; Starr et al., 2009), down-regulation of the mGluR5 in these areas would play a part in pain chronification and following negative affection. I produced the brain map of altered mGluR5 in the pathological pain condition, providing the basis for studying the actions of the neural circuits on the pain and negative emotion.

Whether the mGluR5s are altered in a specific subpopulation of mPFC neurons in pain state remains unknown in my study. Previous studies suggested that the decreased activity of pyramidal neurons in the PrL plays an essential role in pain and

pain-induced affective symptoms (Kelly et al., 2016; Wang et al., 2015a), and increased GABAergic inhibition is responsible for the reduction of pyramidal neuronal activity (Zhang et al., 2015). Although activation of mGluR5 generally promotes neuronal excitability, these previous studies raise the possibility that the upregulation of mGluR5 observed in my PET data might enhance inhibitory effects to the pyramidal neurons. This can be achieved by (1) upregulation of mGluR5 in the GABAergic inhibitory neurons. A recent study performed in non-pain animal showed that the systemic injection of mGluR5 antagonist induces the anti-depressive effect in naïve mice, and this effect is mediated by mGluR5 expressed in parvalbumin-expressing GABAergic interneurons in the mPFC (Lee et al., 2015). Alternatively, (2) the mGluR5 might be upregulated in the glutamatergic neurons in the mPFC which drive excitation of GABAergic neurons. This view is supported by a recent study which showed that the increased GABAergic activity in the PrL of neuropathic pain animal critically depends on the enhanced excitatory synaptic input onto the GABAergic neurons (Zhang et al., 2015). Thus, upregulation of the mGluR5 might occur in the specific glutamatergic neurons in the mPFC area, which leads to facilitation of feed-forward inhibition to the pyramidal neurons via increased glutamate release to the GABAergic neurons. By dissecting the subpopulation of neurons associated with upregulated mGluR5 in the further study, more detailed mechanisms and novel therapies could be discovered.

Currently, both chronic pain diseases and depressive disorders lack methods for objective evaluation in the clinic, and the techniques to investigate mGluR5 level in the brain are considered to be a promising approach for the assessment of the pain and/or depression in clinical trials. In the case of non-pain depression, however, there is an inconsistency in the previous studies regarding the alteration of brain mGluR5 (Abdallah et al., 2017; DeLorenzo et al., 2015; Deschwanden et al., 2011; Esterlis et al., 2017; Gray et al., 2015). A previous study has reported that the female patients

with major depressive disorder showed the higher levels of mGluR5 gene expression in the PFC subregion whereas male patients showed the lower levels of mGluR5 (Gray et al., 2015). Interestingly, a previous animal study has reported that male rats but not female rats show higher levels of prefrontal mGluR5 in the depressive state induced by prenatal chronic mild stress (Wang et al., 2015b). Other studies have reported that male mice with mGluR5 knockout showed increased depressive-like behavior, indicating that the activity of the mGluR5 primarily facilitates the depression (Lee et al., 2015; Witkin et al., 2007). In that, the inconsistency shown from human studies is likely due to differences in gender (Gray et al., 2015), age, onset time, pathophysiological differences of the subjects (DeLorenzo et al., 2015), and a specific subpopulation of the neurons in which mGluR5 is altered (Lee et al., 2015). As the depression is the complex mental problem, there might be discrepancies as well as common mechanisms between non-pain depressive disorders and depression following pain. Thus, whether suffering negative mood with the different origins for a long period in the certain circumstances eventually upregulate or downregulate prefrontal mGluR5 might be case-specific. In this regards, further studies are necessary for the diagnostic application of the prefrontal mGluR5 measurement to human subjects. A translational step is also required regarding the debate over the homology between regions in rodent and primate prefrontal cortex.

The anti-depressive effect of mGluR5 antagonists, in contrast, has been consistently reported from both of pre-clinical and clinical studies (Chaki et al., 2013; Fuxe and Borroto-Escuela, 2015; Hashimoto et al., 2013; Hughes et al., 2013; Kato et al., 2015; Lee et al., 2015; Lindemann et al., 2015; Palucha and Pilc, 2007; Park et al., 2015; Pilc et al., 2008). As such, the PrL-MPEP treatment in my study showed a rapid anti-depressive effect comparable to fast-acting antidepressant drugs, as the treatment reduced immobility time in the FST which was performed at 30 minutes after single-

time injection. In addition, the current study supports that the mPFC-mGluR5 could be an attractive therapeutic target for the chronic pain as well as depressive disorder. In the von Frey test, the effect of consecutive PrL-MPEP treatment on the paw withdrawal threshold had not fully disappeared after 24 hours, suggesting the possible long-term plastic change. These characteristics make the mPFC-mGluR5 an attractive target of intervention which might overcome the limit of current therapeutic approaches.

Table 1. Brain regions with significant differences between sham and SNL rats (Sham < SNL, two-sample t-test, $p < 0.005$, $K_e > 20$). The peak voxel location is represented by the distance from the bregma (mm).

Sham < SNL

Brain region	K_e	T	Z	Peak p	Location (mm)		
					ML	AP	DV
Medial prefrontal cortex (Prelimbic and infralimbic cortices)	97	5.50	4.06	2.54E-06	0.2	2.6	-4.8
Primary somatosensory cortex (Dysgranular zone)	24	5.88	4.23	1.16E-05	-4.6	-0.2	-3.4
Primary, secondary somatosensory cortices and caudate putamen	37	4.42	3.52	0.0002	4.8	-0.4	-5.2
Retrosplenial cortex	25	6.70	4.56	2.45E-05	0.2	-4.6	-2.4
Medial septum	30	3.51	2.98	0.0014	0.4	-0.8	-4.8

Table 2. Brain regions with significant differences between sham and SNL rats (Sham > SNL, two-sample t-test, $p < 0.005$, $K_e > 20$). The peak voxel location is represented by the distance from the bregma (mm).

Sham > SNL

Brain region	K_e	T	Z	Peak p	Location (mm)		
					ML	AP	DV
Insular cortex and piriform cortex	102	7.64	4.89	4.98E-07	-3.2	3.6	-7.0
		4.73	3.69	0.0001	-3.4	3.0	-7.6
		4.60	3.62	0.0001	-3.6	2.6	-5.8
Insular cortex and primary somatosensory cortex	31	4.12	3.35	0.0004	-4.8	3.4	-4.8
Endopiriform nucleus	20	4.06	3.32	0.0005	3.8	1.4	-7.2
Nucleus accumbens	30	3.74	3.12	0.0009	1.6	1.8	-6.4
Piriform cortex	61	3.72	3.11	0.0009	-6.2	-4.8	-8.6
Corpus callosum and caudate putamen	36	3.71	3.11	0.0009	1.6	-0.4	-3.4
Corpus callosum and caudate putamen	76	3.65	3.07	0.0011	3.6	-2.0	-3.8

Chapter 2.

Distinct corticolimbic patterns of metabotropic glutamate receptor 5 encode the degree of neuropathic pain

Summary

Susceptibility to neuropathic pain and the degree of pain amplification vary among individuals. However, methods for objective evaluation of pain status have not been well established. Using an animal model, I identified the brain signature of neuropathic pain, and developed a method for the objective evaluation of pain degree. I analyzed paw withdrawal thresholds from rats that were subjected to right L5 spinal nerve ligation (SNL) surgery, and regressed them to the brain levels of metabotropic glutamate receptor 5 (mGluR5) using [11C] ABP688 PET image data from my previous research. I found clusters with a significant correlation to paw withdrawal threshold localized in brain areas involved in sensory, cognitive, and affective aspects of pain processing. Strikingly, mGluR5 levels in the identified brain regions showed distinct patterns in the neuropathic pain group but not in the control group. I successfully elucidated the degree of pain sensing behavior using the neuropathic pain-specific pattern of mGluR5 levels. This study provides new insight into the signature of neuropathic pain in the brain, and offers a novel diagnostic method for objectively decoding the status of individual neuropathic pain.

Introduction

Once neuropathic pain is established, patients perceive normally innocuous external sensory stimuli as noxious, and suffer from intractable pain. For many patients, neuropathic pain symptoms are not treatable with conventional methods, and the direct cause of neuropathic pain cannot be identified even with close examination. Moreover, there is currently no established standard method for objective assessment of neuropathic pain status, although studies on neuropathic pain have been actively conducted over the past decades. The manifestation of chronic pain symptoms after nerve injury and the degree of pain experienced vary among individuals, making it difficult to identify common circuits and develop standard evaluation methods.

Research in humans with neuropathic pain is difficult because of the variation in symptoms and degree of pain as well as psychosicial effects. Therefore, identifying factors that determine the execution of the pain behavior in the animal model is advantageous for understanding mechanisms of neuropathic pain. Various animal models of neuropathic pain have been developed and studied to clarify mechanisms underlying abnormal sensory information processing in the nervous system of patients with neuropathic pain. In many rodent models of neuropathic pain, mononeuropathy is surgically induced by unilaterally injuring the nerve innervating hind paw, leading to tactile mechanical allodynia in the affected paw. In such models, evaluation of the paw withdrawal response using the von Frey test is the most commonly applied method for assessing tactile mechanical allodynia. When successful, surgically induced neuropathic pain reduces the tactile threshold and evokes sensitized withdrawal behavior in response to a mechanical stimulus applied to the affected paw.

Interestingly, the degree of reduction in paw withdrawal threshold following neuropathic pain modeling varies among individual animals, despite being subjected to the same surgical procedures and experimental environment, and being of the same genetic background (Hogan et al., 2004). Reduction of the paw withdrawal threshold involves supraspinal as well as spinal mechanisms (Detloff et al., 2010; Ossipov et al., 2000; Saadé et al., 2006), and the stochastic neural responses to an aberrant pain signal in the circuits are thought to underlie such variation. Previous studies have revealed various neural factors that correlate with paw withdrawal thresholds in animal models of neuropathic and inflammatory pain (Baliki et al., 2015; Coffeen et al., 2010; Kras et al., 2014; Massart et al., 2016; Wei et al., 2017).

Recent neuroimaging techniques have provided a strong foundation for the study of the functional relationship between brain parameters and animal behavior (Litaudon et al., 2017). The significance of higher cortical functions in pain behavior has been the subject of much attention based on observations from clinical studies. Indeed, neuroimaging studies of animal models of neuropathic pain and human patients with chronic pain emphasize the critical role of corticolimbic structures of the brain in accounting for the probability, severity, and duration of pain symptoms, independently from spinal level mechanisms (Baliki and Apkarian, 2015; Baliki et al., 2012, 2015; Davis et al., 2016; Vachon-Presseau et al., 2016).

In this study, I focused on the metabotropic glutamate receptor 5 (mGluR5), a key player in the modulation of the neural transmission in the brain. mGluR5 plays a significant role in information processing of neurons, and thus the levels of mGluR5 in various brain regions are critically involved in the physiological and pathological functions of the brain circuitry. My primary hypothesis was that the sensitized paw withdrawal behavior observed during neuropathic pain is tightly connected to mGluR5 levels in sensory and limbic brain structures. I analyzed brain images from

my previous study (Chung et al., 2017) of chapter 1, which were acquired using positron emission tomography (PET) with mGluR5-specific radiotracer [11C] ABP688. These brain images contain information of the non-displaceable binding potential of [11C] ABP688, which reflects the level of mGluR5 availability. I analyzed the variation in paw withdrawal threshold of neuropathic pain rats and regressed the thresholds to the [11C] ABP688-PET images. Here, I report the brain regions in which the mGluR5 levels are involved in the paw withdrawal behavior in response to tactile stimuli in neuropathic pain rats. Strikingly, mGluR5 levels showed distinct regional patterns in the brain of neuropathic rats but not control rats. Further, I show that the withdrawal threshold of the individual neuropathic pain subject could be successfully determined from an [11C] ABP688 PET image using this pattern.

Results

Variation of the paw withdrawal threshold following nerve injury-induced neuropathic pain

I adopted the data from 103 rats that were subjected to the right L5 SNL surgery during the study period of my previous research (Chung et al., 2017) of chapter 1. The paw withdrawal threshold was successfully and persistently reduced after the SNL surgery in the majority of subjects (Fig. 7A). As previously described, there was some variation in the degree of behavioral responses of the animal models of neuropathic pain, despite being subjected to identical procedures (Hogan et al., 2004). Consistent with previous studies, paw withdrawal thresholds were distributed with positive skew (Fig. 7B), and in approximately 15 % of the animals (14 out of 103 rats) the threshold was merely reduced (> 50% of baseline threshold) despite SNL surgery. This ratio is in agreement with reports of SNL surgery in the same rodent strain (Sprague-Dawley rats) (Felice et al., 2011). I focused on the brains of animals that demonstrated successful induction of neuropathic pain; non-allodynic animals did not undergo [11C] ABP688-PET scan. Rats with appropriately non-sensitive hind paw response during baseline measurement (paw withdrawal threshold > 10 g) and successful induction of mechanical allodynia (paw withdrawal threshold at 15 days post-surgery < 5 g) were subjected to PET scan (n=10 SNL rats; Fig 7B and 7C, red data points). I further confirmed that the observed variation was common across the 31 surgery batches performed during the research period (Fig. 7C).

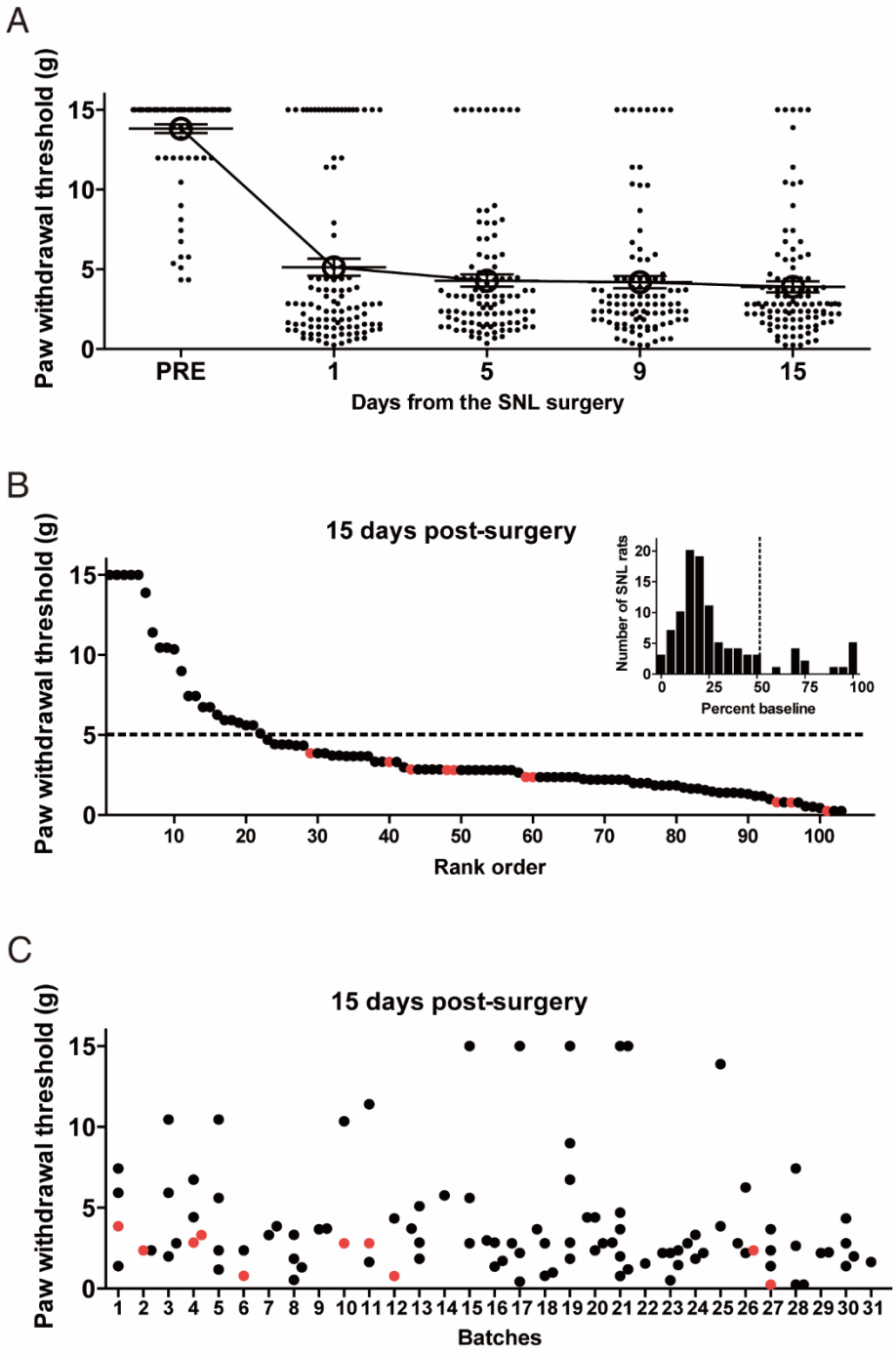
A
Paw withdrawal threshold (g)
15
10
5
0
PRE
1
5
9
15
Days from the SNL surgery
B
15 days post-surgery
Paw withdrawal threshold (g)
Number of SNL rats
20
15
10
5
0
0
25
50
75
100
Percent baseline
Rank order
C
15 days post-surgery
Paw withdrawal threshold (g)
Batches

Figure 7. Distribution of paw withdrawal thresholds of the SNL rats

A. SNL surgery reduces withdrawal threshold of the affected hind paw in the majority of subjects. The paw withdrawal thresholds measured 1 day before and 1, 5, 9, and 15 days after the SNL surgery are plotted (n=103).

B. The paw withdrawal thresholds measured at 15 days post-surgery are plotted by rank order (n=103). Histogram analysis of the SNL-induced reduction of paw withdrawal threshold (inset) revealed the positively skewed distribution of the data, as the paw withdrawal threshold was merely reduced (> 50% of baseline threshold) in 14 out of 103 rats in spite of SNL surgery. I further set the experimental criterion for the PET scan (the paw withdrawal threshold < 5 g), and [11C] ABP688 PET images were successfully acquired from the 10 SNL rats (red dots).

C. Paw withdrawal thresholds measured at 15 days post-surgery plotted by surgery batch (n=103). The data points from 103 rats were acquired from 31 batches of surgery during a year of the study period. The variation was common across surgery batches.

Brain regions in which mGluR5 level is correlated to behavioral response

In the next analysis, I sought to identify the brain regions involved in the processing of behavioral coping strategy in SNL animals. Using regression analysis of the [11C] ABP688-PET images from this group, I investigated the brain regions in which mGluR5 levels are tightly connected to paw withdrawal thresholds. The results of this analysis revealed that mGluR levels in several sensory and limbic brain structures were correlated with paw withdrawal thresholds in SNL animals (Table 3 and Table 4).

A negative interaction with the paw withdrawal thresholds was shown in (1) the striatum cluster including the caudate putamen (contralateral to nerve injury) connected to the secondary somatosensory cortex (Fig. 8A), (2) the rostral striatum (contralateral to nerve injury) (Fig. 8B) connected to the insular cortex (Fig. 8C), and (3) the hippocampus (ipsilateral to nerve injury) (Fig. 8D) of SNL animals. This translates into a greater mGluR5 levels in these regions, with more sensitive paw withdrawal behavior.

Conversely, a positive interaction with the paw withdrawal thresholds was shown in (1) the cingulate cortex (Fig. 9A), (2) the ipsilesional trunk region of the primary somatosensory cortex connected to the hippocampus (Fig. 9B), (3) the hypothalamus (Fig. 9C), (4) the contralesional trunk region, dysgranular zone, and barrel field of the primary somatosensory cortex (Fig. 9D), (5) the ipsilesional secondary somatosensory cortex (Fig. 9E), and (6) the ipsilesional hindlimb region of the primary somatosensory cortex (Fig. 9F) of SNL animals. This translates into a greater mGluR5 level in these regions, with a less sensitive paw withdrawal behavior.

Based on the significant clusters from the regression analysis, regions-of-interest (ROIs) were set as the 0.5 mm radius sphere in each region (Fig. 10A). The mGluR5 levels of each ROI was extracted from the SNL group, and correlations between the

paw withdrawal threshold and the individual BP_{ND} from each ROI were calculated. These analyses confirmed significant correlations between paw withdrawal threshold and mGluR5 levels of each region (Fig. 8 and Fig. 9).

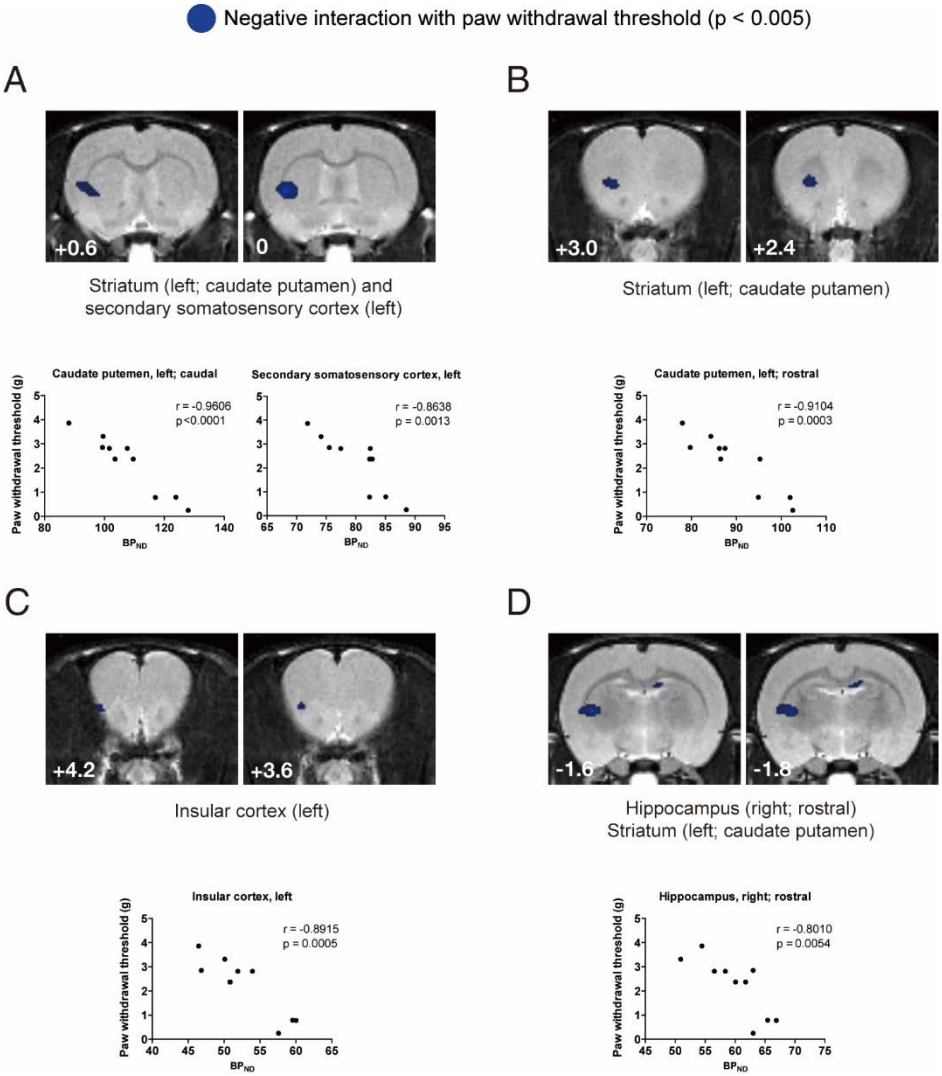
Negative interaction with paw withdrawal threshold (p < 0.005)
A
+0.6
0
Striatum (left; caudate putamen) and secondary somatosensory cortex (left)
Caudate putemen, left; caudal
r = -0.9606
p<0.0001
Secondary somatosensory cortex, left
r = -0.8638
p = 0.0013
Paw withdrawal threshold (g)
BPND
B
+3.0
+2.4
Striatum (left; caudate putamen)
Caudate putemen, left; rostral
r = -0.9104
p = 0.0003
C
+4.2
+3.6
Insular cortex (left)
Insular cortex, left
r = -0.8915
p = 0.0005
D
-1.6
-1.8
Hippocampus (right; rostral)
Striatum (left; caudate putamen)
Hippocampus, right; rostral
r = -0.8010
p = 0.0054

Figure 8. Brain regions in which mGluR5 level is negatively correlated to paw withdrawal threshold in the SNL group. This translates into higher levels of mGluR5 in regions with a more sensitive right hind paw.

A. A cluster including the left striatum (caudate putamen) connected to the secondary somatosensory cortex.

B. A cluster in the left striatum (caudate putamen).

C. A cluster in the left insular cortex connected to a small portion of orbitofrontal cortex.

D. Clusters in the left striatum (caudate putamen) and right hippocampus (CA3).

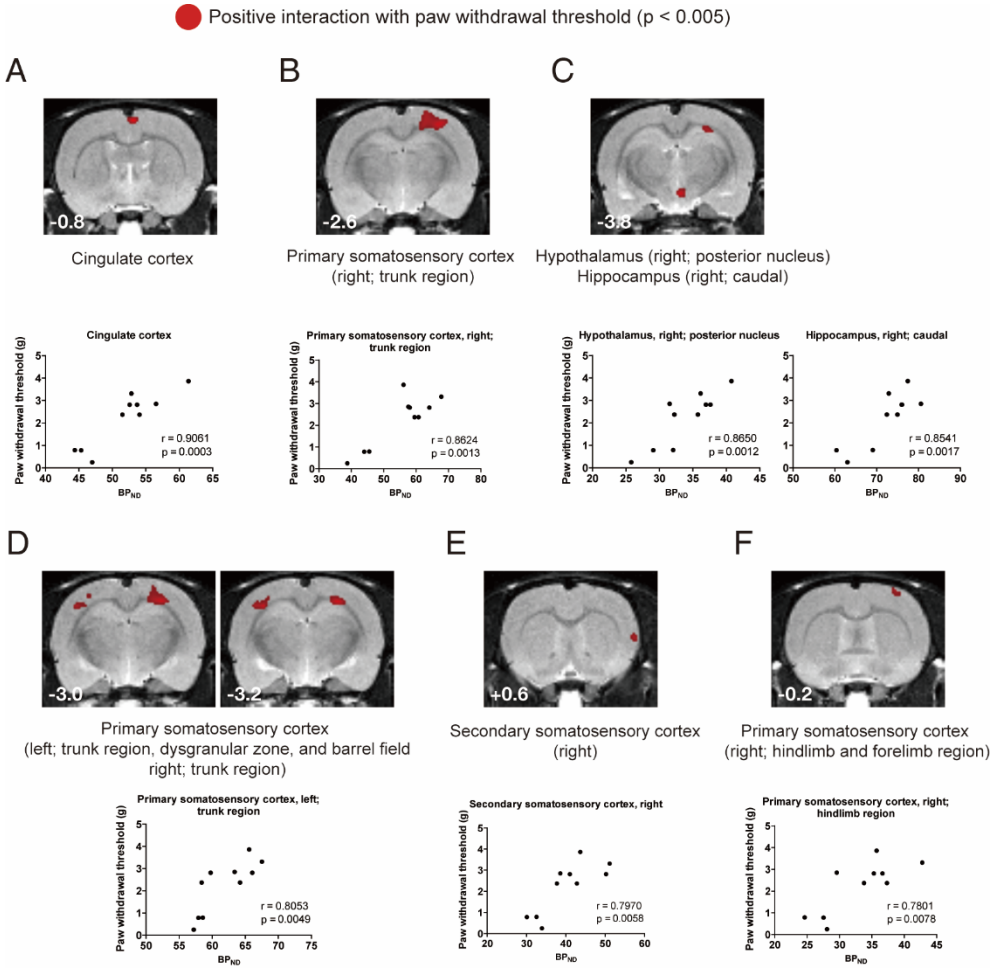
Positive interaction with paw withdrawal threshold (p < 0.005)
A
B
C
-0.8
-2.6
-3.8
Cingulate cortex
Primary somatosensory cortex (right; trunk region)
Hypothalamus (right; posterior nucleus)
Hippocampus (right; caudal)
Cingulate cortex
r = 0.9061
p = 0.0003
Primary somatosensory cortex, right; trunk region
r = 0.8624
p = 0.0013
Hypothalamus, right; posterior nucleus
r = 0.8650
p = 0.0012
Hippocampus, right; caudal
r = 0.8541
p = 0.0017
Paw withdrawal threshold (g)
BPND
D
E
F
-3.0
-3.2
+0.6
-0.2
Primary somatosensory cortex (left; trunk region, dysgranular zone, and barrel field right; trunk region)
Secondary somatosensory cortex (right)
Primary somatosensory cortex (right; hindlimb and forelimb region)
Primary somatosensory cortex, left; trunk region
r = 0.8053
p = 0.0049
Secondary somatosensory cortex, right
r = 0.7970
p = 0.0058
Primary somatosensory cortex, right; hindlimb region
r = 0.7801
p = 0.0078

Figure 9. Brain regions in which mGluR5 level is positively correlated to the paw withdrawal threshold in the SNL group. This translates into higher levels of mGluR5 in regions with a less sensitive right hind paw.

A. A cluster in the cingulate cortex.

B. A cluster in the right primary somatosensory cortex (trunk region).

C. Clusters in the hypothalamus and right hippocampus.

D. Bilateral clusters in the primary somatosensory cortices. The cluster in the left primary somatosensory cortex includes the trunk region, dysgranular zone, and barrel field. The cluster in the right primary somatosensory cortex is largely constituted by the trunk region and connected to the right hippocampus.

E. A cluster in the right secondary somatosensory cortex.

F. A cluster in the right primary somatosensory cortex (hindlimb and forelimb regions).

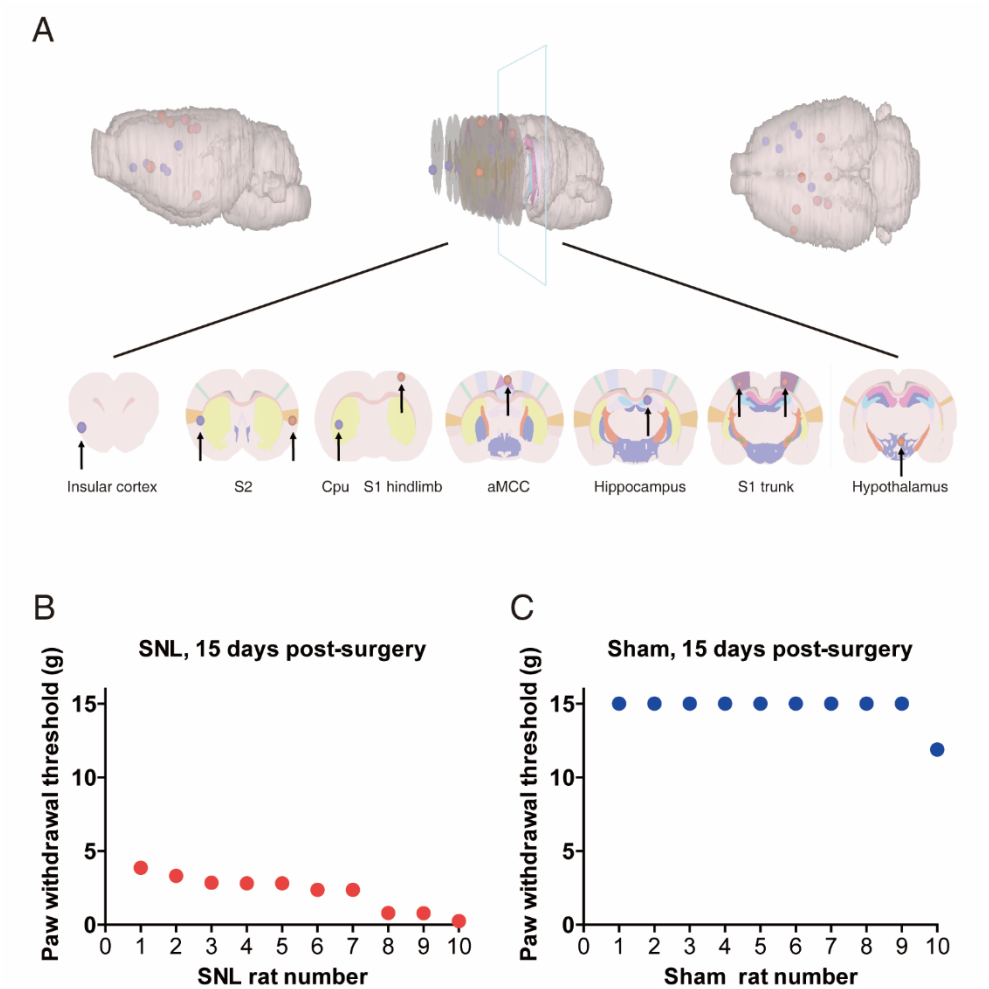

Figure 10. Extraction of ROIs from the brain regions of SNL group and sham group animals.

A. Extraction of ROIs. ROIs were set as the 0.5 mm radius sphere in the significant clusters of somatosensory cortices and the limbic areas.

B. The paw withdrawal thresholds of SNL group animals.

C. The paw withdrawal thresholds of sham group animals.

Correlation of mGluR5 levels between brain regions of SNL animals

As the brain regions were chosen on the basis of their interactions with functional outcome (i.e. paw withdrawal thresholds), the mGluR5 levels in each region should have inter-subject correlations with each other. Indeed, the SNL group showed a high correlation between ROIs (Fig. 11A). There was a clear contrast between the clusters of positive and negative correlations in the matrix of r-value (Fig.11A, left). These correlations were significant (P-value summary, Fig. 11A, right).

I aimed to assess whether this manifestation of inter-subject correlations is a feature specific to neuropathic pain group, rather than an intrinsic feature of the brain. To investigate this, the BP_{ND} of each ROI was extracted from the sham group and their correlations were computed. Sham group showed only a few significant correlations in the matrices (Fig. 11B). The majority of the ROIs did not correlate with other regions, with only a few significant correlations in the matrices (Fig.11B).

The significant regions that were correlated with paw withdrawal threshold in SNL group were not overlapped with the significant regions extracted by voxel-by-voxel two-sample t-test between SNL group and sham group. Therefore, it is suspected that the mGluR5 levels in the regions of correlation would not be different between the SNL and sham groups. To confirm this, the BP_{ND} measurements of each ROI were compared using two-sample t-tests and F-tests. No significant differences were observed (Fig. 12). This suggests that the mGluR5 levels in these brain regions of the SNL group are in a normal range, despite the abnormal paw withdrawal threshold (Fig. 10B and 10C).

These results demonstrate that mGluR5 levels in the sensory and limbic regions form distinct patterns in animals that underwent the neuropathic pain procedure, but not in controls. This raises the prospect that from a group-level perspective, mGluR5 levels in these regions are ‘re-aligned’ according to the paw withdrawal threshold

following neuropathic pain. Consequently, the mGluR5 levels of the ROIs show inter-subject correlations with each other in the neuropathic pain group. Notably, this re-alignment of mGluR5 level following neuropathic pain does not make the mGluR5 levels in these regions exceed the physiological range.

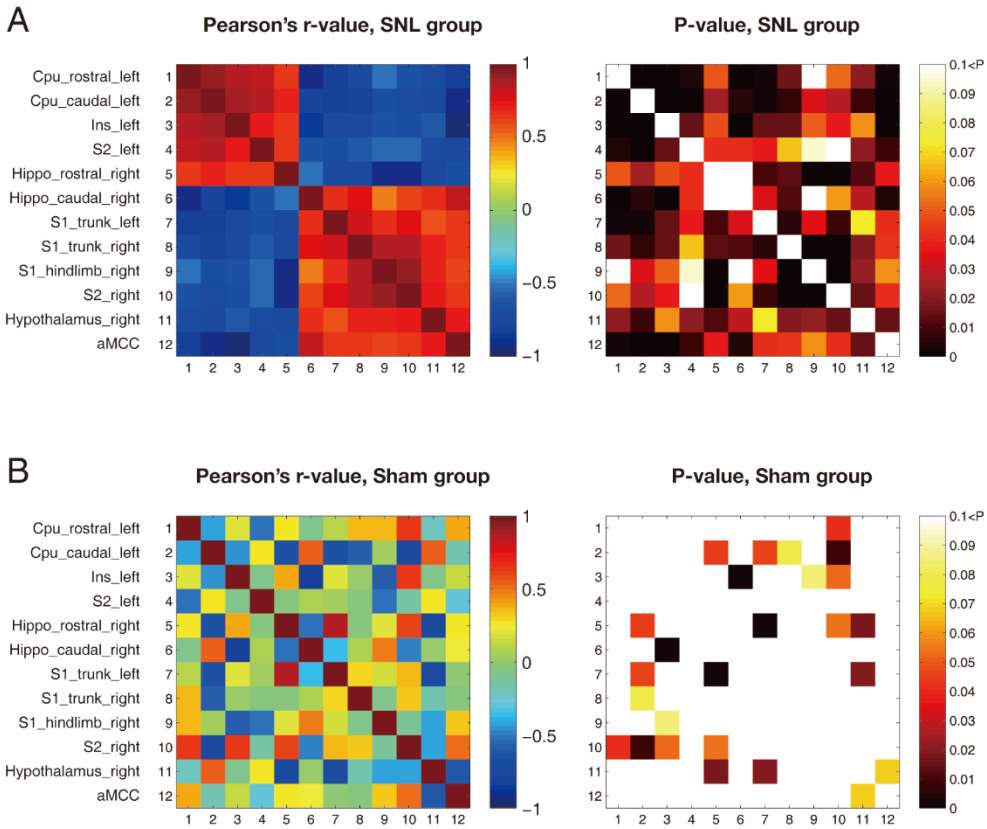

Figure 11. The correlation coefficient between mGluR5 levels in the brain. mGluR5 levels in the corticolimbic areas show distinct correlation patterns in the SNL group only.

A. Correlation coefficient matrices of SNL group. A clear contrast between the clusters of positive and negative correlations was shown in the matrix of r-value (left). The significances of the correlations were further confirmed by their p-values (right).

B. Correlation coefficient matrices of the sham group. The majority of the ROIs did not correlate with other regions, shown by small r-values (left). The majority of the p-values did not reach significance (right).

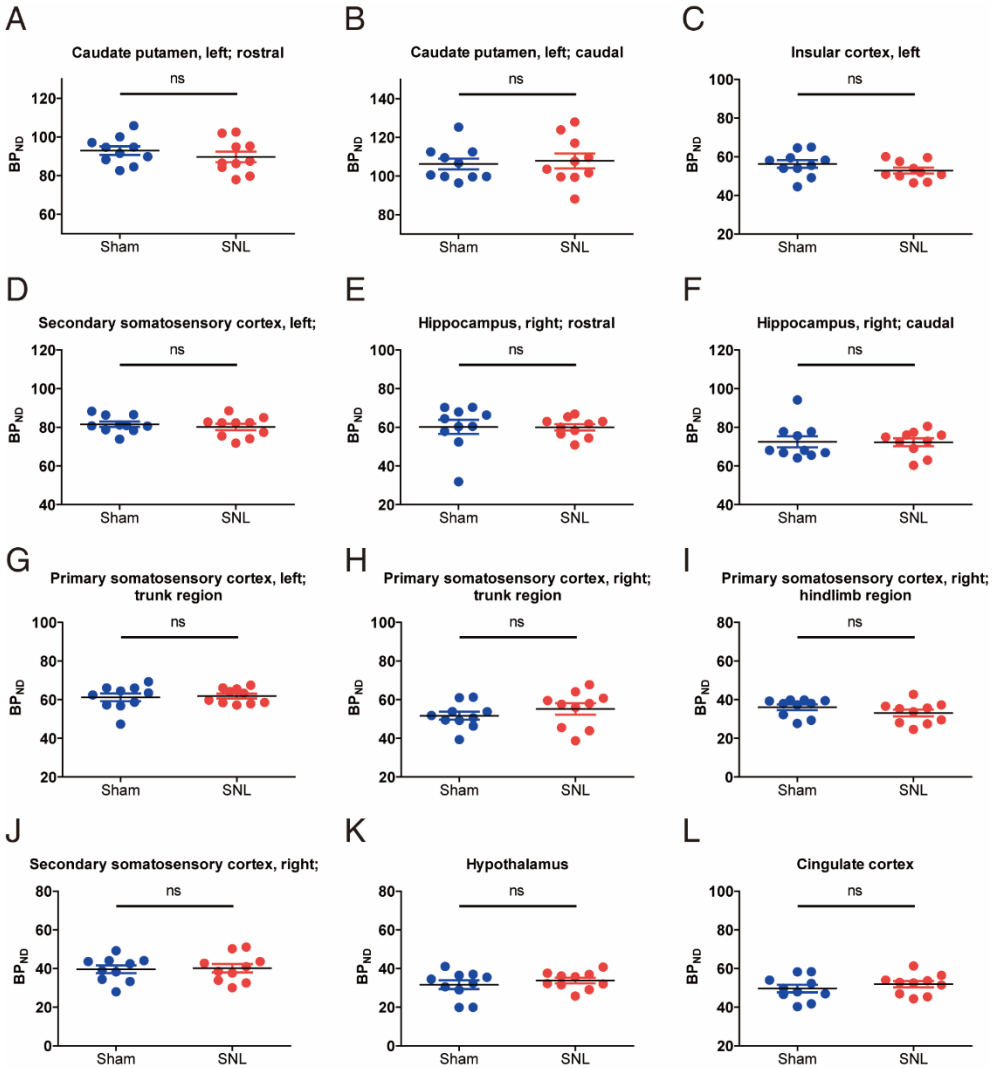

Figure 12. Comparisons of the mGluR5 levels between SNL group and sham group animals. BP_{ND} of each ROI were compared using two-sample t-tests and F-tests. No significant differences were observed from each test, indicating that the mGluR5 levels in the ROIs of the SNL group were in a normal range.

Decoding of the paw withdrawal threshold based on the mGluR5 patterns of neuropathic pain brain

To assess the distribution range of the mGluR5 levels in each region, the BP_{ND} of each ROI was plotted by group (Fig. 13A and 13B). For normalization, all values were scaled in proportion to the average values of each region in the sham group (Fig. 13C and 13D). A representative template of the SNL group pattern was produced by regression of the normalized mGluR5 levels to the paw withdrawal thresholds (Fig. 13E). Thus, each row of the template represents the pattern of normalized mGluR5 levels in each brain regions of a hypothetical SNL rat that has a corresponding paw withdrawal threshold.

The degree of match of the original pattern with the regressed pattern was computed using Pearson's correlation coefficient method. The correlation coefficient between the pattern of each SNL rat (Fig.13C) and the template (Fig.13E) was calculated row-by-row, and the results of each rat were plotted in the columns (Fig. 14A and 14B). Thus, each column of the r-value and p-value matrices represents the result from an individual rat. As the template was produced from the SNL data which had been normalized in proportion to the average value, high correlations ($r > 0.5$) were shown on either side of the average level, depending on the original paw withdrawal threshold value of the subject. The matched patterns were shown by the range of the r-value (Fig. 14C). The range of $r > 0.595$ or $r > 75$ percentile value was plotted to show the best-match between the mGluR5 pattern of the subject and the template, with the original paw withdrawal threshold of the subject assessed using the von Frey test (Fig. 14C). Only the correlations satisfying $p < 0.05$ (Fig. 14B) were considered. The results showed a good match between the original mGluR5 patterns of the SNL group animals and the patterns of the regressed template.

I questioned whether the mGluR5 patterns of the sham group animals matched the patterns of the SNL template by chance. To investigate this, the patterns of sham group animals (Fig. 13C) were compared to the SNL template (Fig. 13E) with the same method. No match showed a significant correlation (Fig. 14D and 14E). To classify the image into SNL or sham group, values of the columns were investigated in the matrices of both groups. The columns that contain the match satisfying $r > 0.595$ and $p < 0.05$ were predicted to be the SNL group. In the criteria, individual PET image could be predicted with 100% accuracy, regardless of the experimental group (Fig. 14F).

Further, I investigated the sensitivity of my method using a leave-one-out cross-validation paradigm. In this method, the pattern data of one subject (a row in the Fig. 13C) were left out, and the regressed template was created from data of the remaining nine subjects. Then data of the subject which had been left out were applied, to calculate the degree of match. This method was repeated subject-by-subject to predict all the paw withdrawal thresholds of SNL subjects. I observed that all the SNL subjects were correctly predicted by the method with 100% sensitivity, showing the existence of matches satisfying $r > 0.595$ and $p < 0.05$ in all of the SNL subjects (Fig. 14G and 14H). The high correlation range in this leave-one-out analysis was plotted with the paw withdrawal thresholds assessed using the von Frey test (Fig. 14I). All the paw withdrawal threshold values were in a range of good-match (range of $r > 0.595$). This confirms that the paw withdrawal threshold of the SNL animal can be precisely predicted by decoding the pattern of regional mGluR5 levels in the brain.

Together, these results show that once a model template is established from the [11C] ABP688 PET images of neuropathic pain group, the status of the individual subject can be decoded using the pattern of the regional mGluR5 levels. I could

precisely predict which group the sample subject belonged to with 100% accuracy, and further estimate the extent of paw withdrawal threshold of SNL group animal using mGluR5 patterns. Regarding the significant role of mGluR5 in regulating neuronal excitability, I propose that the mGluR5 “fingerprints” imprinted within the sensory and limbic structures of neuropathic pain brain reflect the functional crosstalk between sensory perception and behavioral coping.

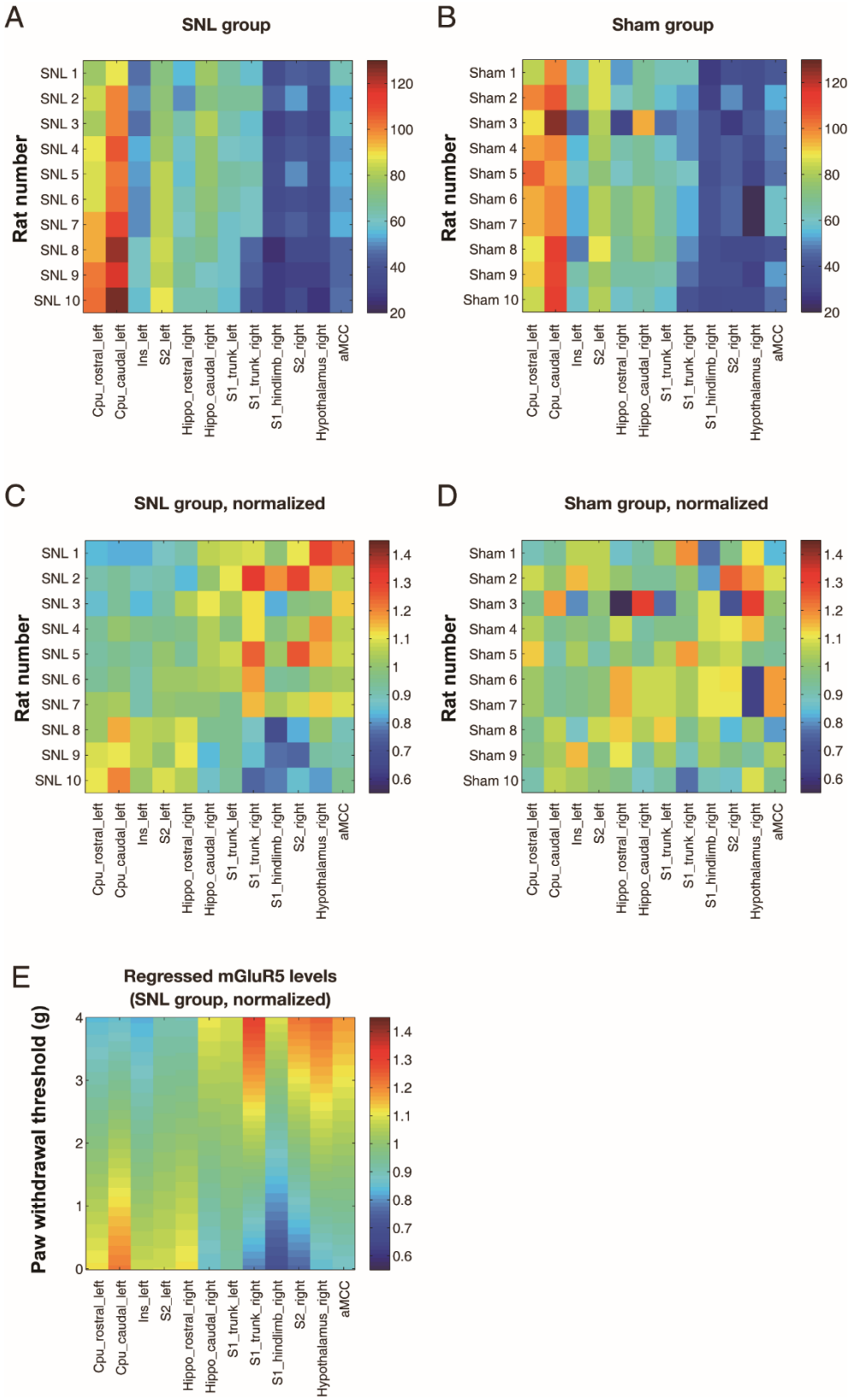
A
SNL group
Rat number
SNL 1
SNL 2
SNL 3
SNL 4
SNL 5
SNL 6
SNL 7
SNL 8
SNL 9
SNL 10
120
100
80
60
40
20
Cpu_rostral_left
Cpu_caudal_left
Ins_left
S2_left
Hippo_rostral_right
Hippo_caudal_right
S1_trunk_left
S1_trunk_right
S1_hindlimb_right
S2_right
Hypothalamus_right
aMCC
B
Sham group
Rat number
Sham 1
Sham 2
Sham 3
Sham 4
Sham 5
Sham 6
Sham 7
Sham 8
Sham 9
Sham 10
120
100
80
60
40
20
Cpu_rostral_left
Cpu_caudal_left
Ins_left
S2_left
Hippo_rostral_right
Hippo_caudal_right
S1_trunk_left
S1_trunk_right
S1_hindlimb_right
S2_right
Hypothalamus_right
aMCC
C
SNL group, normalized
Rat number
SNL 1
SNL 2
SNL 3
SNL 4
SNL 5
SNL 6
SNL 7
SNL 8
SNL 9
SNL 10
1.4
1.3
1.2
1.1
1
0.9
0.8
0.7
0.6
Cpu_rostral_left
Cpu_caudal_left
Ins_left
S2_left
Hippo_rostral_right
Hippo_caudal_right
S1_trunk_left
S1_trunk_right
S1_hindlimb_right
S2_right
Hypothalamus_right
aMCC
D
Sham group, normalized
Rat number
Sham 1
Sham 2
Sham 3
Sham 4
Sham 5
Sham 6
Sham 7
Sham 8
Sham 9
Sham 10
1.4
1.3
1.2
1.1
1
0.9
0.8
0.7
0.6
Cpu_rostral_left
Cpu_caudal_left
Ins_left
S2_left
Hippo_rostral_right
Hippo_caudal_right
S1_trunk_left
S1_trunk_right
S1_hindlimb_right
S2_right
Hypothalamus_right
aMCC
E
Regressed mGluR5 levels
(SNL group, normalized)
Paw withdrawal threshold (g)
4
3
2
1
0
1.4
1.3
1.2
1.1
1
0.9
0.8
0.7
0.6
Cpu_rostral_left
Cpu_caudal_left
Ins_left
S2_left
Hippo_rostral_right
Hippo_caudal_right
S1_trunk_left
S1_trunk_right
S1_hindlimb_right
S2_right
Hypothalamus_right
aMCC

Figure 13. mGluR5 levels in each ROI, and a representative template of mGluR5 pattern in the SNL group.

A. The distribution range of mGluR5 levels in each ROI in the SNL group.

B. The distribution range of mGluR5 levels in each ROI in the sham group.

C. The mGluR5 levels in each region of SNL animals were scaled in proportion to the average values of each region in the sham group.

D. Scaled mGluR5 levels in the sham group.

E. A representative template of the SNL group pattern. Proportionally scaled mGluR5 levels of SNL rats were regressed to the paw withdrawal thresholds. Each row of the template represents the pattern of normalized mGluR5 levels in each brain region of a hypothetical SNL rat which has a corresponding paw withdrawal threshold.

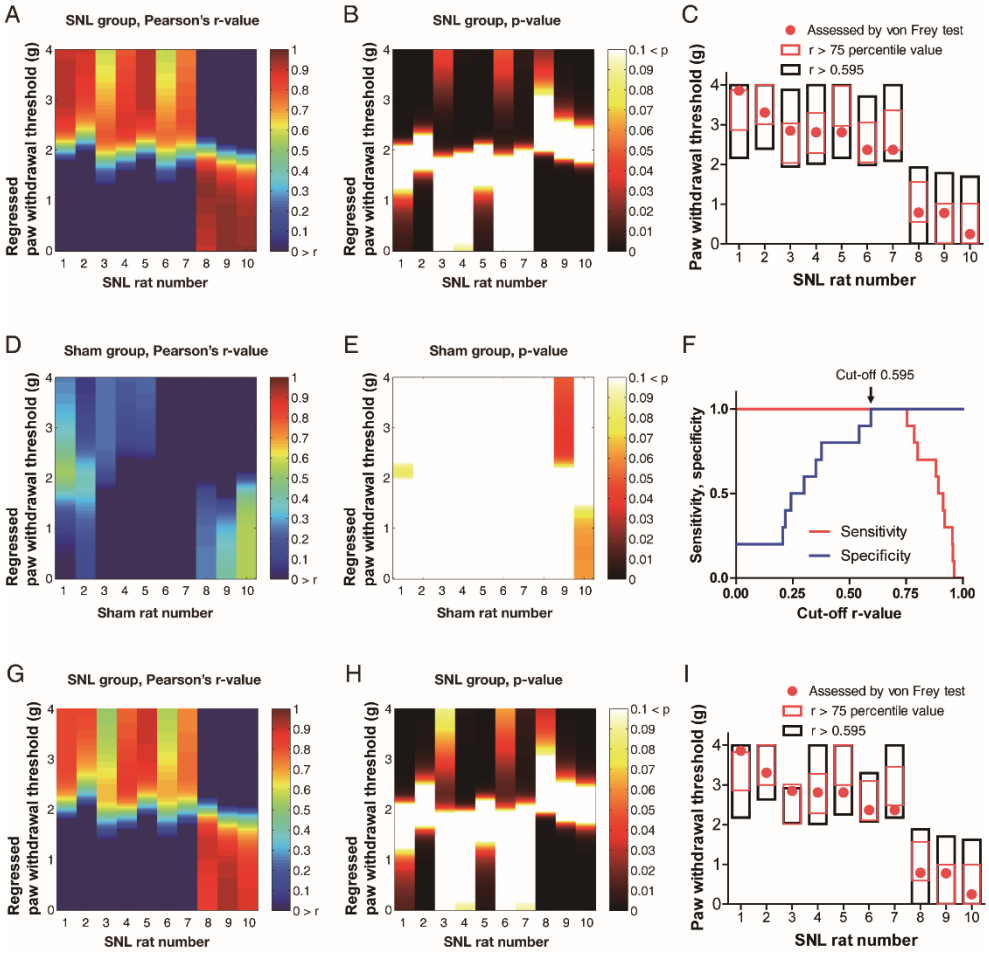
A
SNL group, Pearson's r-value
Regressed paw withdrawal threshold (g)
SNL rat number
0 > r
B
SNL group, p-value
0.1 < p
C
Assessed by von Frey test
r > 75 percentile value
r > 0.595
Paw withdrawal threshold (g)
SNL rat number
D
Sham group, Pearson's r-value
Sham rat number
E
Sham group, p-value
F
Cut-off 0.595
Sensitivity, specificity
Sensitivity
Specificity
Cut-off r-value
G
SNL group, Pearson's r-value
H
SNL group, p-value
I
Assessed by von Frey test
r > 75 percentile value
r > 0.595
Paw withdrawal threshold (g)
SNL rat number

Figure 14. The correlation between mGluR5 patterns of the regressed template and model animal predicts the presence and degree of neuropathic pain.

A. The correlation coefficients between the pattern of each SNL rat and the regressed SNL template. Each column represents the result from an individual rat. mGluR5 values from SNL rats showed high correlation with values of the SNL template.

B. The p-value matrix of SNL group. The matches of high correlation reached the significance ($p < 0.05$)in the SNL group.

C. Best-match ranges. The match ranges of the pattern correlation successfully predicted the original paw withdrawal threshold of the subject.

D. The correlation coefficients between the pattern of each sham rat and the regressed SNL template. The mGluR5 values of sham rats showed poor correlations with the values of the SNL template.

E. The p-value matrix of the sham group. The vast majority of the matches did not reach significance in the sham group.

F. Receiver- operating characteristic curve. The subject which contained an r-value above the cut-off level was predicted as SNL group. The subject could be predicted whether it belonged to the SNL or sham group with 100% accuracy, when the cut-off level was in the range of $0.595 < r < 0.754$.

G. The r-values of the SNL group derived from leave-one-out cross-validation.

H. The p-values of the SNL group derived from leave-one-out cross-validation.

I. The best-match ranges from leave-one-out cross-validation.

Discussion

Variation in paw withdrawal threshold in neuropathic pain animals (Fig. 7) might involve the degree of peripheral hypersensitivity, amplified aversive perception of the nervous system, and altered response strategy for coping behavior following nociception. With the analysis of [11C] ABP688-PET images, I demonstrated the brain regions in which the mGluR5 level is correlated with paw withdrawal threshold of neuropathic pain model animals. The brain regions are mainly constituted of sensory and limbic structures which are known to participate in sensory processing, decision making, and coping behaviors. Although it is difficult to interpret whether these correlations reflect passive change of mGluR5 following peripheral pain amplification or intrinsic regional function of mGluR5 as a determinant responsible for the execution of pain behavior, the critical role of the corticolimbic system in defensive avoidance behaviors is in agreement with previous studies.

I found that the striatal (caudate putamen) mGluR5 is negatively correlated (Fig. 8 A, 8B and 8D) whereas the somatosensory mGluR5 is positively correlated (Fig. 9B, 9D, 9E and 9F), with paw withdrawal thresholds (with the exception of a negative correlation of the left secondary somatosensory cortex in Fig. 8A). Thus, the higher levels of striatal mGluR5 or the lower levels of somatosensory mGluR5 are connected to a more sensitive paw withdrawal behavior to tactile stimulus. The hippocampus showed both a positive and negative correlation depending on subregion. Strikingly, these brain areas overlap with the regions identified by a previous analysis of fMRI-based connectivity. Baliki et al (Baliki et al., 2015) demonstrated that the hippocampus shows increased functional connectivity to the striatum and decreased functional connectivity to the sensorimotor cortex in neuropathic pain animals, and that these changes correlate with the degree of nerve injury-induced reduction of paw withdrawal thresholds. According to that study, the

hippocampus-striatum connectivity is negatively correlated whereas the hippocampus-sensorimotor cortex connectivity is positively correlated with the paw withdrawal thresholds. Thus, the higher level of hippocampus-striatum connectivity or the lower level of hippocampus-sensorimotor connectivity of neuropathic pain animals is connected to a more sensitive paw withdrawal behavior for tactile stimulus. They proposed that the interconnection between these brain regions plays a significant role in the manifestation of neuropathic pain. The results from my PET analysis support this view, and further implicate mGluR5 as a determinant of connectivity between these brain regions.

Besides the hippocampus and the striatum, significant clusters of mGluR5 were also located in other limbic structures such as the cingulate cortex (Fig. 9A) and the hypothalamus (Fig. 9C). In the case of the cingulate cortex, the anterior-posterior range of the significant cluster was -0.4 mm ~ -1.4mm from bregma, located in the anterior part of the midcingulate cortex (aMCC) (Vogt and Paxinos, 2014). This region is involved in error detection (conflict monitoring) and cognitive control (Parvaz et al., 2014; Procyk et al., 2014), and engaged in evaluating the necessity of behavioral adaption (Wessel et al., 2012). My data suggest that mGluR5 in this region affects decision making related to the execution of behavioral coping, and thus correlates with the von Frey stimuli-induced avoidance behavior. In the case of the hypothalamus, a significant mGluR5 cluster was located on the posterior nucleus of the right side. Regarding the sympathetic dependency of SNL-induced neuropathic pain (Kim et al., 1997), the positive correlation of a significant cluster suggests that mGluR5 in the posterior nucleus of hypothalamus suppresses withdrawal behavior via control of autonomic nervous tone.

One unexpected result was the significant correlation of paw withdrawal threshold with the hindlimb region of ipsilateral but not contralateral primary somatosensory

cortex. SNL rats were subjected to the right L5 SNL surgery, and therefore the withdrawal threshold of the right hind paw was assessed and used for regression analysis. Although many significant clusters in other subregions of primary somatosensory cortices were located bilaterally (Fig. 9D), correlation with hindlimb region was shown only in the right (ipsilateral to nerve injury) primary somatosensory cortex (Fig. 9F). mGluR5 level in the hindlimb region of the right primary somatosensory cortex was positively correlated with the paw withdrawal threshold, which indicates that the higher mGluR5 level was, the less withdrawal behavior of the right hind paw was elicited. This might be explained by interhemispheric inhibition of the contralateral corresponding hindlimb area by the ipsilateral primary somatosensory cortex (Clarey et al.; Hlushchuk and Hari, 2006). Unilateral somatosensory cortex participates in interhemispheric inhibition of the contralateral sensorimotor cortices, and thus influences sensory discrimination of transcallosal somatosensory cortex and aids in the motor control (Iwata et al., 2016; Lei and Perez, 2017; Zapallow et al., 2013).

In the case of the secondary somatosensory cortex, the left and right secondary somatosensory cortices showed an opposite direction in terms of the correlation to paw withdrawal threshold (Fig. 8A and Fig. 9E), further supporting the idea above. The positive correlation of right secondary somatosensory cortex, and the negative correlation of left secondary somatosensory cortex with paw withdrawal threshold, translate into a less sensitive hind paw with higher mGluR5 levels in the right secondary somatosensory cortex and/or lower mGluR5 levels in the left secondary somatosensory cortex. This suggests that among the bilateral somatosensory cortices, only mGluR5 in the left secondary somatosensory cortex exacerbates tactile hypersensitivity of the right hind paw. In contrast, mGluR5 levels in the right secondary somatosensory cortex, trunk region of the bilateral primary somatosensory cortices, and hindlimb region of the right primary somatosensory

cortex mitigate the hypersensitivity of the right hind paw.

In the previous analysis (chapter 1), I compared the mGluR5 levels in the brains of SNL surgery animals and sham surgery animals using voxel-by-voxel two-sample t-tests (Fig. 2). The resulting significant ROI clusters did not overlap in a coordinated space with the results of current regression analysis, although some clusters were located within the same anatomical structures (e.g., insular cortex, somatosensory cortices, and striatum). This disagreement between clusters with SNL-induced mGluR5 alteration and clusters which correlate to the withdrawal thresholds implies that the mGluR5 levels of each neural circuits represent separate stages of pain processing. According to the dynamic causal model of a recent study (Roy et al., 2014), a system of interconnected regions including the caudate putamen, hippocampus and ventromedial prefrontal cortex (vmPFC) encodes expectancies of behavioral outcome (expected pain and avoidance value), and activity of the putamen is most closely related to the expected value. In this causality model, the expected value signals from the putamen and the prediction error signals calculated in the midbrain periaqueductal gray are then transmitted to orbitofrontal cortex and anterior midcingulate cortex (aMCC), updating the value in the dorsomedial prefrontal cortex (dmPFC). While that study was conducted in humans and the model was produced based on fMRI experiments, participating brain regions revealed in that model largely overlap with ROIs extracted from my analyses. I interpret the aberrant levels of mGluR5 in affected brain regions (such as the prelimbic subregion of the mPFC) in the SNL-sham group comparison analysis of chapter 1 as maladaptation in the chronic pain state which affects updating appraisal of internal perception. In contrast, mGluR5 levels in the brain regions of behavioral correlation in the current regression analysis were in a normal range (Fig. 12), and thus their correlation with withdrawal threshold might reflect the normal physiological mGluR5 function of the system which affects encoding behavioral strategies (Roy et

al., 2014) or regulating the sensory perception. This is in agreement with the view that the altered paw withdrawal thresholds of SNL animals stem from pathologically intensified aversive perception and resulting reactive coping strategy, rather than normal perception and proactive behavioral decision making. Furthermore, as the identified regions overlap with sensory and limbic areas which are well known to play a significant role in pain processing, the correlations imply that the mGluR5 in certain brain regions actively participates in the manifestation of pain behavior, rather than being passively affected by information transfer from the peripheral sensation. I propose that mGluR5 in the significant brain regions affects the withdrawal threshold of nerve-injured subjects via functional regulation of sensory processing and behavioral coding in the somatosensory and limbic circuitry.

In conclusion, I report the correlation between brain mGluR5 levels and nerve injury-induced reduction of paw withdrawal threshold in a rodent model of neuropathic pain. A correlation was observed in the somatosensory cortices and limbic structures of the brain, emphasizing a critical role of mGluR5 in these regions with respect to neuropathic pain perception and resulting reactive behavior. These findings suggest that despite the fact that peripheral nerve injury is capable of inducing neuropathic pain, the manifestation of pain behavior is eventually determined by functional influences from relevant brain regions, possibly via interaction between interconnected circuitry. Owing to the interactions between sensory perception and behavioral coping, regional mGluR5 levels form distinct patterns in the brain of neuropathic pain subjects. Using the distinct “fingerprints” of mGluR5 levels, the status of individuals could be precisely predicted. Together with the study of chapter 1, the current study reveals a significant involvement of brain mGluR5 in the manifestation of neuropathic pain, and identifies brain circuits that may be further studied to clarify the mechanisms underlying altered sensory perception and behavioral coping in neuropathic pain subjects.

Table 3. Brain regions in which mGluR5 levels show negative correlations with the paw withdrawal threshold (Multiple regression with paw withdrawal threshold of SNL group, $p < 0.005$, $K_e > 20$). The peak voxel location is represented as distance from bregma (mm).

Negative interaction with paw withdrawal threshold

Brain region	K_e	T	Z	Peak p	Location (mm)		
					ML	AP	DV
Striatum (left; caudate putamen) and secondary somatosensory cortex (left)	543	9.92	4.44	4.5E-06	-4.2	-1.6	-5.8
		9.42	4.36	6.6E-06	-4.4	0	-6.0
		5.02	3.29	0.0005	-5.0	-1.8	-5.6
Striatum (left; caudate putamen) and insular cortex (left)	179	6.37	3.70	0.0001	-2.6	2.4	-5.2
		4.96	3.26	0.0006	-3.4	4.2	-5.6
Hippocampus (right; rostral)	27	4.20	2.97	0.0015	1.4	-1.8	-3.6

Table 4. Brain regions in which the mGluR5 levels show a positive correlation with the paw withdrawal threshold (Multiple regression with paw withdrawal threshold of SNL group, $p < 0.005$, $K_e > 20$). The peak voxel location is represented as the distance from bregma (mm).

Positive interaction with paw withdrawal threshold

Brain region	K_e	T	Z	Peak p	Location (mm)		
					ML	AP	DV
Cingulate cortex	53	6.40	3.71	0.0001	0.4	-0.8	-1.4
Primary somatosensory cortex (right; trunk region) and hippocampus (right; caudal)	395	5.73	3.51	0.0002	3.0	-3.2	-2.2
		5.50	3.44	0.0003	3.4	-2.6	-1.8
		4.85	3.22	0.0006	2.2	-2.8	-1.8
Hypothalamus (right; posterior nucleus)	43	5.60	3.48	0.0003	0.4	-3.8	-8.2
Primary somatosensory cortex (left; trunk region, dysgranular zone, and barrel field)	66	5.37	3.40	0.0003	-3.8	-3.2	-2.6
		4.72	3.17	0.0008	-4.6	-3.0	-2.6
		3.51	2.65	0.0040	-3.4	-3.0	-1.6
Secondary somatosensory cortex (right)	23	4.55	3.11	0.0009	6.0	0.6	-5.6
Primary somatosensory cortex (right; hindlimb and forelimb region)	26	4.40	3.05	0.0012	3.6	-0.2	-1.2

Chapter 3.

Dysregulation of metabotropic glutamate receptor 5 in the periaqueductal gray perpetuates neuropathic pain

Summary

The pain becomes chronic with dysfunction of an endogenous pain processing system in the central nervous system. However, underlying mechanisms remain largely unknown. Here I demonstrate that the metabotropic glutamate receptor 5 (mGluR5) in the periaqueductal gray (PAG) is persistently active in normal condition to maintain an appropriate sensory transmission, and decline of the activity is responsible for chronic pain. In the condition of peripheral nerve injury, the activity-dependently expressed immediate early gene Homer1a is expressed in the PAG and causes the decline of mGluR5 activity, which results in reduced excitability of PAG neurons. Notably, I found that single-time inactivation of the PAG-mGluR5 results in long-lasting pain even in the absence of peripheral injury, which is related to long-term depression of the excitatory drive on the endogenous pain modulatory pathway. Conversely, activation of mGluR5 in the PAG of chronic neuropathic pain rat eliminated pain behavior and completely reversed pain-induced alteration of brain activity. These findings reveal novel mechanisms underlying maintenance of neuropathic pain and provide new insight into how the pain becomes chronic with the maladaptive coping of the PAG to pain sensation.

Introduction

Decreased endogenous pain inhibition and increased pain facilitation are shared characteristics of many pathological chronic pain conditions including nerve injury-induced neuropathic pain (Staud, 2012). Owing to the malfunction of endogenous pain modulatory system, neuropathic pain patients suffer from long-lasting severe pain still after the nerve injury-induced peripheral change is diminished (Tracey and Mantyh, 2007; Ossipov, Dussor and Porreca, 2010; Ossipov, Morimura and Porreca, 2014). In contrast to detailed understandings of increased pain transmission in the primary afferent and spinal cord, however, mechanisms underlying abnormal pain modulation in the brain in the chronic neuropathic pain state are largely unknown.

Periaqueductal gray (PAG), the key area of the endogenous pain modulatory system, regulates sensory signals via rostral ventromedial medulla (RVM). Excitatory drive on the PAG mainly suppresses pain although the action of the RVM can be engaged to promote as well as prevent pain signals. The decline of excitatory influences on the PAG might produce modulatory dysfunction and distort sensory signals to be painful (Ho, Cheng and Chiou, 2013). I focused on the role of metabotropic glutamate receptor 5 (mGluR5) in the PAG. Group I mGluRs including mGluR5 play dual roles in the pain processing of the nervous system, enhancing pain transmission in ascending pathways and inhibiting pain at endogenous modulatory pathway of PAG-RVM (Kim, Calejesan and Zhuo, 2002). According to previous studies, activation of the mGluR5 in the PAG (PAG-mGluR5) enhances neuronal activity and induces analgesic effect (Drew, Mitchell and Vaughan, 2008; Wilson-poe, Mitchell and Vaughan, 2013; Kolber, 2015).

Activation of mGluR5 triggers various downstream signaling cascades and affects neuronal excitability. Although mGluR5 has been shown to be persistently active in certain circumstance (Young et al., 2013) and promote firing of neurons (Davies et

al., 1995; Young, Bianchi and Wong, 2008; D'Ascenzo et al., 2009), the in-vivo existence and physiological roles in brain function of such an activity have not been reported. Here I report that the mGluR5 in the PAG is persistently active in normal state, and its conditional inactivation underlies chronic pain. I demonstrate that the persistent activity of PAG-mGluR5 is required for regulation of neuronal excitability, and suspension of it is sufficient to induce long-lasting pain in the naïve animal. Further, I investigate the alteration of whole-brain activity in chronic pain animal using PET imaging and reveal the basal PAG-RVM activity is down-regulated. Activation of the PAG-mGluR5 completely reverses the pain-induced alteration of brain activity and rescues neuropathic pain behavior. My results demonstrate a critical involvement of persistent PAG-mGluR5 activity in pain processing and provide new insight into how the PAG-RVM pathway becomes dysfunctional as it contributes to chronic pain.

Results

Activation of the PAG-mGluR5 eliminates neuropathic pain symptom

I questioned whether the PAG-mGluR5 activates the endogenous pain modulatory function sufficient to reverse chronic neuropathic pain. Spinal nerve ligation (SNL) was adopted as a neuropathic pain model (Kim and Chung, 1992) and paw withdrawal threshold of affected hindpaw was measured from model animals to confirm the emergence of mechanical allodynia. Then I administered 3,5-dihydroxyphenylglycine (DHPG), the agonist of mGluR5, into the unilateral PAG of the model animal via implanted cannula (Fig. 15A) and measured paw withdrawal threshold. DHPG treatment into the PAG (PAG-DHPG) evoked powerful analgesic effect and completely abolished SNL-induced mechanical allodynia (Fig. 15C and 16A). This analgesic effect lasted more than an hour and disappeared within next 24 hours (Fig. 15C and 16A).

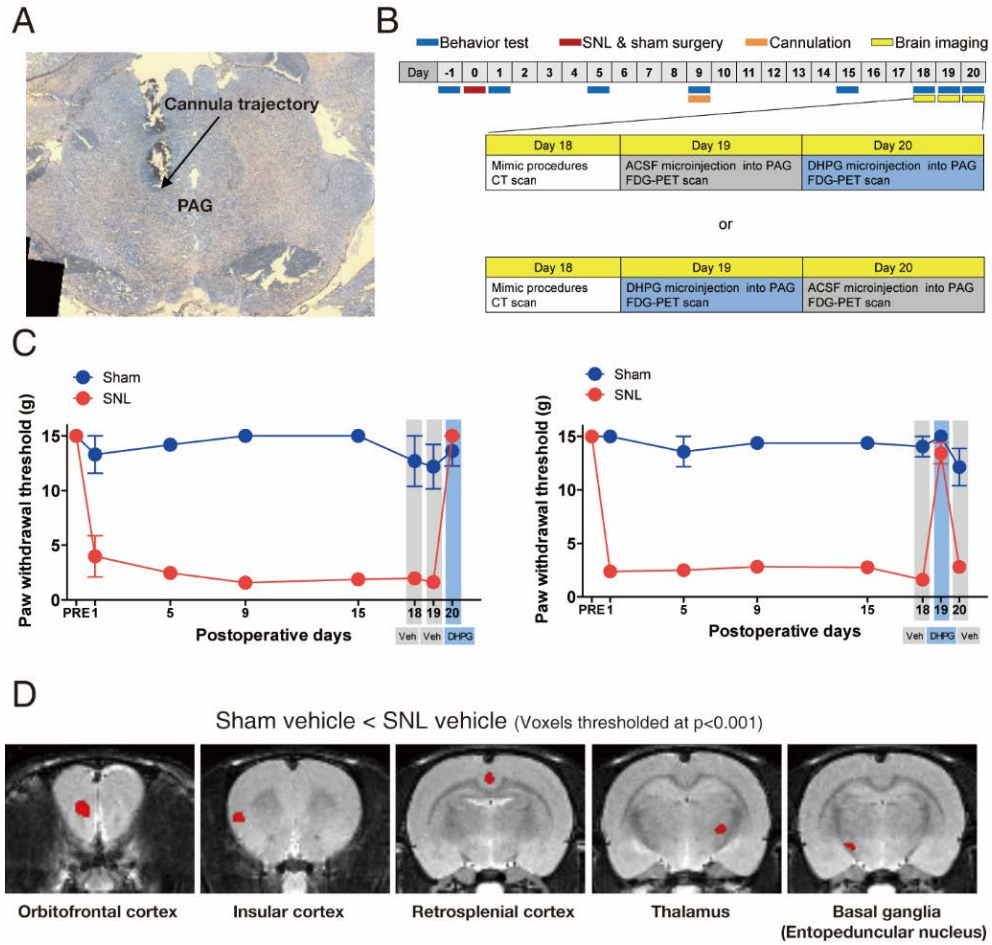

Figure 15. Microinjection of DHPG into the PAG and FDG-PET experiments.

A. Location of microinjection site in the PAG.

B. Experimental design for the FDG-PET scans.

C. Mechanical hypersensitivity induced by SNL surgery is abolished by PAG-DHPG.

D. Brain regions showing higher activity in SNL group compared to sham group (PAG-vehicle condition, independent two-sample t-test, $p<0.001$, $K_e > 20$).

Activation of the PAG-mGluR5 rescues chronic neuropathic pain-related alteration of brain activity

To measure the alteration of the whole-brain activity in neuropathic pain state and PAG-driven analgesic state *in vivo*, I performed two separate brain scans to each animal using [^{18}F] - fluorodeoxyglucose (FDG) – PET imaging technique, with microinjection of vehicle (PAG-vehicle) and DHPG (PAG-DHPG) into the PAG, respectively (Fig. 15B and 15C). First, I compared the brain activity of SNL group and sham surgery group using images of vehicle-treated state (SNL-vehicle vs. Sham-vehicle) with a conventional threshold of uncorrected $p < 0.001$. In this PAG-vehicle condition, SNL group showed significantly lower activity from the PAG and the RVM compared to sham group (Fig. 16B, Table 5). The orbitofrontal cortex (OFC), insular cortex (IC), retrosplenial cortex (RSC), thalamus and basal ganglia (BG), which are brain regions involved in pain processing, showed higher activity in SNL group compared to sham group (Fig. 15D, Table 5). Next, I compared SNL and sham animals of analgesic state using images of DHPG-treated state (SNL-DHPG vs. Sham-DHPG). Under the PAG-DHPG condition, inter-group differences were completely eliminated and no significant alteration was observed. PAG, RVM, OFC, IC, RSC, thalamus and BG no longer showed activity differences even at the more relaxed statistical criterion of uncorrected $p < 0.005$.

Further, I analyzed the effect of the PAG-DHPG on brain activity using pairs of images from each animal. Differences between vehicle-treated state and DHPG-treated state were compared with a conventional threshold of uncorrected $p < 0.001$ by each group. In SNL group (SNL-vehicle vs. SNL-DHPG), DHPG-induced metabolic increase was observed from entire PAG (Fig. 16D), although unilateral caudal ventrolateral PAG was targeted, implying broad excitatory connection among the region (Beitz, 1989). RVM as well showed a metabolic increase in this condition

(Fig. 16D, table 5), which is in line with the well-known PAG-RVM pathway. Interestingly, however, the response was different in the sham group (Sham-vehicle vs. Sham-DHPG). The metabolic increase was observed from only dorsal part of the PAG and focal injected site of ventral part (Fig. 16C). Activity increase of the ventral or rostral part PAG was less prominent in sham group compared to SNL, for voxels of these areas could not survive significance level in the sham group. I further explore these phenomena using merged results of the drug-status and surgery-status analyses with a more relaxed p-value threshold of uncorrected $p < 0.005$, showing: (i) In SNL group, PAG-DHPG increases the activity of the PAG region which is related to neuropathic pain (Fig. 16F), which is consistent with my model. (ii) The PAG-DHPG effect is insufficient to increase the activity of the same region in the sham group (Fig. 16E), possibly because of a ceiling effect. (iii) The decrease of activity is observed mainly from remote cortical areas in both groups (Table 6 and Table 7). Fig. 16E and 16F clearly show the difference of DHPG effect on the PAG activity between sham and SNL group, and imply altered activity of the PAG region in neuropathic pain condition is related to the mGluR5 status. Taken together, these data show the decline of the PAG-RVM activity during chronic neuropathic pain state and suggest the involvement of PAG-mGluR5 activity.

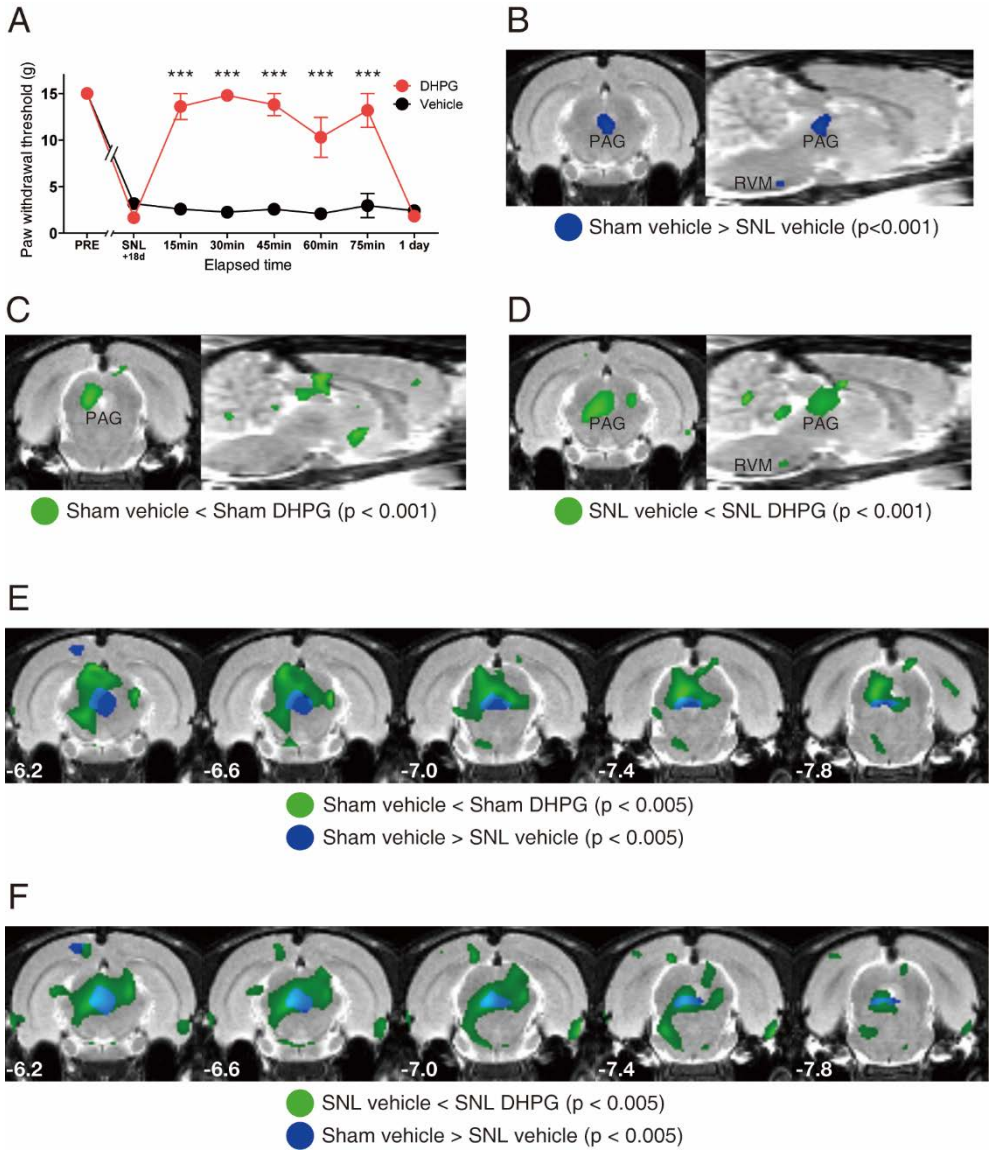
A
Paw withdrawal threshold (g)
15
10
5
0
***
***
***
***
***
DHPG
Vehicle
PRE
SNL +18d
15min
30min
45min
60min
75min
1 day
Elapsed time
B
PAG
PAG
RVM
Sham vehicle > SNL vehicle (p<0.001)
C
PAG
Sham vehicle < Sham DHPG (p < 0.001)
D
PAG
PAG
RVM
SNL vehicle < SNL DHPG (p < 0.001)
E
-6.2
-6.6
-7.0
-7.4
-7.8
Sham vehicle < Sham DHPG (p < 0.005)
Sham vehicle > SNL vehicle (p < 0.005)
F
-6.2
-6.6
-7.0
-7.4
-7.8
SNL vehicle < SNL DHPG (p < 0.005)
Sham vehicle > SNL vehicle (p < 0.005)

Figure 16. Activation of PAG-mGluR5 ameliorates pain behavior and rescues pain-induced alteration of brain activity.

A. Effect of DHPG microinjection into the PAG on SNL-induced mechanical allodynia (n=5 animals per each group, ***$p<0.001$, repeated ANOVA with Bonferroni).

B. Brain areas of which the activity is lower in SNL group compared to sham group (n=11 animals per each group).

C. Brain areas which responded to DHPG microinjection into the PAG in sham rats.

D. Brain areas which responded to DHPG microinjection into the PAG in SNL rats.

E. Merged results from each analysis (analyses used in B and C) with a p-value of 0.005. Ventral part PAG does not respond to the DHPG treatment in the sham group. The distance from bregma is indicated in the lower left corner (in mm). Voxels with a significant difference are shown as blue or green color. Voxels in the images are thresholded at the indicated p-value in independent (surgery-status, blue) or paired (drug-status, green) two-sample t-test, and overlaid to MRI template image. Brain regions and their significances are listed in Table 5, 6 and 7.

F. Merged results from each analysis (analyses used in B and D) with a p-value of 0.005. PAG-DHPG treatment increases glucose metabolism in the entire PAG, including ventral regions.

PAG-mGluR5 is persistently active in normal state, and a suspension of it is sufficient to induce chronic pain

I then questioned why the DHPG treatment could not increase activity from the broad ventral PAG regions in the sham group. One possible explanation is that the neurons within this area are already active to a considerable degree in a normal state, and therefore DHPG could not promote a further increase in the sham group. mGluR5 is known to be persistently active in certain circumstance (Young et al., 2013) and promote firing of neurons (D'Ascenzo et al., 2009; Davies et al., 1995; Young et al., 2008). To identify the persistent activity of mGluR5, I administered mGluR5 inverse-agonist (antagonist which can block the persistent activity) 2-methyl-6-(phenylethynyl)pyridine (MPEP) into the bilateral PAG of naïve rats, and measured behavioral change. Pharmacological blockade of the PAG-mGluR5 using MPEP (PAG-MPEP) resulted in tactile hypersensitivity manifested by a reduction of paw withdrawal threshold, which was comparable to nerve injury-induced mechanical allodynia (Fig. 17A). The inverse-agonist of mGluR1 also induced similar effect (Fig. 18A). These findings show that PAG-mGluRs are persistently active to consistently modulate sensory signals in a normal state. Furthermore, tactile hypersensitivity produced by PAG-MPEP did not decay along with the time. The stability of this hypersensitivity was independent to diffusion of the injected drug in that the allodynia was not attenuated even a month after single-time administration of MPEP (Fig. 17A). These data indicate that the malfunction of the pain modulatory system induced by conditional inactivation of regional mGluR5 is eventually able to produce chronic pain even in the absence of amplified ascending pain signal originating from peripheral damage.

PAG-mGluR5 is persistently active to regulate neuronal excitability in normal condition and is attenuated in chronic pain condition

Previous findings reported the persistent effect of mGluR5 activation under certain circumstances (Ireland and Abraham, 2002; Sourdet et al., 2003). To identify the persistent action of mGluR5, I assessed the excitability of PAG neurons from brain slices of naïve rats before and after MPEP treatment. Bath application of MPEP significantly decreased the number of action potentials (AP) from 10 out of 14 recorded neurons (total 40.96% reduction of AP numbers averaged from 14 neurons) (Fig. 17B, 17C, and 17G). Reduction of APs accompanied decrease of input resistance (Fig. 17D) and was expressed by abrupt cessation of firing (Fig. 17B, left) or increased spike frequency adaptation (Fig. 17B, right), which was rescued by bath application of mGluR5 agonists after washout of MPEP (Fig. 17B and Fig. 18B). These results are coherent with the previous report which showed that the activation of mGluR5 in hippocampal neuron leads to an increase in input resistance and a reduction in spike frequency adaptation (Davies et al., 1995). Together, my findings demonstrate that mGluR5 is persistently active to regulate the excitability of vlPAG neurons in normal condition.

In the following sets of experiments, I tested whether the persistent mGluR5 activity is declined in PAG neurons of chronic pain animals. Intrinsic excitability of PAG neuron was measured in sham surgery control and SNL surgery animal before and after MPEP treatment. Consistent with results from naïve rats, MPEP treatment resulted in a reduction of excitability of PAG neurons from sham surgery-performed rats, showing AP attenuation from 13 out of 19 neurons tested (total 39.74% reduction of AP numbers averaged from 19 neurons) (Fig. 17E and 17G). In contrast, MPEP could not reduce excitability from the majority of PAG neurons in SNL group in that only 7 out of 19 neurons showed AP attenuation (total 15.74% reduction of

AP numbers averaged from 19 neurons) (Fig. 17F and 17G). The occlusion of the MPEP effect suggests that the persistent PAG-mGluR5 activity is readily attenuated in neuropathic pain condition. I propose that the decline of mGluR5 activity resulted in a reduction of PAG neuronal excitability in SNL rats, as the proportion of transient-spiking cells before MPEP treatment was more prominent in SNL rats (Fig. 17H).

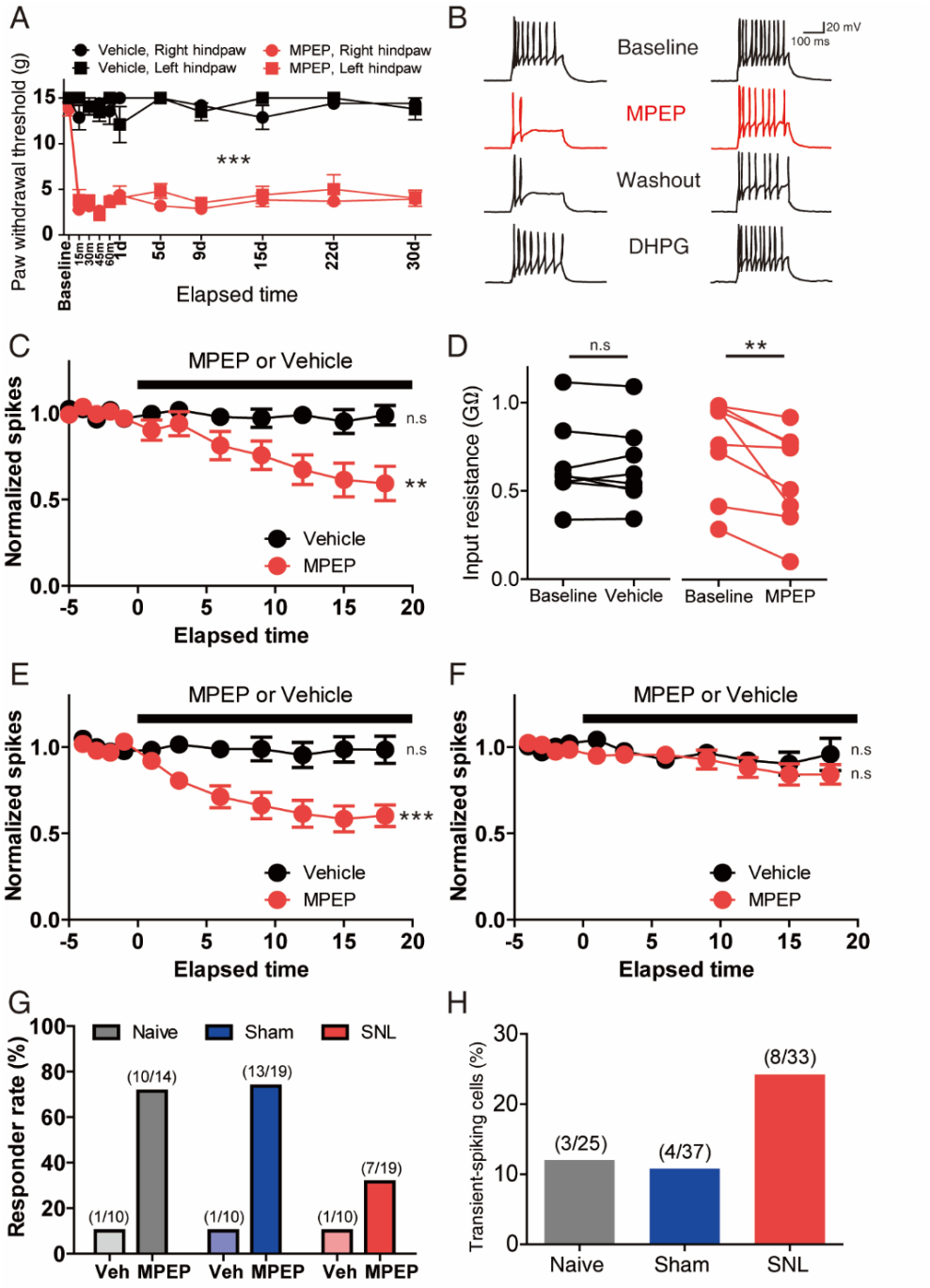
A
Vehicle, Right hindpaw
Vehicle, Left hindpaw
MPEP, Right hindpaw
MPEP, Left hindpaw
Paw withdrawal threshold (g)
***
Baseline
15m
30m
45m
60m
1d
5d
9d
15d
22d
30d
Elapsed time
B
Baseline
MPEP
Washout
DHPG
20 mV
100 ms
C
MPEP or Vehicle
Normalized spikes
n.s
**
Vehicle
MPEP
Elapsed time
D
n.s
**
Input resistance (GΩ)
Baseline
Vehicle
Baseline
MPEP
E
MPEP or Vehicle
Normalized spikes
n.s
***
Vehicle
MPEP
Elapsed time
F
MPEP or Vehicle
Normalized spikes
n.s
n.s
Vehicle
MPEP
Elapsed time
G
Naive
Sham
SNL
Responder rate (%)
(10/14)
(13/19)
(7/19)
(1/10)
(1/10)
(1/10)
Veh MPEP
Veh MPEP
Veh MPEP
H
Transient-spiking cells (%)
(3/25)
(4/37)
(8/33)
Naive
Sham
SNL

Figure 17. PAG-mGluR5 is persistently active in a normal state to regulate neuronal excitability, and a disturbance of it is responsible for neuropathic pain.

A. Long-lasting mechanical allodynia induced by MPEP microinjection into the PAG in naïve rats (n=5 each, ***$p<0.001$ at all the time points, repeated ANOVA with Bonferroni).

B. Bath application of MPEP results in abrupt cessation of firing (left) or increased spike frequency adaptation (right) of PAG neurons from naïve rats.

C. Reduction of spike firing after MPEP treatment in PAG neurons from naïve rats (MPEP n=14, vehicle n=10).

D. The decrease of input resistance after MPEP treatment.

E. Effect of MPEP on the excitability of PAG neurons from the sham group (MPEP n=19, vehicle n=10). Wilcoxon matched pairs test was used for the excitability analyses (*$p<0.05$, **$p<0.01$, ***$p<0.001$)

F. Effect of MPEP on the excitability of PAG neurons from SNL group (MPEP n=19, vehicle n=10).

G. The ratio of MPEP responder neurons in naïve, sham and SNL group.

H. The ratio of transient-spiking PAG neurons in each group (baseline state).

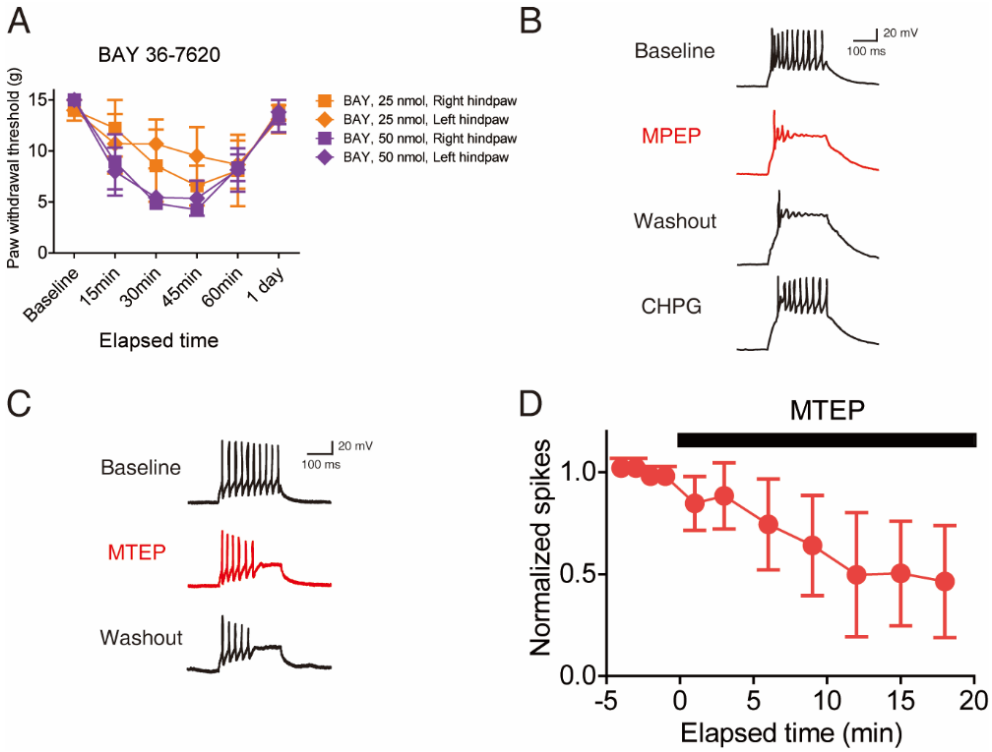

Figure 18. Persistent activity of PAG-mGluRs in naïve rats.

A. Inactivation of PAG-mGluR1 using BAY 36-7620 induces mechanical hypersensitivity which decays along with the time.

B. MPEP reduces excitability of PAG neurons from naïve rats. Bath application of mGluR5 agonist CHPG rescues a cease of spike firing induced by MPEP.

C. Administration of MTEP reduces excitability of PAG neurons from naïve rats, which is consistent with the effect of MPEP.

D. MTEP decreased the number of APs from 2 out of 3 recorded neurons (total 53.67% reduction of AP numbers averaged from 3 neurons).

Decline of PAG-mGluR5 activity in chronic pain state results in reduced excitatory drive on the PAG-RVM pathway

As the PAG itself is the major source of glutamatergic input to the PAG (Beitz, 1989), reduced excitability of glutamatergic PAG neurons would result in decreased excitatory output to other PAG neurons. To assess the effect of mGluR5 on the excitatory activity of the PAG network, I recorded spontaneous excitatory postsynaptic currents (sEPSC) of PAG neurons before and after mGluR5 antagonism in brain slices from naïve rats. 3-((2-methyl-1,3-thiazol-4-yl)ethynyl)pyridine (MTEP) was used in this experiment. Blockade of persistent mGluR5 activity with MTEP also reduced neuronal excitability (Fig. 18C and 18D). As I expected, MTEP treatment resulted in a reduction of the frequency of sEPSC in PAG neurons from naïve rats showing 41.54% reduction (Fig. 19A and 19B). Change of amplitude was not significant, although a subset of neurons showed reduced sEPSC amplitude after MTEP treatment (Fig. 19C).

I wondered whether the alteration of mGluR5 property in neuropathic pain state changes excitatory network activity and affects PAG-RVM circuit. To investigate the sEPSC on PAG neurons which project to RVM (PAG-RVM neuron) specifically, I identified the PAG-RVM neurons by retrograde tracing technique and recorded sEPSC in these neurons from each group animals (Fig. 20A and 20B). The PAG-RVM neurons from sham animals responded to MTEP and showed reduced frequency of sEPSC (Fig. 19D, left), which is consistent with the result of PAG neurons from naïve rats. In the case of SNL rats, in contrast, neurons barely responded to MTEP treatment (Fig. 19D, middle and right), indicating occlusion of the effect. Change of amplitude was not significant in both groups (Fig. 19E). Inter-group analysis revealed that sEPSC before MTEP treatment is already lower in SNL group compared to sham group (Fig. 19F and 19G), which suggests that the loss of

persistent mGluR5 activity resulted in the reduced excitatory drive across the PAG. On the contrary, GABAergic spontaneous inhibitory postsynaptic currents (sIPSCs) were increased in SNL group (Fig. 20B and 20D), implicating that the decline of the mGluR5 activity could not reduce the activity of inhibitory neurons. Taken together, these data show that mGluR5 persistently regulates excitatory influences on the PAG-RVM pathway in a normal state, and confirm decline of the effect in neuropathic pain state.

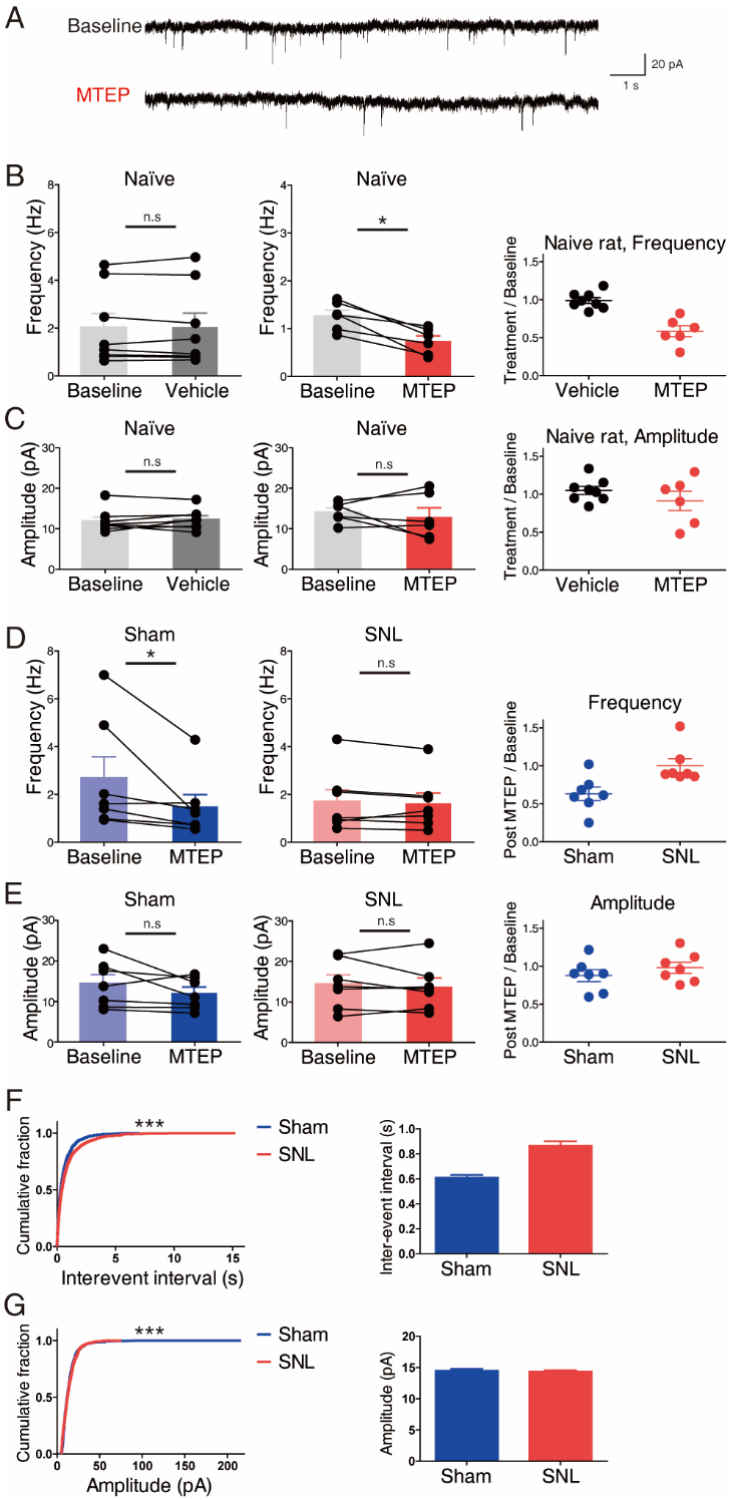
A
Baseline
MTEP
20 pA
1 s
B
Naïve
Frequency (Hz)
n.s
Baseline
Vehicle
Naïve
*
Baseline
MTEP
Naive rat, Frequency
Treatment / Baseline
Vehicle
MTEP
C
Naïve
Amplitude (pA)
n.s
Baseline
Vehicle
Naïve
n.s
Baseline
MTEP
Naive rat, Amplitude
Treatment / Baseline
Vehicle
MTEP
D
Sham
*
Frequency (Hz)
Baseline
MTEP
SNL
n.s
Frequency (Hz)
Baseline
MTEP
Frequency
Post MTEP / Baseline
Sham
SNL
E
Sham
n.s
Amplitude (pA)
Baseline
MTEP
SNL
n.s
Amplitude (pA)
Baseline
MTEP
Amplitude
Post MTEP / Baseline
Sham
SNL
F
***
Cumulative fraction
Interevent interval (s)
Sham
SNL
Inter-event interval (s)
Sham
SNL
G
***
Cumulative fraction
Amplitude (pA)
Sham
SNL
Amplitude (pA)
Sham
SNL

Figure 19. Persistent PAG-mGluR5 activity is attenuated in neuropathic pain state, which results in a reduction of excitatory input on the PAG-RVM pathway.

A. Effect of MTEP on spontaneous EPSC of vlPAG neurons from the naïve rats.

B. Effect of MTEP on the frequency of spontaneous EPSC of vlPAG neurons from the naïve rats.

C. Effect of MTEP on the amplitude of spontaneous EPSC of vlPAG neurons from the naïve rats.

D. Effect of MTEP on the frequency of spontaneous EPSC of PAG-RVM projection neurons from sham or SNL groups (n=7 each, *$p<0.05$, Wilcoxon matched pairs test). The effect of MTEP is absent in SNL group, implicating the occlusion.

E. Effect of MTEP on the amplitude of spontaneous EPSC of PAG-RVM projection neurons from sham or SNL groups (n=7 each, *$p<0.05$, Wilcoxon matched pairs test).

F. The frequency of spontaneous EPSC is reduced in SNL rats compared to sham control in baseline state (n=7 each, before the MTEP treatment, ***$p<0.001$, Kolmogorov-Smirnov two-sample test).

G. The amplitude of spontaneous EPSC in baseline state (n=7 each, before the MTEP treatment).

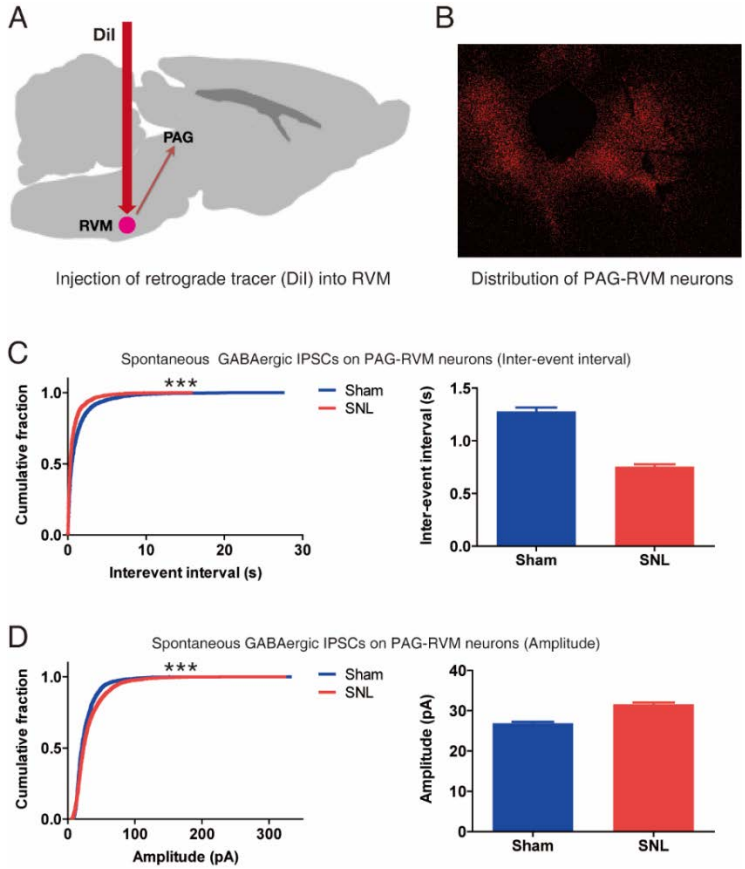

Figure 20. Identifying PAG neurons which project to the RVM (PAG-RVM projection neurons) and recording postsynaptic currents.

A. Microinjection of retrograde tracer (DiI) into RVM.

B. The distinct distribution pattern of PAG-RVM neurons can be seen from midbrain slice. Dorsolateral columns of the PAG lacks PAG-RVM neurons.

C. The frequency of spontaneous GABAergic IPSC is increased in SNL rats, shown by the decreased inter-event interval (n=16 each, ***p<0.001, Kolmogorov-Smirnov two-sample test).

D. The amplitude of spontaneous GABAergic IPSC is increased in SNL rats (n=16 each, ***p<0.001, Kolmogorov-Smirnov two-sample test).

Homer1a is involved in the decline of PAG-mGluR5 activity in chronic neuropathic pain state

Functions of mGluR5 are regulated by intracellular interacting molecules, such as scaffolding protein Homer (Brakeman et al., 1997; Xiao et al., 1998). Among the Homer family, a short splice variant Homer1a is activity-dependently expressed, and acts as a dominant negative competitor for other long-form Homer proteins. Although the Homer1a induces long-lasting constitutive activity of mGluR5 in certain circumstances (Fagni et al., 2003), the functional effect of Homer1a on the sustained activation of mGluR5 seems to differ based on neuronal conditions (see chapter 4). In the current study, I found the Homer1a counteracts sustained activation of PAG-mGluR5.

I observed the increased Homer1a expression in the vlPAG of SNL rats (Fig. 21A). To see the functional effect of the Homer1a induction on the pain behavior, I injected virus expressing Homer1a into the bilateral PAG of naïve rats, and measured paw withdrawal threshold for 21 days. The overexpression of Homer1a resulted in the manifestation of tactile hypersensitivity in naïve rats (Fig. 21B), which was comparable to SNL-induced mechanical allodynia. This implicates the Homer1a expression in the PAG acts as a pain inducer. Thus, the functional effect of the Homer1a expression was same with the PAG-MPEP treatment.

To further confirm the functional effect of the Homer1a within the PAG, experiments were performed with knock-down strategy using virus expressing Homer1a shRNA (shHomer1a). The virus expressing luciferase shRNA (shLuci) was used as a control. The SNL surgery was performed 3 weeks after the virus injection into the bilateral PAG. As I expected, the knock-down of Homer1a in the PAG prevented the transition to chronic pain following SNL surgery (Fig. 21C). Despite the mechanical allodynia was successfully developed by the surgery, the

symptom was gradually recovered along with the time in the shHomer1a-treated group. These data demonstrate that the increased Homer1a in the PAG is the cause of the maintenance of chronic pain after the peripheral nerve injury.

In the slice patch-clamp experiment of the PAG-MPEP treatment, the decline of mGluR5 activity in the control group resulted in reduction of neuronal excitability (Fig. 17C and 17E). On the contrary, the MPEP treatment could not further reduce neuronal excitability in the PAG slices from SNL rats (Fig. 17F), implicating the occlusion. In that, I supposed the excitability of PAG neuron would be decreased in SNL group due to the decline of the persistent mGluR5 activity. Indeed, PAG neurons of SNL group showed significantly lower baseline excitability compared to sham group (Fig. 21D). Consistent with the behavior experiment, the neuronal excitability was rescued by knock-down of Homer1a prior to SNL surgery (Fig. 21D). The excitability of the PAG neurons from shHomer1a-injected SNL group was comparable to, or even higher than, the sham group. Furthermore, the persistent activity of mGluR5 in the PAG neurons was preserved despite of the SNL surgery in the shHomer1a-injected group, shown by reduction of the excitability in response to the slice MTEP treatment (Fig. 21E).

Taken together, these data demonstrate the increased Homer1a within the PAG is involved in the decline of mGluR5 persistent activity in neuropathic pain condition. I propose a model of Homer1a-mediated maintenance of chronic neuropathic pain as follows: In the early stages, peripheral nerve injury directly induces pain. Homer1a within the PAG is increased activity-dependently, with the activated endogenous pain modulatory system. Sustained activation of the system accumulates Homer1a, which eventually leads to the decline of persistent mGluR5 activity. This causes reduction of neuronal excitability, followed by a hypoactivity of PAG neurons which project to the RVM. Consequently, the dysfunction of endogenous pain modulatory system is fixed by the positive feedback, and pain goes chronic.

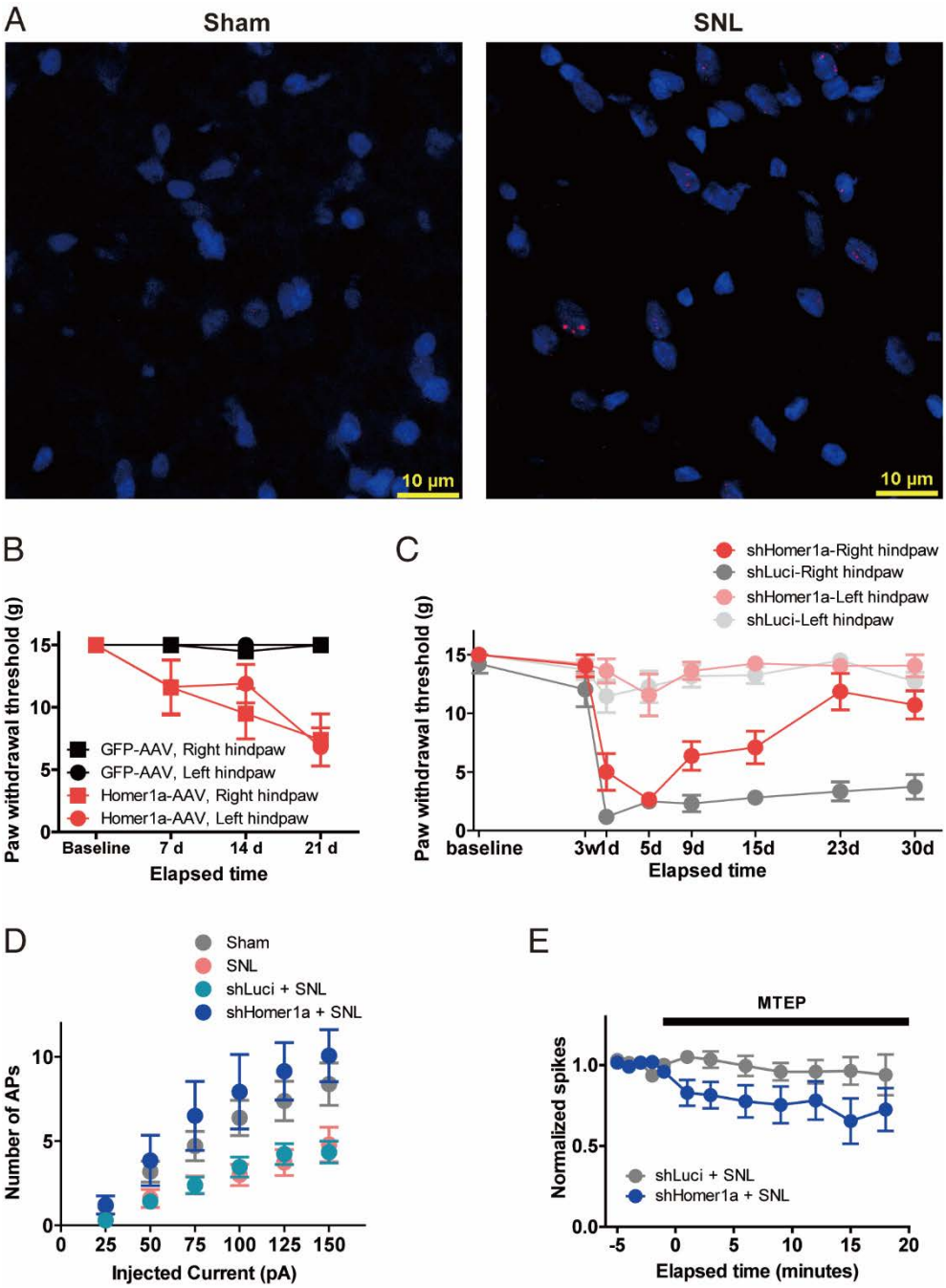
A
Sham
SNL
10 μm
10 μm
B
Paw withdrawal threshold (g)
GFP-AAV, Right hindpaw
GFP-AAV, Left hindpaw
Homer1a-AAV, Right hindpaw
Homer1a-AAV, Left hindpaw
Baseline
7 d
14 d
21 d
Elapsed time
C
shHomer1a-Right hindpaw
shLuci-Right hindpaw
shHomer1a-Left hindpaw
shLuci-Left hindpaw
Paw withdrawal threshold (g)
baseline
3w1d
5d
9d
15d
23d
30d
Elapsed time
D
Sham
SNL
shLuci + SNL
shHomer1a + SNL
Number of APs
Injected Current (pA)
E
MTEP
Normalized spikes
shLuci + SNL
shHomer1a + SNL
Elapsed time (minutes)

Figure 21. Identifying PAG neurons which project to the RVM (PAG-RVM projection neurons) and recording postsynaptic currents.

A. Homer1a is increased in the PAG of SNL rats.

B. Homer1a overexpression in the naïve rat PAG induces mechanical allodynia (n=6 each).

C. Homer1a knock-down in the PAG prevents chronic pain following SNL surgery (shHomer1a, n=8; shLuci, n=6).

D. Intrinsic excitability of PAG neuron is reduced in SNL group, which can be prevented by Homer1a knock-down prior to SNL surgery (Sham, n=21; SNL, n=15; shLuci + SNL, n=26; shHomer1a + SNL, n=14).

E. Homer1a knock-down prevents SNL-induced attenuation of MTEP effect (shLuci, n=9; shHomer1a, n=13).

Discussion

These findings primarily support the involvement of endogenous pain modulatory system in the pathophysiology of chronic neuropathic pain. In my FDG-PET scan, neuropathic pain rats showed lower activities of the PAG and RVM compared to control rats. It is noteworthy that these brain images contains information of conscious, resting-state brain activity, as rats were kept to be in a fully awake state in their home-cage and no external noxious stimulus was given during the uptake period of FDG. Thus, these data confirm that the basic state of the PAG-RVM system is maladjusted in the chronic neuropathic pain state, even in the condition without the external nociceptive stimulus.

I have identified that PAG-mGluR5 is persistently active in normal state and the activity is attenuated in neuropathic pain state. Although the persistent activity of mGluR5 has been reported from previous brain slice studies, the *in-vivo* physiological existence of such an activity has not been reported. In addition, persistent mGluR5 activity has been reported only from the condition of wash-out following agonist-induced activation in the brain slice. Thus, previous researchers have used the agonist of mGluR5 in baseline condition to activate it, assuming that mGluR5 is not in the active state in the normal condition. I used inverse-agonist (antagonist) in baseline condition to reveal that the mGluR5 is an active state already. Regarding the essential role of the mGluR5 in the plastic change of the nervous system, my approach has implications on the broad fields of neuroscience.

Persistent PAG-mGluR5 activity turned out to regulate the excitability of PAG neurons, which is consistent with the findings from previous agonist studies of other brain regions (D'Ascenzo et al., 2009; Davies et al., 1995; Ireland and Abraham, 2002; Sourdet et al., 2003; Young et al., 2008, 2013). Regarding the results from the occlusion experiments, I contend that decline of persistent PAG-mGluR5 activity

following peripheral nerve injury, and ensuing reduction of neuronal excitability, causes a hypofunction of PAG-RVM system and leads to dysfunction of pain modulation. Activation of PAG-mGluR5 in neuropathic pain animals cancels out mechanical allodynia and restores the alteration of the PAG-RVM activity, supporting the idea above. Furthermore, pain-related facilitation of activity in the OFC, IC, RSC, BG and thalamus was also reversed by pharmacological activation of the PAG-mGluR5, implying the causal relationship between down-regulation of pain modulatory system and altered pain perception in the brain.

Conversely, single-time pharmacological deactivation of PAG-mGluR5 in naïve animals induced long-lasting mechanical allodynia. These findings are of especial interest because, as yet, the emergence of chronic pain has been reported to be the consequence of the injury-induced peripheral and spinal change. The long-term potentiation (LTP) in the spinal cord, one of the most studied mechanisms of chronic pain, cannot explain the spread of pain sensation to distant body regions and mechanical allodynia typical for chronic pain (Ruscheweyh et al., 2011). In addition, the hyperalgesia induced by spinal LTP eventually decays after 6-9 days (Price and Inyang, 2015; Sandkühler and Gruber-Schoffnegger, 2012). My study fills the gap and presents a novel explanation for the prolonged amplification of nociception.

The functions of mGluR5 are regulated by intracellular interacting molecules. I found that the intracellular scaffolding protein Homer (Xiao et al., 1998) is involved in the initial deactivation of PAG-mGluR5 in the neuropathic pain condition. Homer proteins modulate mGluR5 coupling to intracellular effectors (Kammermeier and Worley, 2007) and are tightly connected to the constitutive activity of mGluRs (Ango et al., 2001). Homer1a, the short-form splice variant of Homer family, is activity-dependently expressed and acts as a dominant negative competitor for other long-form Homer proteins. Homer1a expression in the PAG neuron leads to the decline of the sustained activity of mGluR5, which results in the reduced neuronal

excitability. I propose this Homer1a upregulation in the PAG causes dysfunction of the endogenous pain modulatory system, which is responsible for the prolonged pain.

The molecular mechanisms underlying long-lasting characteristic of allodynia induced by one-time blockade of the PAG-mGluR5 in the naïve rat is unclear. A possible explanation is that once mGluR5 is deactivated in the PAG, specific conditions are required for re-acquisition of initial persistent activity (Young et al., 2008). Loss of interaction with other molecules due to a conformational change of the mGluR5 might be candidate mechanism (Schröder et al., 2009). Alternatively, suspension of PAG-mGluR5 activity may induce a long-lasting change of neuronal excitability or synaptic transmission in the brain network which is related to the PAG.

Recently, mGluR5 antagonists have emerged as promising candidates for the treatment of chronic pain. Regarding its dual roles in the pain processing and the prospect that the maladaptive coping of the PAG to pain sensation induces long-lasting pain, I concern that the systemic treatment of mGluR5 antagonists might induce paradoxical chronic pain via decline of the PAG activity. Development of peripheral mGluR5 antagonist which is unable to penetrate blood-brain barrier might be required to prevent possible side effects. I suggest that although mGluR5 antagonists have beneficial clinical effects, care should be taken for its use in the treatment of other neurological disorders.

Table 5. Brain regions with significant differences between sham and SNL rats. The images of PAG-vehicle condition were used (voxel-by-voxel two-sample t-test, $p < 0.001$, $K_e > 20$). The peak voxel location is represented by the distance from the bregma (mm).

Table 5-1.
SNL-vehicle < Sham-vehicle

Brain region	K_e	T	Z	p level	Location (mm)		
					ML	AP	DV
Periaqueductal gray	205	4.83	3.78	<0.001	0.4	-6.2	-5.6
Rostral ventromedial medulla	24	4.54	3.62	<0.001	0.6	-9.4	-10.2
Secondary visual cortex	102	4.10	3.37	<0.001	-2.2	-5.2	-1.4

Table 5-2.
SNL-vehicle > Sham-vehicle

Brain region	K_e	T	Z	p level	Location (mm)		
					ML	AP	DV
Orbitofrontal cortex	188	5.06	3.90	<0.001	-1.4	4.6	-4.8
		4.40	3.54	<0.001	-0.4	5.4	-5.6
Insular cortex	48	4.79	3.76	<0.001	-4.6	2.2	-5.6
Retrosplenial cortex	55	4.38	3.53	<0.001	0	-1.8	-2.2
Basal ganglia	22	4.21	3.43	<0.001	-2.4	-2.4	-8.0
Thalamus	31	4.04	3.33	<0.001	3.0	-3.0	-6.6

Table 6. Brain regions with significant differences between vehicle and DHPG condition in sham group rats (voxel-by-voxel paired t-test, $p < 0.001$, $K_e > 20$).
*The cluster which includes the PAG region. **The cluster adjacent to the RVM region. However, the cluster does not include the RVM even at a more relaxed threshold of $p < 0.005$

Table 6-1.
Sham-vehicle < Sham-DHPG

Brain region	K_e	T	Z	Location (mm)		
				ML	AP	DV
Retrosplenial cortex	*2085	19.42	5.17	0	-5.6	-2.8
Cerebellum (lobule 3)		10.04	4.26	-0.8	-9.4	-4.6
Anterior pretectal nucleus		8.49	4.00	-2.4	-5	-6
Retrosplenial cortex	24	6.52	3.59	-2.8	-9	-3.2
		5.74	3.39	-3.6	-9.4	-2.6
Retrosplenial cortex	22	5.56	3.34	1.6	-7.6	-2.2
Cerebellum (lobule 7)	25	6.95	3.69	-0.4	-12.8	-3.6
		5.27	3.25	-0.8	-13.6	-4.2
Cerebellum (lobule 9)	21	6.26	3.53	0	-13.2	-6
Cerebellum (paraflocculus)	58	9.41	4.16	-5.6	-11.4	-6.6
Thalamus	56	9.09	4.11	1	-2	-5.6
		6.12	3.49	0.4	-2.6	-5.4
Thalamus and hypothalamus	236	8.21	3.95	0.2	-2.8	-7.6
		7.42	3.80	-0.8	-3	-8.6
		6.64	3.62	0.2	-2	-7.2
Prelimbic cortex	98	11.15	4.41	0.6	2.6	-3.4
Superior colliculus	41	11.11	4.40	2.6	-6.4	-4.8
Subthalamic nucleus	34	10.47	4.32	-2.2	-4	-8.6
Pons (reticulotegmental nucleus)	**32	7.90	3.89	-0.6	-8.8	-9.8

Table 6-2.
Sham-vehicle > Sham-DHPG

Brain region	K_e	T	Z	Location (mm)		
				ML	AP	DV
Primary somatosensory cortex	335	18.18	5.08	4.8	-2.2	-4.8
Primary somatosensory cortex	463	10.11	4.27	5.2	1.4	-4.4
Secondary somatosensory cortex		8.44	3.99	6.4	-0.2	-4.6
Insular cortex		9.86	4.23	4.6	1.8	-5.8
Insular cortex	76	6.66	3.63	5.4	-1	-7.6
Primary somatosensory cortex	21	6.64	3.62	-4.8	-1.2	-4.6
Primary somatosensory cortex	128	6.84	3.67	-4.4	1	-4.4
		6.76	3.65	-4.8	1.6	-5.2
Primary somatosensory cortex	202	7.22	3.75	-5.6	0.4	-3
Secondary somatosensory cortex		8.91	4.08	-7	-0.8	-5
		8.44	3.99	-6.8	0	-5.6
Secondary somatosensory cortex	24	6.81	3.66	-7	-3.8	-4
Insular cortex	142	12.49	4.57	-3.8	4.2	-5.6
		7.61	3.84	-4.6	3.4	-5
		7.09	3.73	-3.8	4.4	-4.4
Insular cortex	193	11.16	4.41	-5.4	1.4	-7.8
		9.80	4.22	-5.8	1	-7
Reticular nucleus	32	8.42	3.99	2.4	-11.8	-9.6
Reticular nucleus	52	7.45	3.80	-2.8	-11.4	-9.4
Cerebellum (Simple lobule and Crus1)	70	12.72	4.60	3.6	-11.6	-3.8
		6.86	3.67	2.8	-11.4	-4.8

Table 7. Brain regions with significant differences between vehicle and DHPG condition in SNL group rats (voxel-by-voxel paired t-test, $p < 0.001$, $K_e > 20$).
*The cluster which includes the PAG region. **The cluster which includes the RVM region. The result with the threshold of $p < 0.005$ includes a larger cluster of the RVM.

Table 7-1.
SNL-vehicle < SNL-DHPG

Brain region	K_e	T	Z	Location (mm)		
				ML	AP	DV
Hippocampus	*1663	11.14	4.41	0	-4.2	-3.4
Cerebellum (lobule 2)		10.88	4.37	-1	-10.2	-6
		8.09	3.93	0.8	-9.4	-5.6
Retrosplenial cortex	35	6.54	3.60	-1.8	-7.2	-1.8
		5.06	3.18	-1.4	-6.2	-1
Cerebellum (lobule 8)	90	14.84	4.81	-0.2	-12.2	-4.6
Hypothalamus	61	7.11	3.73	-1.8	-2.8	-8.8
		5.13	3.20	-1	-3.6	-9
Hippocampus and piriform cortex	42	5.57	3.34	-4.4	-4.8	-8.4
Entorhinal cortex	84	8.90	4.08	6.6	-7.4	-8
Secondary visual cortex	71	8.48	4.00	-4.8	-8.4	-2.2
Superior colliculus	236	7.23	3.75	2.2	-5.8	-4.2
		5.66	3.36	2.2	-7	-5
Pedunculopontine tegmental nucleus	42	6.32	3.54	-2.2	-7.4	-7.8
Pons (reticulotegmental nucleus)	**20	6.92	3.69	-0.2	-9	-9.8

Table 7-2.
SNL-vehicle > SNL-DHPG

Brain region	K_e	T	Z	Location (mm)		
				ML	AP	DV
Thalamus (VPL)	251	8.45	4.00	-6.6	-3	-3.4
Primary somatosensory cortex		7.12	3.73	-6.6	-1.4	-3.6
Auditory cortex		6.83	3.67	-7.2	-4.2	-4.2
Primary somatosensory cortex	128	8.84	4.07	-5.6	0.6	-3.8
Primary somatosensory cortex	156	6.66	3.63	-5.2	-1	-4.4
Caudate putamen		5.88	3.43	-4.4	-0.2	-5.2
Secondary somatosensory cortex		5.64	3.36	-4.8	0.6	-5.4
Secondary somatosensory cortex	45	7.54	3.82	-5.2	-2	-6.2
Primary somatosensory cortex	390	7.83	3.88	4.2	2.6	-4.4
		7.83	3.88	5	3	-4.4
		5.03	3.17	5.6	2	-5.6
Primary somatosensory cortex	29	6.66	3.62	6	-0.6	-3.2
Piriform cortex	22	5.89	3.43	-6.8	-4.6	-8.8
		5.40	3.29	-6.2	-3.4	-9.4
Piriform cortex	152	8.20	3.95	-5	-1.6	-10
		5.65	3.36	-4.8	0.6	-9.2
Piriform cortex	24	10.21	4.28	-3.4	1.6	-7.8
Piriform cortex	260	6.51	3.59	-4.2	2.6	-8
Orbital cortex		8.94	4.08	-3.2	5.2	-4.2
Insular cortex		8.65	4.03	-3.8	4	-6
Piriform cortex	547	8.77	4.05	5	1	-8.4
		7.93	3.90	4	1.4	-8
		7.15	3.74	3.8	2	-7.4
Piriform cortex	38	8.38	3.98	6	-2.6	-9.4
Insular cortex	34	5.67	3.37	-4.6	2.4	-5.6
Insular cortex	110	6.33	3.54	3.8	4	-5.6
Primary motor cortex	69	19.11	5.15	-2.4	3.2	-3
Parvicellular reticular nucleus	42	7.98	3.91	-2.2	-11	-8.8
Prelimbic cortex	118	7.17	3.74	1.6	3	-3.6
Corpus callosum (forceps minor)		6.54	3.60	1.6	4.4	-4
Corpus callosum (forceps minor)		5.30	3.26	1.4	3.6	-4.2
Corpus callosum (forceps minor)	27	6.93	3.69	-2.2	4.4	-4
Auditory cortex	237	20.01	5.20	7.2	-4.6	-4.6
Temporal association cortex		8.78	4.06	7.2	-4.6	-6.2
Ectorhinal cortex		8.23	3.96	7	-7	-6
Olfactory tubercle	27	16.16	4.92	2.6	1.2	-10
Hippocampus	23	6.44	3.57	4.2	-4.2	-3.6
Caudate putamen	20	6.07	3.48	3.6	0	-3.6

Chapter 4.

Sustained activity of metabotropic glutamate receptor: Homer, arrestin, and beyond

Summary

When activated, metabotropic glutamate receptors (mGluRs) exert long-lasting changes within the glutamatergic synapses. One mechanism is a tonic effect of downstream signal transduction pathways via sustained activation of mGluR itself. Like many other G-protein coupled receptors (GPCRs), mGluR can exist in a constitutively active state, which persists agonist-independently. In this chapter, I review the current knowledge of the mechanisms underlying the constitutive activity of group I mGluRs. The issues concerning Homer1a mechanism in the constitutive activity of group I mGluRs and recent findings regarding the significant role of β-arrestin in sustained GPCR activity are also discussed. I propose that once in a state of sustained activation, the mGluR persistently activates downstream signaling pathways, including various adaptor proteins and kinases, such as β-arrestin and mitogen-activated protein kinases. In turn, these effector molecules bind to or phosphorylate the mGluR C-terminal binding domains and consequently regulate the activation state of the mGluR.

Introduction

Efficient transmission of information in the nervous system is mediated by various neurotransmitters and neuromodulators. Glutamate, the most abundant neurotransmitter in the nervous system, acts as an excitatory signal in the synapses and plays a key role in the regulation of neuronal activity. In the synaptic loci, glutamate released from presynaptic vesicles binds to postsynaptic glutamate receptors, and synaptic activation of the postsynaptic ionotropic glutamate receptors, such as N-methyl-D-aspartate (NMDA) and α-amino-3-hydroxy-5-methyl-4-isoxazolepropionic acid (AMPA) receptors, directly contributes to the generation of action potentials in the postsynaptic neurons. Activation of the metabotropic glutamate receptor (mGlu), on the other hand, exerts indirect long-lasting influences throughout the neuron, primarily via the activation of heterotrimeric G proteins (Gladding et al., 2009; Lüscher and Huber, 2010; Willard and Koochekpour, 2013).

Based on intracellular signaling pathways, the eight subtypes of mGluRs can be classified into three subgroups (I, II, and III). Among the eight mGluR subtypes, the most extensively studied mGluRs are mGluR1 and mGluR5, which constitute group I mGluRs (Piers et al., 2012; Wang and Zhuo, 2012). The activation of group I mGluRs stimulates phospholipase C (PLC) β, resulting in activation of a diacylglycerol (DAG)-mediated protein kinase C (PKC) pathway, and exerts calcium response by facilitating the opening of plasma membrane calcium channels and the release of inositol triphosphate (IP_3)-mediated calcium from the intracellular calcium stores (Niswender and Conn, 2010). The intracellular signaling cascades activated by group I mGluRs play an essential role in the plasticity of neuronal excitability (Niswender and Conn, 2010). This is achieved by endocannabinoid-mediated suppression of presynaptic vesicle release probability, modulation of the receptor and channel availability in the postsynaptic neuronal membrane, and alteration in the

transcription of genes related to various regulatory signaling molecules (Wang and Zhuo, 2012).

Akin to many other GPCRs (Corder et al., 2013; Gilliland et al., 2013; Meye et al., 2014; Thomsen et al., 2016), mGluRs exist in a state of equilibrium between being active or inactive, regardless of agonist binding (Ango et al., 2001; Fagni et al., 2003; Panaccione et al., 2013). As such, mGluRs can show sustained activity under certain circumstances. The persistence of mGluR activity after agonist washout as well as the constitutive mGluR activity independent of agonist binding have been reported in previous studies (Ango et al., 2001; Young et al., 2008, 2013). The sustained cellular effects of mGluR activation are mediated by downstream effectors, including G proteins or β-arrestins, and play a critical role in modulating neuronal plasticity (Eng et al., 2016; Newell and Matosin, 2014; Niswender and Conn, 2010; Stoppel et al., 2017). Further, previous studies have reported that the persistent effect of mGluR activation is involved in physiological function and pathological dysfunction of the nervous system (Bianchi et al., 2009; Fagni et al., 2003; Young et al., 2013).

In this chapter, I will focus on the sustained activity of group I mGluR signaling and intracellular mechanisms underlying the persistent effect of receptor activation. I will review current knowledge regarding the significant role of the intracellular scaffold, Homer1a, in constitutive activity of group I mGluRs. Further, I will discuss recent findings of β-arrestin function in sustained G protein activity in the intracellular GPCRs, addressing its possible relevance to the persistently active mGluR signaling. I conclude with a discussion of intracellular mGluR function and the suspected role of downstream mitogen-activated protein kinase (MAPK) signaling in the maintenance of sustained mGluR activity.

Main

Persistent action of the mGluRs following activation

The persistent activation is a common phenomenon among GPCRs (Cahill et al., 2017; Ritter and Hall, 2009; Thomsen et al., 2016). Sustained G protein signaling after agonist washout has been reported for many GPCRs. This long-lasting action can be derived from the persistent effect of downstream cascades following agonist binding to the receptor, and/or agonist-independent persistent activation of the receptor itself. Previous studies have shown that the activation of mGluR downstream cascades exerts long-lasting influences on glutamatergic synaptic transmission, and persistent changes in synaptic efficacy elicited by mGluR activation are reversibly suppressed by mGluR antagonists (Lodge et al., 2013). For instance, a long-term depression (LTD) can be induced by the stimulation of group I mGluR using the agonist, 3,5-dihydroxyphenylglycine (DHPG), in hippocampal neurons. This group I mGluR-mediated LTD is fully or partially reversed by the application of the mGluR antagonists, such as α-methyl-4-carboxyphenylglycine (MCPG), 2-amino-2-(3-cis and trans-carboxycyclobutyl-3-(9-thioxanthyl)propionic acid (LY393053), α-amino-4-carboxy-2-methylbenzeneacetic acid (LY367385), or 2-methyl-6-(phenylethynyl)-pyridine hydrochloride (MPEP). The phenomenon is not specific to the group I mGluR. The group II and group III mGluR-mediated LTD is also reversed by representative antagonists (Lodge et al., 2013). These findings raise the possibility that prolonged alteration in neuronal activity induced by group I mGluR activation is mediated by the persistent activity of the mGluRs themselves (Young et al., 2013). This suggested role of persistent activation can lead to modulation of neuronal activity in the physiological as well as pathological state (Panaccione et al., 2013; Tronson et al., 2010; Young et al., 2013).

The necessary condition for this persistent activity might differ based on the

neuronal state and mGluR subtypes. In the case of the mGluR5 in CA3 hippocampal neurons, DHPG application at a sufficiently high temperature (30–31 °C) for a sufficient period of time (> 30 min) is necessary for the manifestation of persistent activation (Young et al., 2008). Under this condition, neuronal excitability was altered because of a change in state of the potassium channels, and therefore, persistent suppression of afterhyperpolarization (AHP), which is mediated by a p38 MAPK- and protein synthesis-dependent signaling pathway. The necessary condition (high temperature) in this case implicates that temperature-sensitive enzymes and/or ion channels might be involved in this mGluR5-mediated persistent AHP suppression (Frank, 2016; Talavera et al., 2008; Wang et al., 2014; Young et al., 2008). In the case of the mGluR1, the ion channel was transiently affected but the persistent change of state was not elicited by the same stimulation (Young et al., 2008). Interestingly, another study has reported the persistent CA3 neuronal responses to the group I mGluR agonist DHPG were reversed by mGluR1 antagonist LY367385 or (hydroxyimino)cyclopropa[b]chromen-1a-carboxylate ethyl ester (CPCCOEt), and to a lesser extent by the mGluR5 antagonist MPEP, indicating that the mGluR1 is primarily involved (Young et al., 2013). In spite of the inconsistency, these studies commonly implicate the persistent activity and functional relevance of group I mGluR to long-lasting changes in neuronal activity.

Constitutive, agonist-independent activity of mGluRs

Many GPCRs exhibit agonist-independent activity. Although the exact mechanisms underlying the sustained signaling of GPCRs have not been fully understood, many investigations on the phenomenon have revealed that constitutive activity is an intrinsic feature of GPCRs (Corder et al., 2013; Gilliland et al., 2013; Meye et al., 2014; Thomsen et al., 2016). The sustained activation of GPCRs can be modulated

by signaling molecules, as well as endogenous ligands, and plays a significant role in maintaining both physiological and pathological state.

Group I mGluRs have been reported to show constitutive activity (Fagni et al., 2003; Panaccione et al., 2013; Ronesi et al., 2012; Tronson et al., 2010). As a GPCR, the mGluR also has intracellular domains that can interact with numerous kinases, phosphatases, and proteins. These molecules modulate the action of the receptors and many of them are shared by other GPCRs signaling pathways. Constitutive activity of mGluRs can result from changes in receptor conformation induced by these interacting molecules. Previous studies showed that mutation of specific allosteric binding domain residues results in conformational changes and modulates the constitutive activity of mGluRs (Malherbe et al., 2003; Yanagawa et al., 2009). Recently it has been revealed that the constitutive activity of group I mGluRs can be modulated by mGluRs coupling to specific intracellular interacting molecules, such as the Homer family of scaffold proteins (Ango et al., 2001; Fagni et al., 2003).

Involvement of Homer proteins in the mGluRs constitutive activity

In the case of mGluR, the involvement of the Homer family of intracellular proteins is the most studied mechanism of the constitutive activity. Homer proteins are intracellular scaffolding proteins that interact with various membrane receptors including mGluRs (Shiraishi-Yamaguchi and Furuichi, 2007; Xiao et al., 1998, 2000). With the conserved Ena/VASP Homology (EVH) 1 domain, Homer proteins bind to the C-terminal PPXXF motif of receptors and act as a scaffold for various intracellular effector interactions. The Homer family comprises of many alternative splicing variants from three Homer genes and these multiple isoforms can be categorized into either long-form or short-form Homer proteins. The long-form Homer proteins (Homer 1b, 1c, 2, and 3) have a coiled-coil domain and form dimers

with other intracellular effectors. The short-form Homer protein (Homer 1a), in contrast, only has an EVH1 domain and lacks a coiled-coil domain. Homer1a acts as a dominant negative competitor for other long-form Homer proteins by binding to the receptors and disrupting intracellular signaling. The Homer1a is expressed in an activity-dependent manner, whereas other long-form Homer proteins are constitutively expressed. Homer1a is believed to counteract the hyperexcitability of neurons and thus play a key role in endogenous neuroprotection (Brakeman et al., 1997; Sakagami et al., 2005; Shiraishi-Yamaguchi and Furuichi, 2007; Wang et al., 2015c; Yamamoto et al., 2005).

Other than such a homeostatic regulatory role, Homer1a is also involved in the constitutive activation of the mGluR (Ango et al., 2001; Fagni et al., 2003). As a dominant negative competitor for other long-form Homer proteins binding to the mGluR, Homer1a disrupts mGluR-Homer3 interaction when expressed. Because the Homer3 is constitutively expressed and acts as a negative regulator of mGluR constitutive activity via stabilization of the receptor, disruption of mGluR-Homer3 binding by Homer1a induction results in the development of neuronal conditions for mGluRs constitutive activation (Fagni et al., 2003).

Although the involvement of Homer1a in the constitutive activity of mGluR is widely accepted, this concept does not clarify the basal mechanisms underlying constitutive activation of mGluR. The Homer1a mechanism for the induction of constitutive activity depends on its dominant-negative effect on mGluR-Homer3 binding. The study of the Homer1a-mediated constitutive activity of mGluR was performed in the cerebellum, where basal Homer3 expression is known to be high (Ango et al., 2001). As the expression of Homer3 differs depending on the brain regions and neuronal subtypes, it is speculated that the induction of constitutive mGluR activity by Homer1a might be inconsistent depending on the cellular

condition. If Homer3 binding stabilizes mGluR and blocks the constitutive activation of the receptor, and Homer1a induces mGluR constitutive activity by disrupting mGluR-Homer3 binding, it is not appropriate to state that Homer1a is a necessary condition for the constitutive activity of mGluR. Thus, in the neuronal condition where Homer3 is absent, the mGluR constitutive activity might be conserved even without the presence of Homer1a. Rather, regarding the original Homer1a action of disrupting the binding of the mGluR to various interacting molecules, Homer1a would prevent the activation of certain intracellular pathways downstream in the mGluR signaling pathway. For instance, the disruption of mGluR interaction with Homer1b/c or Homer2 would affect calcium signaling and MAPK phosphorylations (Mao et al., 2005; Worley et al., 2007; Yang et al., 2004). The degree of interruption in the mGluRs downstream pathways by Homer proteins varies among different neurons and on the composition of the signaling pathways (Worley et al., 2007). In that, the expression of Homer1a can decrease (Minami et al., 2003; Tappe et al., 2006; Tu et al., 1998) as well as increase (Abe et al., 2003; Ango et al., 2001; Minami et al., 2003) the rise in calcium levels in response to mGluR stimulation, depending on the neuronal subtype (Worley et al., 2007). Furthermore, the stimulation of mGluRs activates several downstream pathways (Hu et al., 2012; Stoppel et al., 2017), and Homer binding to mGluR does not uniformly activate or deactivate all these pathways (Hu et al., 2012). Therefore, the functional effect of Homer on the sustained downstream activation of the mGluR might be pathway specific.

The role of the β-arrestin pathway

I speculate that β-arrestin might be involved in the modulation of mGluR activity. In the classical view, β-arrestin had been regarded as a terminator of GPCR activity. According to this classical concept, agonist activation of the surface GPCR leads to

GPCR kinases (GRKs)-induced phosphorylation of the receptor, followed by β-arrestin binding, and the binding of β-arrestin to the receptor results in desensitization and internalization of the receptor (Ritter and Hall, 2009). However, it is now clear that the action of β-arrestin is not limited to the desensitization or internalization of the receptor (Crépieux et al., 2017). β-arrestin acts as an adaptor or a scaffold, and its binding to the GPCR can activate signaling pathways independent of the G protein, to induce cellular change (Magalhaes et al., 2012; Peterson and Luttrell, 2017). β-arrestin interacts with most of the GPCRs including mGluRs (Eng et al., 2016; Stoppel et al., 2017). A recent study showed that the β-arrestin-induced G protein-independent signaling pathways of group I mGluR play a significant role in LTP and LTD in hippocampal neurons, and the involved pathways differ between CA1 neurons and CA3 neurons (Eng et al., 2016). The authors of the study found that genetic ablation of β-arrestin2 results in deficits in LTD mediated by mGluR1 in CA3 neurons and by mGluR5 in CA1 neurons. They also have reported that the β-arrestin2 knock-out mice have a deficiency in long-term potentiation (LTP) induced by low-frequency, paired stimulation of mossy fiber inputs to CA3 pyramidal neurons (Eng et al., 2015), but not in LTP induced by high-frequency stimulation (Eng et al., 2016). An early study of CA3 pyramidal neurons revealed that NMDA receptor potentiation by mGluR5 is mediated by a G protein-dependent pathway, whereas potentiation by mGluR1 is mediated by a G protein-independent pathway (Benquet et al., 2002). The study demonstrated that the DHPG application could induce LTP under conditions of G-protein blockade using GDPβS. This DHPG-LTP was blocked by the Src inhibitor. The authors discussed that the β-arrestin-mediated recruitment of Src kinase underlies the G-protein-independent action of mGluR1 (Benquet et al., 2002; Gerber et al., 2007). Therefore, I can speculate that the β-arrestin downstream pathways of mGluR might be in an active state even under circumstances in which mGluR ceased its G protein-dependent

pathways.

In addition to the activation of G protein-independent signaling pathways, the coupling of β-arrestin to mGluRs might determine the activity status of the receptors. According to previous studies, GPCRs with weak coupling to β-arrestin (Class A GPCRs) interact transiently with β-arrestin due to relatively low affinity and thus, are recycled back to the plasma membrane shortly after endocytosis. GPCRs with stronger binding affinity to β-arrestin (Class B GPCRs), on the other hands, show stable coupling and thus, have been thought to experience endosomal degradation following β-arrestin-induced endocytosis (Cahill et al., 2017; Thomsen et al., 2016). Recent studies, however, have challenged this classical concept of β-arrestin-mediated cessation of GPCR activity. According to the studies, the binding of β-arrestin to GPCRs results in the sustained activity of the G protein, mainly in the internalized GPCRs (Gilliland et al., 2013; Thomsen et al., 2016). In this new concept, β-arrestin and the G protein can bind simultaneously to the GPCR. This is achieved by β-arrestin binding to the C terminus and the G protein binding to the transmembrane core of the receptor (Thomsen et al., 2016). The binding of β-arrestin to the C-terminal tail mediates receptor internalization and intracellular signaling, but does not induce desensitization of G protein signaling (Cahill et al., 2017; Gilliland et al., 2013; Thomsen et al., 2016). Thus, the high affinity of the C-terminal tail of the class B GPCRs to β-arrestin allows for the condition in which the G protein couples with the transmembrane core and simultaneously, β-arrestin couples with the C-terminal, which results in internalization of the receptor by β-arrestin and conserved G-protein signaling in the internalized receptor (Cahill et al., 2017; Thomsen et al., 2016). Consequently, the simultaneous activation of G protein-dependent and independent signaling pathways can occur in the internalized GPCR (Thomsen et al., 2016). Although the interaction status of the transmembrane core and C-terminal tail to the G protein and β-arrestin in active mGluR is unclear, β-

arrestin-mediated sustained signaling in the internalized GPCRs suggests a feasible mechanism for the constitutive activity (Fig. 22).

β-arrestin is also critically involved in modulating the plasticity of glutamatergic synaptic transmission (Eng et al., 2016; Stoppel et al., 2017). A recent study showed that the β-arrestin pathway is required for a certain type of group I mGluR-mediated plasticity, which involves the extracellular signal-regulated kinase (ERK) pathway and is mediated by mGluR1 in the CA1 neurons and mGluR5 in the CA3 neurons (Eng et al., 2016). I speculate that β-arrestin is further involved in the constitutive activity of the mGluRs.

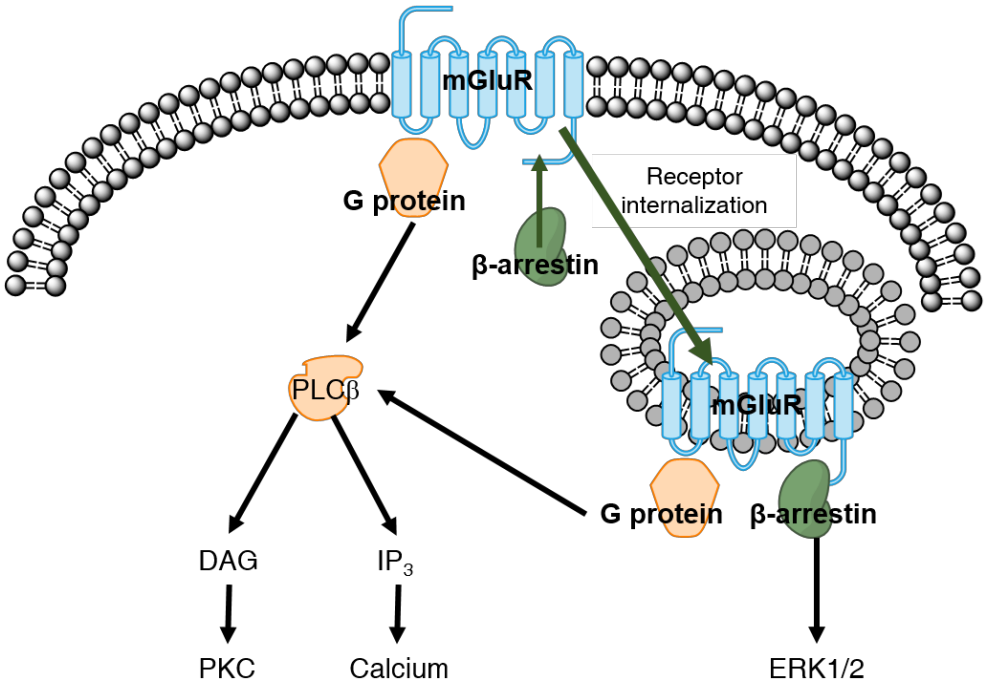

Fig. 22. Proposed model of sustained mGluR activation. β-arrestin binding to the mGluR internalizes the receptor. With stable binding to the mGluR C-terminal, β-arrestin mediates receptor internalization and activates ERK1/2 MAPK, but does not induce desensitization of G protein signaling. In this condition, the β-arrestin tightly binds only to the C-terminal tail but not to the transmembrane region, and thus the G protein can simultaneously bind to the transmembrane core of the receptor. The downstream pathways are activated without interfering with each other. The convergence of the downstream pathways on common effectors and their reciprocal interactions are omitted in this figure.

Involvement of intracellular mGluR5

Recently revealed intracellular activity of mGluR5 supports the idea above. According to the studies, more than 60% of mGluR5 are located in the intracellular site (Hubert et al., 2001; Vincent et al., 2016), and activation of the intracellular mGluR5 leads to sustained cytosolic calcium responses (Jong et al., 2009; Kumar et al., 2012; Purgert et al., 2014; Vincent et al., 2016). Regarding the β-arrestin-mediated sustained activity of GPCR that takes place with receptor internalization, the high composition ratio of intracellular mGluR5 inspires the idea that the intracellular mGluR5 activity is correlated with β-arrestin binding and sustained receptor signaling.

This intracellular mGluR5 activity plays a significant role in maintaining physiological and pathological plasticity during hippocampal LTD (Purgert et al., 2014) and nerve injury-induced hyperexcitability of spinal neurons (Vincent et al., 2016). Interestingly, the signaling cascades induced by intracellular mGluR5 activation is distinct from the downstream signaling of mGluR5 in the plasma surface membrane (Jong et al., 2009; Kumar et al., 2012). Only intracellular mGluR5, not surface membrane mGluR5, cause ERK1/2 phosphorylation. This was demonstrated by the upregulation of ERK1/2 phosphorylation in response to the treatment of membrane-permeable agonist, quisqualate, in the presence of impermeable, nontransported antagonist, LY393053. The quisqualate-mediated upregulation of ERK1/2 phosphorylation could be blocked by the membrane-permeable antagonist MPEP. Conversely, the impermeable, nontransported agonist, DHPG, could not induce an increase in ERK1/2 phosphorylation. Similar discrepancies regarding ERK1/2 activation have been shown in a recent study of the β-arrestin-dependent downstream signaling pathway of mGluR5 activation (Stoppel et al., 2017).

ERK1/2 MAPK pathway

In the signaling cascades of many GPCRs, G protein and β-arrestin-mediated pathways share common downstream effectors of ERK1/2 MAPK (Cassier et al., 2017; Eishingdrelo and Kongsamut, 2013; Zimmerman et al., 2011). The binding of β-arrestin to activated GPCRs contributes to ERK1/2 phosphorylation, and sustained phosphorylation of ERK1/2 promotes GPCR internalization and constitutive signaling (Beautrait et al., 2017; Cassier et al., 2017; Eishingdrelo and Kongsamut, 2013; Khoury et al., 2014; Lin et al., 1999; Paradis et al., 2015). In the case of the mGluR1/5, agonist stimulation of the receptor results in ERK1/2 phosphorylation, which plays a significant role in the synapse (Gallagher et al., 2004; Kelleher et al., 2004; Sweatt, 2004). This ERK1/2 activation is unaffected or only partially affected by inhibitors of PLC (Mao et al., 2005), which is a downstream effector of the G protein-mediated pathway (Peterson and Luttrell, 2017). Recent studies showed that mGluR5-mediated ERK1/2 activation was completely blocked by genetic reduction of β-arrestin2 (Eng et al., 2016; Stoppel et al., 2017). This suggests that the mGluR5-mediated ERK1/2 activation is β-arrestin pathway-dependent but not G-protein pathway-dependent (Stoppel et al., 2017). As discussed above, this biased involvement for the phosphorylation of ERK1/2 is a shared characteristic in studies of intracellular mGluR5 activation and mGluR5-mediated β-arrestin signaling pathway.

Interestingly, activated ERK, in turn, regulates the binding of β-arrestin and Homer proteins to the receptor. The actions of β-arrestin on the GPCRs are regulated by an ERK-mediated feedback mechanism, as activated ERK preferentially phosphorylates receptor-bound β-arrestin (Coffa et al., 2011; Luttrell et al., 2001; Peterson and Luttrell, 2017) and regulate its function (Lin et al., 1999). Furthermore,

activated ERK1/2 phosphorylates the serine-proline motif of mGluR1 and mGluR5, and the phosphorylation sites include the Homer binding site of mGluRs C-terminal (Hu et al., 2012; Mao and Wang, 2016). Thus, it is likely that once the β-arrestin pathway of intracellular mGluR is sufficiently activated, subsequent ERK activation would affect receptor coupling to β-arrestin and Homer proteins, and eventually modulate the downstream signaling of mGluRs (Fig. 23). Whether the ERK-induced phosphorylation of Homer binding site of mGluR results in activation or deactivation of mGluR signaling might be case specific, as Homer modulation of mGluR signaling would differ based on neuronal conditions (Mao and Wang, 2016; Worley et al., 2007). I propose that, under certain circumstances, binding of Homer and β-arrestin to the receptor adjusted by kinase phosphorylation would lead to sustained activation of the mGluR.

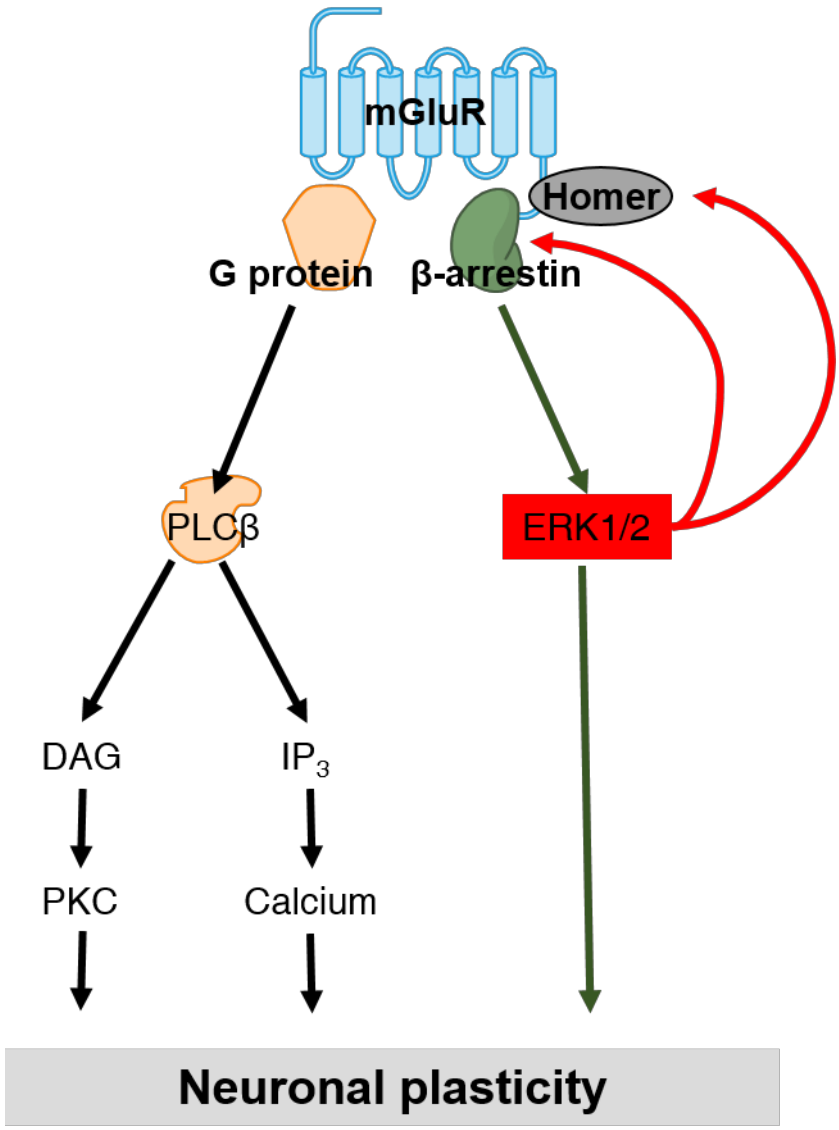

Fig. 23. Feedback modulation of mGluR activity by ERK1/2. Stable binding of β-arrestin to the receptor upregulates ERK1/2 activation, whereas transient binding β-arrestin downregulates it. The activated ERK1/2 preferentially phosphorylates receptor-bound β-arrestin and regulates its function. In addition, the activated ERK1/2 phosphorylates the Homer binding site of mGluRs C-terminal. These feedback mechanisms might play a role in keeping the mGluR persistently active.

Regulation of the interactions

The coupling of the Homer proteins to the receptor is affected by phosphorylation of the binding sites. In group I mGluR, the proline-directed kinases, such as ERK1/2 and cyclin-dependent kinase (CDK) 5, phosphorylate group I mGluR at the Homer binding site, and control the downstream signaling pathways (Hu et al., 2012; Orlando et al., 2009). A multi-domain scaffolding protein called Preso1 binds these proline-directed kinases and regulates Homer-mGluR binding (Hu et al., 2012). Furthermore, expression of Homer1a after the induction of LTP in neurons present in the hippocampal dentate gyrus requires the ERK1/2 cascade (Rosenblum et al., 2002). As such, the interaction between kinases and proteins plays an important role in regulating the expression of Homer proteins and their interaction with mGluRs. Since the Preso1-mediated regulation of Homer binding does not influence the surface expression of mGluRs (Hu et al., 2012), it is unlikely that the downstream activation of the Homer-mediated mGluR directly recruits β-arrestin. Rather, it is speculated that the Homer-mediated and the β-arrestin-mediated pathways affect each other by the phosphorylation of the receptor and each protein. Importantly, the proline-directed kinases, which mediate mGluR phosphorylation at the Homer binding site can be activated by numerous signaling pathways, and are not specific to the receptor. This suggests the possibility of receptor crosstalk (Hu et al., 2012) and interaction with β-arrestin signaling. The binding of β-arrestin to the mGluRs critically affects ERK1/2 activation via Raf signaling and protein synthesis following receptor activation. In return, β-arrestin signaling is affected by the ERK-mediated feedback control (Lin et al., 1999). Interestingly, β-arrestin has two different modes of action in the regulation of ERK. A recent study of M_1 muscarinic acetylcholine receptors revealed the bidirectional control of ERK by β-arrestin binding to the receptor, showing that the stable binding of the β-arrestin upregulates ERK1/2 expression, whereas transient binding downregulates it (Jung et al., 2017). Although

details regarding β-arrestin binding to the mGluRs during receptor activation are still unclear, this raises the prospect that the sustained activity of the mGluR is regulated by the functional interaction between Homer proteins and β-arrestin, which is balanced by ERK.

Effects of the interactions

Proteins responsible for long-term expression of synaptic plasticity are rapidly translated in response to mGluR activation. Disrupted regulation, as well as excessive protein synthesis, can result in neuronal disorders (Osterweil et al., 2010). Regarding the role that activated ERK1/2 plays in the regulation of gene expression, the signaling cascades involved in ERK activation would directly affect mGluR-mediated protein synthesis.

Although the binding of Homer1a to the group I mGluR leads to constitutive activation in certain circumstances (Ango et al., 2001), the consequence is manifested by the G protein-dependent downstream cascades, and not the ERK activation cascade. I speculate that the constitutive downstream activation of the G protein cascades is just one of the many possible consequences of Homer1a binding to mGluR. This view is supported by the effects of Homer proteins and β-arrestin on the Ras-mediated activation of the ERK1/2. The Ras protein transduces signals from activated GPCRs to the cytoplasm and nucleus and contributes to the induction of various effector molecules, including MAPKs (Ryu and Lee, 2016). In many GPCRs, the Ras-dependent activation of the ERK1/2 MAPK pathway requires Src kinase signaling, and the interaction between β-arrestin and Src kinase plays an important role in this GPCR-Src-ERK1/2 pathway (Benquet et al., 2002; Orlando et al., 2009). In addition, β-arrestin directly binds to c-Raf (Luttrell et al., 2001) and relieves the autoinhibition of the kinase even without Ras, which leads to the activation of the

ERK cascade (Min, 2011). In the case of the mGluR, it has been proposed that β-arrestin acts as a scaffold to couple the Src kinase to the activated mGluR (Benquet et al., 2002; Eng et al., 2016; Rosenblum et al., 2002), and thus is required for mGluR-mediated ERK1/2 activation (Stoppel et al., 2017). Interestingly, upon activation of the mGluR5 in striatal neurons, only a small portion of ERK1/2 is activated by the PLCβ/IP_3/calcium dependent pathway (Mao et al., 2005), which is a G protein-mediated cascade (Stoppel et al., 2017). In the same condition, much stronger ERK1/2 activation is achieved by the calcium-independent pathway, in a Homer1b/c-dependent manner (Mao et al., 2005). Since the ERK1/2 activation is β-arrestin pathway-dependent, this implicates the crosstalk between the Homer1b/c and β-arrestin downstream pathways. In this neuronal condition, Homer1a binding to mGluR would negatively regulate ERK1/2 activation via inhibition of Homer1b/c binding to mGluR. Indeed, Homer1a strongly attenuates mGluR-dependent activation of ERK1/2 in the spinal cord (Tappe et al., 2006). Notably, the disruption of mGluR-Homer interactions selectively blocks the phosphoinositide 3-kinase (PI3K)-Akt-mammalian target of rapamycin (mTOR) pathway but not the ERK pathway in hippocampal neurons, suggesting the region-specific role of Homer in mGluR signaling (Ronesi and Huber, 2008). As a read-out of the protein synthesis downstream of mGluR5 activation, the ERK change implicates distinct mode of actions of the mGluR5 following its interaction with Homer proteins.

The functional consequences of the interaction are manifested by various physiological and pathological responses in neurons. The glutamate-induced protective signaling of mGluR1 is mediated by sustained, β-arrestin-mediated ERK activation (Emery et al., 2010). In the case of Homer, the binding of the Homer protein to the phosphoinositide 3 kinase enhancer (PIKE) following quisqualate- or DHPG- induced activation of group I mGluR activates PI3K, and prevents neuronal apoptosis (Rong et al., 2003). Therefore, disruption of this interaction would affect

the basal viability of the neuron. In addition, the mechanisms of the group I mGluR-mediated synaptic plasticity involve β-arrestin (Eng et al., 2016; Stoppel et al., 2017) and the Homer protein(Ronesi and Huber, 2008). These interactions are associated with neuronal diseases such as fragile X (Ronesi and Huber, 2008; Ronesi et al., 2012; Stoppel et al., 2017), chronic pain (Obara et al., 2013; Tappe-Theodor et al., 2011; Tappe et al., 2006), and addiction (Szumlinski et al., 2004, 2006), Although these findings suggest the involvement of sustained activation, direct implication of sustained mGluRs activity in the regulation of the synaptic transmission has not yet been established.

Conclusion

Constitutive activity of mGluR plays a critical role in neuronal responses. The coupling of mGluRs to effector molecules including G proteins or β-arrestins not only mediates downstream effectors but also determines the activity of the mGluRs itself. These effectors coupling to the mGluRs, and activation following downstream pathways, could be modulated by reciprocal interactions between the binding molecules including kinases, phosphatases, and proteins. I propose that the Homer proteins, ERK1/2 MAPK, and β-arrestin affect each other and regulate the constitutive activity of mGluR. This regulation would occur in the internalized mGluR following sufficient receptor activation, and the C-terminal binding to interacting molecules would modulate the implementation of downstream signaling.

Materials and Methods

Animals

Adult male Sprague-Dawley rats (Samtako, Seoul, Korea) were housed at a constant temperature of 23 ± 1°C under a 12 h light/dark cycle. Animals were housed two per cage, with free access to food and water. Rats were acclimatized to the facilities at least for 2 weeks before beginning the experiments. All the experimental procedures were approved by the Institutional Animal Care and Use Committee of Seoul National University and were performed according to the Ethical Guidelines of the International Association for the Study of Pain.

Spinal nerve ligation (SNL)

Adult male rats (8-week-old) were subjected to SNL or sham surgery as described by Kim and Chung (Kim and Chung, 1992). Isofluorane was inhaled from 15 minutes before surgery till the end. Under the deep anesthesia with 2% isoflurane, a midline incision was made and the right L6 transverse process was removed. The right L5 spinal nerve was isolated and tightly ligated with 5-0 silk suture. In control group, sham surgery was performed with the identical procedure, except that isolated L5 nerve was not ligated. After the surgery, rats were returned to their home cage and monitored during recovery. Rats with abnormal motor deficiency (foot-drop or paw dragging) after the surgery were excluded from further experiments. Animals exhibiting sensitive hind paws pre-surgery (paw withdrawal threshold < 10g) or weak sensitivity post-SNL surgery (paw withdrawal threshold > 5g) underwent the

von Frey tests during the observation period, but were not considered as the subject of the PET scan and the drug tests.

Paw withdrawal threshold

Paw withdrawal thresholds were evaluated by the von Frey filament testing using Dixon's up-down method (Dixon, 1965). Rats were individually placed under transparent acryl cage on the grid mesh floor table and allowed to habituate for 20 minutes. A series of von Frey filaments (3.61, 3.84, 4.08, 4.31, 4.56, 4.74, 4.93, 5.18) were applied to the test area of right hind paw using the up-down method, and 50% paw withdrawal threshold was calculated as described by Chaplan (Chaplan et al., 1994). Withdrawal threshold of 15 g was used as the cut-off value. Tests were performed one day before SNL surgery and 1, 5, 9, and 15 days after the surgery. Rats with a low mechanical threshold at pre-surgery condition (less than 10g) and rats without mechanical hypersensitivity after SNL surgery were excluded from the PET scan and the drug tests.

ABP688-PET imaging

The ABP688-PET images were acquired from the SNL group and sham group rats, between the 16^{th} and the 25^{th} day after the surgery. Animals were anesthetized and maintained with 1.5% isoflurane and received a tail vein injection of [11C] ABP688 (5.05-16.15 MBq / 100g). Brain scans were processed using a micro-PET/CT scanner (eXplore VISTA, GE Healthcare) which has 47mm axial and 68mm transaxial field-of-view, with a resolution of 1.6mm full-width at half maximum. Data were acquired for 60 minute with list-mode. After finishing scan procedure, list mode data were reconstructed into a single static image of the full 60 minutes and into dynamic frames of 6 * 30 sec, 7 * 60 sec, and 5 * 600 sec duration using 3-

dimensional ordered-subsets expectation maximum (OSEM) algorithm with scatter correction and random correction. Voxel size was 0.3875 * 0.3875 * 0.775 mm. Each image was reconstructed in proportion to standardized uptake value (SUV).

ABP688-PET image preprocessing

The ABP688-PET images were processed using Statistical Parametric Mapping 8 software package (SPM8), MarsBaR toolbox and imgsrtm program of Turku PET Centre. Static images of the full 60 minutes from each dataset were coregistered with a standard rat MRI template (Schweinhardt et al., 2003), and the calculated transformation parameters were applied to the respective binned images. All the results of the coregistration were visually confirmed. Then the time-activity curves (TAC) for the cerebellum were extracted from the series of binned images. The non-displaceable binding potential (BP_{ND}) of [11C] ABP688 was calculated by use of the simplified reference tissue model with the cerebellum as a reference region. The images were cropped to exclude olfactory bulb region, and averaged to make an ABP688-PET brain template image. All the images were spatially normalized to this ABP688-PET brain template image. Voxels were resampled to 0.2 * 0.2 * 0.2 mm and smoothed with a Gaussian filter of 0.8 mm full-width at half maximum.

ABP688-PET image analysis

In the study of chapter 1, a voxel-by-voxel comparison of mGluR5 availability between the two groups was performed using the SPM8 software. A two-sample t-test was used to assess differences between SNL group and sham control. In the study of chapter 2, a voxel-wise regression analysis was used with data from SNL group animals, to investigate the interaction between the mGluR5 level in the brain and

paw withdrawal threshold. An uncorrected p-value threshold of 0.005 and an extent threshold of 20 voxels were used to determine statistical significance. The statistical map was overlaid onto an MRI template image (Schweinhardt et al., 2003) for visualization purpose.

For post-hoc analyses, ROI was set based on the anatomical location of the significant cluster, and BP_{ND} in the 0.5 mm radius sphere of the ROI was extracted using the MarsBaR toolbox. The interaction between paw withdrawal threshold and the mGluR5 level in each ROI was analyzed by calculating Pearson's correlation coefficient. The same method was also used to compute the correlation between the ROIs. The mGluR5 levels of each ROI in the SNL group and the sham group were compared using the two-sample t-test and F-test.

Deciphering the pain status using ABP688-PET image

For normalization, the mGluR5 levels in each ROIs were separately divided by the average values of each ROIs of the sham group. The normalized values of SNL rats were then separately regressed to the paw withdrawal thresholds. The regressed values of each ROIs were then plotted in separate columns. As such, a row of regressed mGluR5 templates represent an ideal mGluR5 pattern of a hypothetical SNL rat that has a corresponding paw withdrawal threshold.

Pearson's correlation coefficients were computed between the pattern of each SNL rat and the template. Thus, a normalized mGluR5 pattern of a rat (a row) was applied to the regressed template row-by-row, to calculate the degree of match. The calculations were repeated for all rats, and the results for each rat were plotted to the separated columns. Thus, each column of the r-value and p-value matrices represents the result from an individual rat. The sensitivity of the method was investigated using

leave-one-out cross-validation. In this paradigm, the pattern data of one subject (a row) was left out, and the regressed template was created from data of the remaining nine subjects. Then, data of the subject that had been left out were applied, to calculate the degree of match. This method was repeated subject-by-subject to predict all the paw withdrawal thresholds of SNL subjects.

FDG-PET imaging

The FDG-PET images were acquired in SNL rats and sham rats. 18 days after surgery (18^{th} day), the animal was transported to PET facility and experienced mimicking procedures for habituation purpose. Two PET scans were performed to each rat on the 19^{th} day and 20^{th} day respectively, with the microinjection of DHPG solution or vehicle solution (aCSF). Rats were deprived of food 12-16 hours prior to each PET scan session to enhance uptake of FDG to the brain.

On each day of the experiment, 0.5 μl of the solution was injected into left ventrolateral PAG of the rat via implanted cannula. One of the solutions (DHPG or aCSF) was randomly assigned to the first PET scan period (19^{th} day) and the counterbalanced solution was used on next PET scan period (20^{th} day). After the injection, the rat was placed in a transparent acryl cage on the grid mesh floor table and acclimatized for 20 minutes. Paw withdrawal threshold was measured in this condition using von Frey filaments.

[18F] FDG (2mCi in the volume of 0.5ml saline) was then injected via tail vein under light isoflurane anesthesia. Rat woke up immediately and was monitored to stay awake in its home-cage during 45 minutes of uptake period. Following the uptake period, the rat was anesthetized with isoflurane and a static image was acquired for 30 minutes using the microPET/CT scanner. After scanning, images

were reconstructed using OSEM algorithm provided by eXplore VISTA, with a voxel size of 0.3875 * 0.3875 * 0.775 mm.

All animals experienced mimicking procedures on the 18th day for acclimation. Mimicking procedures included procedures of intra-PAG injection via implanted cannula, measurement of paw withdrawal threshold, tail vein injection, home-cage waiting and brain-scanning under isoflurane anesthesia. During this mimicking procedure which was performed one day prior to first PET scan session, aCSF was used for intra-PAG injection and saline was used for tail vein injection. CT scan was performed instead of PET scan using the same scanner machine. CT images acquired from this procedure were used to verify the location of the implanted cannula.

FDG-PET image preprocessing

The FDG-PET images were processed and analyzed using the SPM8 software package. All images acquired from FDG-PET scan sessions were coregistered to one space and averaged. The averaged image was coregistered to an MRI template image (Schweinhardt et al., 2003) and all the individual FDG-PET images were coregistered to this averaged image. Afterward, all the individual images were cropped to exclude olfactory bulb region, and then averaged to make a FDG-PET brain template image. All brain images were spatially normalized to this FDG-PET brain template image with heavy nonlinear regularization (value of 10), and resliced with a voxel size of 0.2 * 0.2 * 0.2 mm. The images were smoothed with a Gaussian kernel of 0.6 mm full-width at half maximum. Following normalization, images were classified into separate datasets according to the surgery-status (SNL or Sham) and the treatment-status (DHPG injection or Vehicle injection).

FDG-PET image analysis

FDG-PET images were analyzed using voxel-by-voxel t-tests using the SPM8. Independent two-sample t-tests were performed to compare the difference between the surgery status (SNL vs. sham) and paired t-tests were performed to compare treatment-status (DHPG injection vs. vehicle injection) by the group. Proportional scaling method was used and the day of scanning session (postoperative 19th day or 20th day) was applied as a nuisance covariate. An uncorrected p-value threshold of 0.001 or 0.005, and an extent threshold of 20 voxels were used to determine statistical significance. Survived voxels were overlaid onto an MRI template image (Schweinhardt et al., 2003) for visualization.

Cannula implantation

Under deep anesthesia, the head of each animal was fixed in a stereotaxic frame and animals were deeply anesthetized. The target coordinates were according to the Atlas of Paxinos and Watson (Paxinos and Watson, 2007).

In the study of chapter 1, guide cannulas were implanted into the PrL bilaterally. The coordinates of AP +2.6 mm, ML ±0.8 mm, DV -2.9 mm from the bregma were targeted, which made the tip of the guide cannula locate 0.7 mm above the injection site.

In the study of chapter 3, coordinates of AP -7.8 mm, ML ±0.9 mm, DV -4.5 mm from the bregma were targeted, which made the tip of the guide cannula locate 1.5 mm above the injection site of the PAG. The cannula was implanted unilaterally (left, for DHPG treatment) or bilaterally (for MPEP treatment to naïve rats).

After the fixation of the guide cannula using dental cement and mini screw, rats were returned to their home cage and monitored during recovery from the anesthesia.

At least 7 days of recovery period was given. After the recovery period, the rats were handled once a day for 3 consecutive days prior to drug injection.

Drug injection

In the study of chapter 1, microinjection of drug solution into the target region was conducted using internal cannula which has a length of 0.7 mm additional projection beyond the tip of the guide cannula (final target DV -3.6 mm). In the case of the dorsal and ventral parts, targeted coordinates were identical except final target DV -2.0 mm and -5.4 mm. A volume of 0.5 μl drug solutions (25 nmol of MPEP) was injected to each side of mPFC and behavioral experiments were followed. In the case of MTEP solution, 10 nmol of MTEP in the same volume was used.

In the study of chapter 3, microinjections of the drug into the ventrolateral PAG were conducted using internal cannula which has a length of 1.5 mm additional projection beyond the end of the guide cannula. A volume of 0.5 μl drug solution was injected per site unilaterally or bilaterally over a period of 60 seconds using syringe pump. Drug solutions of DHPG (25 nmol), MPEP (25 nmol), BAY36-7620 (25 and 50 nmol) and 50% DMSO were used.

The internal cannula was kept in place for additional 60 seconds after the microinjection to prevent backflow. All behavioral measurements were initiated 15 minutes after the end of the microinjection.

Confirmation of the injection sites

At the end of the experiments, rats were deeply anesthetized and dye was microinjected to verify the placement of the cannula. For the fixation of the brain, rats were transcardially perfused with phosphate-buffered saline followed by 4%

paraformaldehyde. Brains were extracted, stored in formalin and sliced in coronal sections using cryotome. The injection site was determined under light microscopy from brain sections counterstained with cresyl violet. In the case of the FDG-PET experiment of chapter 3, the placement of the cannula was verified by CT scan. Only data from rat with a confirmed placement of the cannula were included in the studies.

Forced swimming test (FST)

The FST was used in the study of chapter 1. On the 22nd day after SNL or sham surgery, the rat was placed in a swim cylinder (20 cm in diameter and 45 cm height) filled with water at 23°C (depth of 30 cm) and underwent a pre-test swimming of 15 minutes. After the pre-test swimming, the rat was dried with the towels and returned to its home-cage. On the next day (the 23rd day after the surgery), one of the solutions (DMSO vehicle or MPEP solution) was randomly selected and injected into the bilateral PrL of the rat via implanted cannula. At 30 minutes after the injection, the rat was placed in the swim cylinder for a 5 minutes swimming (Slattery and Cryan, 2012). In the case of the experiment with lentiviral expression, 15 minutes of pre-test swimming was performed on the 14th day after the injection of mGluR5-LV or ZsGreen-LV into the bilateral PrL of the naïve rat. Repeated 5 minutes of swimming tests were performed on the 15th and 21st day after the LV injection (Mezadri et al., 2011). All the tests were video-recorded and the immobility time was analyzed from 5 minutes swimming. Immobility was defined as when rat had no activity except for those necessary to keep its head above water.

Open field test (OFT)

The OFT was used in the study of chapter 1. The rat was placed in the center of an

open field box (60 cm * 60 cm square, 30 cm height) under low-light illumination (<20 lux) and was video-recorded during 5 minutes. The experimenter was blinded to the group and total distance moved and time spent in the center zone during the test were analyzed automatically using EthoVision XT software (Noldus). Center zone was defined as a zone of 30 cm * 30 cm center square. In the case of the MPEP experiment, the drug was injected into the medial prefrontal cortex (mPFC) via implanted cannula and the rat was returned to its home-cage. OFT was performed 30 minutes after the drug injection.

Conditioned place preference test (CPP)

The CPP was used in the study of chapter 1. The cannulated rats had a 3 days protocol for 3 chamber CPP test (King et al., 2009). The CPP chamber consisted of two pairing chambers (vertical versus horizontal visual cues) connected by a neutral chamber. All animals were exposed to the experimental room environment three days prior to the beginning of the main experiment for adaptation purpose. On the first day of the main experiment, the animal was allowed to access to all chambers freely for 15 minutes. The time spent in each chamber was analyzed to confirm the absence of pre-conditioning chamber preference. Animals spending less than 20% of the time in any one chamber at this stage were excluded from further experiments. On the second day, the vehicle DMSO solution was injected into the bilateral PrL, and the animal was returned to its home-cage. The 30 minutes of the waiting period was given. Then the animal was placed in a randomly assigned chamber (with vertical or horizontal visual cue) for 30 minutes. After 4 hours, the MPEP solution was injected to the bilateral PrL of the same animal and 30 minutes of home-cage waiting was followed. And then the animal was placed in the counterbalanced chamber for 30 minutes. The animal was not allowed to access to the other chambers during these

pairing periods. On the third day, the animal was placed into the neutral chamber and was allowed to freely access to all chambers for the 15 minutes. The time spent in each chamber was calculated and compared.

Lentiviral overexpression of mGluR5

The lentiviral overexpression technique was used in the study of chapter 1. The lentivirus vector used in the study was a generous gift from Professor Chul Hoon Kim (Yonsei University), and lentivirus expressing mGluR5 or ZsGreen1 was produced and verified as previously described (Shin et al., 2015). In brief, the cDNA of mGluR5 (primer forward: ATGGTCCTTCTGTTGATTCTGTCAG, reverse: TCACAACGATGAAGAACTCTGCG) was amplified and inserted into the lentiviral vector pLVX-EF1α–IRES-ZsGreen1 (Clontech, Catalog No. 631982), and the plasmid was transfected into HEK293FT cells of 60-70% confluency together with psPAX2 (Addgene), pMD2G (Addgene) and polyethyleneimine solution (sigma-Aldrich). Cell media were harvested, centrifuged and then ultracentrifuged. After the re-suspension, the virus was aliquoted and stored at -80°C until use. The virus was validated with Western blot analysis in virus-treated HEK293FT cells using mGluR5 antibody (Abcam, EPR2425Y).

The lentivirus expressing EF1α-IRES-Zsgreen1 (ZsGreen LV, titer=$3*10^8$ TU/ml) or EF1α-mGluR5-IRES-Zsgreen1 (mGluR5 LV, titer=$1*10^8$ TU/ml) was injected to the bilateral mPFC (coordinates of AP +2.6 mm, ML ±0.8 mm, DV -3.6 mm from the bregma) of naïve rats. Behavioral experiments were started 13 days after the virus injection. After finishing the experiments, the brains were extracted from each animal and coronal sections containing the mPFC region were prepared. The correct injection sites were confirmed in all animals. In the brain slices, precise delivery of the virus was confirmed by visualizing ZsGreen1-expressing neurons in the mPFC

region.

Viral manipulation of Homer1a expression

The Homer1a manipulation techniques were used in the study of chapter 3.

The adeno-associated virus (AAV) expressing Homer1a (Homer1a-AAV) was used for the overexpression of Homer1a in the PAG of naïve rats. The AAV expressing green fluorescent protein (GFP-AAV) was used as a control. The Homer1a-AAV and the GFP-AAV were generous gifts from Professor Karen Szumlinski (University of California at Santa Barbara).

For the Homer1a knock-down, the AAV containing short hairpin RNA (shRNA) vectors were constructed. The AAV containing shRNA vector of Homer1a (5'-GCTGCAGAACAAGGAAATT-3') was injected into the PAG to block the endogenous Homer1a expression following SNL surgery (shHomer1a). The AAV containing shRNA vector of luciferase was used as control (shLuci). The red fluorescent protein, dTomato, was co-expressed as an indicator.

Preparations of brain slice for patch-clamp recordings

The techniques related to the patch-clamp recordings were used in the study of chapter 3. Brain slices were obtained from 10-11 weeks old rats (16-25 days after SNL or sham surgery) using protective recovery method (Ting et al., 2014). Rats were decapitated under isoflurane anesthesia and brain was extracted. The 250um-thick coronal brain slices containing PAG regions were dissected using vibrating tissue slicer with NMDG-aCSF (in mM: 93 NMDG, 93 HCl, 2.5 KCl, 1.2 NaH_2PO_4, 30 $NaHCO_3$, 20 HEPES, 25 Glucose, 5 sodium ascorbate, 2 Thiourea, 3 Sodium

pyruvate, 10 $MgSO_4 \cdot 7H_2O$, 0.5 $CaCl_2 \cdot 2H_2O$ at pH 7.3) at room temperature. After dissection, slices were transferred to recovery chamber and allowed to proceed for initial recovery with NMDG-aCSF for 10-12min at 32-33°C. After the initial recovery period, slices were transferred to holding chamber containing recording aCSF (in mM: 124 NaCl, 2.5 KCl, 1.2 NaH_2PO_4, 24 $NaHCO_3$, 5 HEPES, 12.5 Glucose, 2 $MgSO_4 \cdot 7H_2O$, 2 $CaCl_2 \cdot 2H_2O$ at pH 7.3) and were proceeded additional recovery period of at least one hour at room temperature. All aCSF was equilibrated with 95% O_2 and 5% CO_2.

Patch clamp recordings

Brain slices were transferred to a recording chamber and visualized with a fluorescence Olympus BX-50WI light microscope using the 40x objective lens and monitored with a CCD camera. Slices were continuously perfused with recording aCSF at 32°C during recording. Whole-cell patch-clamp recordings were performed in neurons located in the ventrolateral column of the PAG using EPC9 (HEKA) or Multiclamp 700B amplifier. The resistance of the pipette was 4-8 MΩ when filled with internal solution. Series resistance was monitored throughout the experiment, and the recordings were discarded if it changed by more than 20%. Signals were filtered at 2 kHz and digitized. All electrophysiological recordings were started at least 3 minutes after the whole-cell configuration was established.

Measurement of neuronal excitability

In the current-clamp mode, neurons were held with bias current injection at -70 mV in the presence of 10μM NBQX and 100μM picrotoxin. Internal solution was as follows (in mM): 9 KCl, 10 KOH, 120 K-gluconate, 3.48 $MgCl_2$, 10 HEPES, 4 NaCl,

4 Na_2ATP, 0.4 Na_3GTP, 17.5 sucrose at pH 7.25. Neurons were stabilized for at least 7 min before recording the baseline period excitability. Number of AP was measured by recording spike firing of neurons in response to injection of brief depolarizing current (250 ms). Depolarizing current was adjusted to evoke 4-9 spikes at the beginning of the recording and neurons of transient-spiking type (Park et al., 2010) were excluded from further drug study (maximum spike count < 10Hz). Neurons were discarded if resting membrane potential was depolarized more than -50mV or APs were unstable during the baseline period.

Measurement of spontaneous postsynaptic currents

Spontaneous EPSC was measured in the voltage-clamp mode at -70mV in the presence of 100μM picrotoxin. Internal solution was as follows (in mM): 140 Cs-methanesulfonate, 4 NaCl, 10 HEPES, 0.5 $CaCl_2$, 5 EGTA, 2 Mg-ATP, pH 7.3 with CsOH. The analysis of spontaneous EPSC was performed using MiniAnalysis software. From each neuron, 200 events were selected at baseline state and another 200 events were selected at 15-20 min after drug treatment. Amplitudes and inter-event intervals of 200 events were averaged by state respectively to represent the relevant state of the neuron. The effect of drug treatment was compared by paired t-test between the representative averaged points from each neuron. In the inter-group analysis, events selected from baseline state were concatenated to describe the cumulative fractions of spontaneous EPSCs in each group and then compared by a Kolmogorov-Smirnov test. In the case of spontaneous GABAergic IPSC recordings, signals were measured in the presence of 10 μM NBQX and 4 μM strychnine. Internal solution for IPSC recordings was as follows (in mM): 150 CsCl, 1.5 $MgCl_2$, 10 HEPES, 0.1 $CaCl_2$, 1 EGTA, 2 Na_2ATP, 0.4 Na_3GTP, 5 QX-314, at pH 7.3.

Identification of the PAG-RVM projection neurons

At 9 days after SNL or sham surgery, the head of each rat was fixed in a stereotaxic frame under the anesthesia and a hole was drilled into the skull. DiI (0.5 μl of volume, 25 mg/0.5 ml in DMSO) was injected into the RVM with the coordinates of AP -11 mm, ML 0 mm, DV -10.5 mm from bregma. Rats were returned to their home-cages and patch-clamp experiments were performed 7-16 days after injection. The injection site of the RVM was visually confirmed during the preparation of the brain slices, and distribution pattern of the PAG-RVM projection neurons in the PAG was confirmed with DiI sensitive filter during the recordings. Only brains with correct injection site of the RVM was considered and slices with the distinct distribution pattern of the PAG-RVM neurons (absence of PAG-RVM projection neurons in dorsolateral columns of the PAG) was used.

Drugs

2,3-Dioxo-6-nitro-1,2,3,4-tetrahydrobenzo[f]quinoxaline-7-sulfonamide (NBQX), (S)-3,5-Dihydroxyphenylglycine (DHPG), (RS)-2-Chloro-5-hydroxyphenylglycine (CHPG), 2-Methyl-6-(phenylethynyl)pyridine hydrochloride (MPEP), 3-((2-Methyl-1,3-thiazol-4-yl)ethynyl)pyridine hydrochloride (MTEP) and (3aS,6aS)-Hexahydro-5-methylene-6a-(2-naphthalenylmethyl)-1H-cyclopenta[c]furan-1-one (BAY 36-7620) were purchased from Tocris. Picrotoxin and strychnine were obtained from Sigma. 1,1'-Dioctadecyl-3,3,3',3'-Tetramethylindocarbocyanine Perchlorate (DiI) was purchased from Molecular Probes. NBQX, picrotoxin, and strychnine were dissolved in water. DHPG was dissolved in water (50 mM) for slice application, or aCSF without bicarbonate for in vivo microinjection. CHPG was dissolved with 110mM NaOH (100 mM). MPEP, MTEP, and BAY 36-7620 were dissolved with DMSO (100 mM). Stock solutions were diluted to final concentration

with aCSF. Final concentrations of the drugs used in the patch clamp experiments were as follows: 10 μM DHPG, 100 μM CHPG, 20 μM MPEP and 10 μM MTEP.

Statistical analysis

Paw withdrawal thresholds were analyzed using repeated measures ANOVA with time serving as a within-subject factor. In the post-hoc comparisons, the Bonferroni tests were performed between conditions at each time point. For FST and OFT, group data were analyzed using a one-way ANOVA followed by post-hoc test as specified. For CPP experiments, the time difference between pre- and post-conditioning was compared using paired t-test in each group, and the preference to the MPEP-conditioned chamber was compared between groups using Mann-Whitney test. Electrophysiology data were analyzed using Wilcoxon matched pairs test and Kolmogorov-Smirnov two-sample test, as specified. Two-sided testing was used in all the tests. For the excitability analyses, differences between baseline (one minute prior to drug treatment) condition and drug-treated condition (18 minutes after administration) were compared. Data are presented as mean ± S.E.M. All data are representative of at least three experiments. Animals were randomly assigned to groups in all experiments.

References

Abdallah, C.G., Hannestad, J., Mason, G.F., Holmes, S.E., DellaGioia, N., Sanacora, G., Jiang, L., Matuskey, D., Satodiya, R., Gasparini, F., et al. (2017). Metabotropic Glutamate Receptor 5 and Glutamate Involvement in Major Depressive Disorder: A Multimodal Imaging Study. Biol. Psychiatry Cogn. Neurosci. Neuroimaging.

Abe, H., Misaka, T., Tateyama, M., and Kubo, Y. (2003). Effects of coexpression with Homer isoforms on the function of metabotropic glutamate receptor 1alpha. Mol. Cell. Neurosci. *23*, 157–168.

Alexander, W.H., and Brown, J.W. (2012). Medial Prefrontal Cortex as an action-outcome predictor. Nat. Neurosci. *14*, 1338–1344.

Ango, F., Prézeau, L., Muller, T., Tu, J.C., Xiao, B., Worley, P.F., Pin, J.P., Bockaert, J., and Fagni, L. (2001). Agonist-independent activation of metabotropic glutamate receptors by the intracellular protein Homer. Nature *411*, 962–965.

Baliki, M.N., and Apkarian, A.V. (2015). Nociception, Pain, Negative Moods, and Behavior Selection. Neuron *87*, 474–491.

Baliki, M.N., Chialvo, D.R., Geha, P.Y., Levy, R.M., Harden, R.N., Parrish, T.B., and Apkarian, A.V. (2006). Chronic pain and the emotional brain: specific brain activity associated with spontaneous fluctuations of intensity of chronic back pain. J. Neurosci. *26*, 12165–12173.

Baliki, M.N., Petre, B., Torbey, S., Herrmann, K.M., Huang, L., Schnitzer, T.J., Fields, H.L., and Apkarian, A.V. (2012). Corticostriatal functional connectivity predicts transition to chronic back pain. Nat. Neurosci. *15*, 1117–1119.

Baliki, M.N., Chang, P.C., Baria, A.T., Centeno, M. V., and Apkarian, A. V. (2015). Resting-state functional reorganization of the rat limbic system following neuropathic injury. Sci. Rep. *4*, 6186.

Bannerman, D.M., Sprengel, R., Sanderson, D.J., McHugh, S.B., Rawlins, J.N.P., Monyer, H., and Seeburg, P.H. (2014). Hippocampal synaptic plasticity, spatial memory and anxiety. Nat. Rev. Neurosci. *15*, 181–192.

Beautrait, A., Paradis, J.S., Zimmerman, B., Giubilaro, J., Nikolajev, L., Armando, S., Kobayashi, H., Yamani, L., Namkung, Y., Heydenreich, F.M., et al. (2017). A new inhibitor of the β-arrestin/AP2 endocytic complex reveals interplay between GPCR internalization and signalling. Nat. Commun. *8*, 15054.

Beitz, A.J. (1989). Possible Origin of Glutamatergic Projections to the Midbrain

Periaqueductal Gray and Deep Layer of the Superior Colliculus of the Rat. Brain Res. Bull. *23*, 25–35.

Benarroch, E.E. (2016). Involvement of the nucleus accumbens and dopamine system in chronic pain. Neurology *87*, 1720–1726.

Benquet, P., Gee, C.E., and Gerber, U. (2002). Two distinct signaling pathways upregulate NMDA receptor responses via two distinct metabotropic glutamate receptor subtypes. J. Neurosci. *22*, 9679–9686.

Bianchi, R., Chuang, S.-C., Zhao, W., Young, S.R., and Wong, R.K.S. (2009). Cellular plasticity for group I mGluR-mediated epileptogenesis. J. Neurosci. *29*, 3497–3507.

Bordi, F., and Ugolini, A. (1999). Group I Metabotropic Glutamate Receptors : Implications for Brain Diseases. *59*.

Brakeman, P.R., Lanahan, A.A., O'Brien, R., Roche, K., Barnes, C.A., Huganir, R.L., and Worley, P.F. (1997). Homer: a protein that selectively binds metabotropic glutamate receptors. Nature *386*, 284–288.

Bushnell, M.C., Čeko, M., and Low, L.A. (2013). Cognitive and emotional control of pain and its disruption in chronic pain. Nat Rev Neurosci *14*, 502–511.

Cahill, T.J., Thomsen, A.R.B., Tarrasch, J.T., Plouffe, B., Nguyen, A.H., Yang, F., Huang, L.-Y., Kahsai, A.W., Bassoni, D.L., Gavino, B.J., et al. (2017). Distinct conformations of GPCR–β-arrestin complexes mediate desensitization, signaling, and endocytosis. Proc. Natl. Acad. Sci. *114*, 2562–2567.

Cassier, E., Gallay, N., Bourquard, T., Claeysen, S., Bockaert, J., Crépieux, P., Poupon, A., Reiter, E., Marin, P., and Vandermoere, F. (2017). Phosphorylation of β-arrestin2 at Thr ^{383} by MEK underlies β-arrestin-dependent activation of Erk1/2 by GPCRs. Elife *6*.

Chaki, S., Ago, Y., Palucha-Paniewiera, A., Matrisciano, F., and Pilc, A. (2013). mGlu2/3 and mGlu5 receptors: Potential targets for novel antidepressants. Neuropharmacology *66*, 40–52.

Chang, P.C., Pollema-Mays, S.L., Centeno, M.V., Procissi, D., Contini, M., Baria, A.T., Martina, M., and Apkarian, A.V. (2014). Role of nucleus accumbens in neuropathic pain: Linked multi-scale evidence in the rat transitioning to neuropathic pain. Pain *155*.

Chaplan, S.R., Bach, F.W., Pogrel, J.W., Chung, J.M., and Yaksh, T.L. (1994). Quantitative assessment of tactile allodynia in the rat paw. J. Neurosci. Methods *53*, 55–63.

Cheriyan, J., Kaushik, M.K., Ferreira, A.N., and Sheets, P.L. (2016). Specific targeting of the basolateral amygdala to projectionally defined pyramidal neurons in prelimbic and infralimbic cortex. eNeuro *3*.

Chung, G., Kim, C.Y.C.Y., Yun, Y.-C.Y.-C., Yoon, S.H.S.H., Kim, M.-H.M.-H., Kim, Y.K.Y.K., and Kim, S.J.S.J. (2017). Upregulation of prefrontal metabotropic glutamate receptor 5 mediates neuropathic pain and negative mood symptoms after spinal nerve injury in rats. Sci. Rep. *7*, 9743.

Clarey, J.C., Tweedale, R., and Calford, M.B. Interhemispheric modulation of somatosensory receptive fields: evidence for plasticity in primary somatosensory cortex. Cereb. Cortex *6*, 196–206.

Coffa, S., Breitman, M., Hanson, S.M., Callaway, K., Kook, S., Dalby, K.N., and Gurevich, V. V. (2011). The Effect of Arrestin Conformation on the Recruitment of c-Raf1, MEK1, and ERK1/2 Activation. PLoS One *6*, e28723.

Coffeen, U., Ortega-Legaspi, J.M., de Gortari, P., Simón-Arceo, K., Jaimes, O., Amaya, M.I., and Pellicer, F. (2010). Inflammatory Nociception Diminishes Dopamine Release and Increases Dopamine D2 Receptor mRNA in the Rat's Insular Cortex. Mol. Pain *6*, 1744-8069-6–75.

Corder, G., Doolen, S., Donahue, R.R., Winter, M.K., Jutras, B.L., He, Y., Hu, X., Wieskopf, J.S., Mogil, J.S., Storm, D.R., et al. (2013). Constitutive μ-opioid receptor activity leads to long-term endogenous analgesia and dependence. Science *341*, 1394–1399.

Crépieux, P., Poupon, A., Langonné-Gallay, N., Reiter, E., Delgado, J., Schaefer, M.H., Bourquard, T., Serrano, L., and Kiel, C. (2017). A Comprehensive View of the β-Arrestinome. Front. Endocrinol. (Lausanne). *8*, 32.

D'Ascenzo, M., Podda, M.V., Fellin, T., Azzena, G.B., Haydon, P., and Grassi, C. (2009). Activation of mGluR5 induces spike afterdepolarization and enhanced excitability in medium spiny neurons of the nucleus accumbens by modulating persistent Na+ currents. J. Physiol. *587*, 3233–3250.

Davies, C.H., Clarke, V.R., Jane, D.E., and Collingridge, G.L. (1995). Pharmacology of postsynaptic metabotropic glutamate receptors in rat hippocampal CA1 pyramidal neurones. Br. J. Pharmacol. *116*, 1859–1869.

Davis, D.A., Ghantous, M.E., Farmer, M.A., Baria, A.T., and Apkarian, A.V. (2016). Identifying brain nociceptive information transmission in patients with chronic somatic pain. PAIN Reports *1*, e575.

DeLorenzo, C., Sovago, J., Gardus, J., Xu, J., Yang, J., Behrje, R., Kumar, J.S.D., Devanand, D.P., Pelton, G.H., Mathis, C.A., et al. (2015). Characterization of brain mGluR5 binding in a pilot study of late-life major depressive disorder using positron emission tomography and [11C]ABP688. Transl. Psychiatry *5*, e693.

Deschwanden, A., Karolewicz, B., Feyissa, A.M., Treyer, V., Ametamey, S.M., Johayem, A., Burger, C., Auberson, Y.P., Sovago, J., Stockmeier, C.A., et al. (2011). Reduced metabotropic glutamate receptor 5 density in major depression determined by [11C]ABP688 PET and postmortem study. Am. J. Psychiatry *168*, 727–734.

Detloff, M.R., Clark, L.M., Hutchinson, K.J., Kloos, A.D., Fisher, L.C., and Basso, D.M. (2010). Validity of acute and chronic tactile sensory testing after spinal cord injury in rats. Exp. Neurol. *225*, 366–376.

Dixon, W.J. (1965). The up-and-down method for small samples. J. Am. Stat. Assoc. *60*, 967–978.

Duman, R.S., Aghajanian, G.K., Sanacora, G., and Krystal, J.H. (2016). Synaptic plasticity and depression: new insights from stress and rapid-acting antidepressants. Nat. Med. *22*, 238–249.

Eishingdrelo, H., and Kongsamut, S. (2013). Minireview: Targeting GPCR Activated ERK Pathways for Drug Discovery. Curr. Chem. Genomics Transl. Med. *7*, 9–15.

Emery, A.C., Pshenichkin, S., Takoudjou, G.R., Grajkowska, E., Wolfe, B.B., and Wroblewski, J.T. (2010). The Protective Signaling of Metabotropic Glutamate Receptor 1 Is Mediated by Sustained, β-Arrestin-1-dependent ERK Phosphorylation. J. Biol. Chem. *285*, 26041–26048.

Eng, A., Hedrick, T., and Swanson, G. (2015). mGluR1-β-arrestin 2 Signaling Mediates Induction of Excitatory Synaptic Plasticity. FASEB J. *29*, 934–935.

Eng, A.G., Kelver, D.A., Hedrick, T.P., and Swanson, G.T. (2016). Transduction of group I mGluR-mediated synaptic plasticity by b-arrestin2 signalling. Nat. Commun. *7*, 13571.

Esterlis, I., DellaGioia, N., Pietrzak, R.H., Matuskey, D., Nabulsi, N., Abdallah, C.G., Yang, J., Pittenger, C., Sanacora, G., Krystal, J.H., et al. (2017). Ketamine-induced reduction in mGluR5 availability is associated with an antidepressant response: an [11C]ABP688 and PET imaging study in depression. Mol. Psychiatry.

Etkin, A., Egner, T., and Kalisch, R. (2011). Emotional processing in anterior cingulate and medial prefrontal cortex. Trends Cogn. Sci. *15*, 85–93.

Fagni, L., Ango, F., Prezeau, L., Worley, P.F., Pin, J.-P., and Bockaert, J. (2003). Control of constitutive activity of metabotropic glutamate receptors by Homer proteins. Int. Congr. Ser. *1249*, 245–251.

Felice, M. De, Sanoja, R., Wang, R., Vera-portocarrero, L., Oyarzo, J., King, T., Ossipov, M.H., Vanderah, T.W., Lai, J., Dussor, G.O., et al. (2011). Engagement of descending inhibition from the rostral ventromedial medulla protects against chronic neuropathic pain. Pain *152*, 2701–2709.

Frank, M.G. (2016). Circadian Regulation of Synaptic Plasticity. Biology (Basel). *5*.

Fuxe, K., and Borroto-Escuela, D.O. (2015). Basimglurant for treatment of major depressive disorder: a novel negative allosteric modulator of metabotropic glutamate receptor 5. Expert Opin. Investig. Drugs *24*, 1247–1260.

Gallagher, S.M., Daly, C.A., Bear, M.F., and Huber, K.M. (2004). Extracellular

signal-regulated protein kinase activation is required for metabotropic glutamate receptor-dependent long-term depression in hippocampal area CA1. J. Neurosci. *24*, 4859–4864.

Gerber, U., Gee, C.E., and Benquet, P. (2007). Metabotropic glutamate receptors: intracellular signaling pathways. Curr. Opin. Pharmacol. *7*, 56–61.

Gilliland, C.T., Salanga, C.L., Kawamura, T., Trejo, J., and Handel, T.M. (2013). The Chemokine Receptor CCR1 Is Constitutively Active, Which Leads to G Protein-independent, β-Arrestin-mediated Internalization. J. Biol. Chem. *288*, 32194–32210.

Gladding, C.M., Fitzjohn, S.M., and Molnar, E. (2009). Metabotropic Glutamate Receptor-Mediated Long-Term Depression: Molecular Mechanisms. Pharmacol. Rev. *61*, 395–412.

Gorelova, N., and Yang, C.R. (1996). The course of neural projection from the prefrontal cortex to the nucleus accumbens in the rat. Neuroscience *76*, 689–706.

Gray, A.L., Hyde, T.M., Deep-Soboslay, A., Kleinman, J.E., and Sodhi, M.S. (2015). Sex differences in glutamate receptor gene expression in major depression and suicide. Mol. Psychiatry *20*, 1057–1068.

Gupta, A., Silman, A.J., Ray, D., Morriss, R., Dickens, C., MacFarlane, G.J., Chiu, Y.H., Nicholl, B., and McBeth, J. (2007). The role of psychosocial factors in predicting the onset of chronic widespread pain: Results from a prospective population-based study. Rheumatology *46*, 666–671.

Hashimoto, K., Malchow, B., Falkai, P., and Schmitt, A. (2013). Glutamate modulators as potential therapeutic drugs in schizophrenia and affective disorders. Eur. Arch. Psychiatry Clin. Neurosci. *263*, 367–377.

Hlushchuk, Y., and Hari, R. (2006). Transient Suppression of Ipsilateral Primary Somatosensory Cortex during Tactile Finger Stimulation. J. Neurosci. *26*, 5819–5824.

Hogan, Q., Sapunar, D., Modric-Jednacak, K., and McCallum, J.B. (2004). Detection of neuropathic pain in a rat model of peripheral nerve injury. Anesthesiology *101*, 476–487.

Hoppa, M.B., Gouzer, G., Armbruster, M., Ryan, T.A., DeNardo, L.A., Berns, D.S., DeLoach, K., and Luo, L. (2015). Connectivity of mouse somatosensory and prefrontal cortex examined with trans-synaptic tracing. Nat. Neurosci. *84*, 778–789.

Hu, J., Yang, L., Kammermeier, P.J., Moore, C.G., Brakeman, P.R., Tu, J., Yu, S., Petralia, R.S., Li, Z., Zhang, P., et al. (2012). Preso1 dynamically regulates group I metabotropic glutamate receptors. *15*.

Hubert, G.W., Paquet, M., and Smith, Y. (2001). Differential subcellular localization of mGluR1a and mGluR5 in the rat and monkey Substantia nigra. J Neurosci *21*, 1838–1847.

Hughes, Z.A., Neal, S.J., Smith, D.L., Sukoff Rizzo, S.J., Pulicicchio, C.M., Lotarski, S., Lu, S., Dwyer, J.M., Brennan, J., Olsen, M., et al. (2013). Negative allosteric modulation of metabotropic glutamate receptor 5 results in broad spectrum activity relevant to treatment resistant depression. Neuropharmacology *66*, 202–214.

Ireland, D.R., and Abraham, W.C. (2002). Group I mGluRs increase excitability of hippocampal CA1 pyramidal neurons by a PLC-independent mechanism. J Neurophysiol *88*, 107–116.

Iwata, Y., Jono, Y., Mizusawa, H., Kinoshita, A., and Hiraoka, K. (2016). Interhemispheric Inhibition Induced by Transcranial Magnetic Stimulation Over Primary Sensory Cortex. Front. Hum. Neurosci. *10*, 438.

Jong, Y.-J.I., Kumar, V., and O'Malley, K.L. (2009). Intracellular metabotropic glutamate receptor 5 (mGluR5) activates signaling cascades distinct from cell surface counterparts. J. Biol. Chem. *284*, 35827–35838.

Jung, S.-R., Kushmerick, C., Seo, J.B., Koh, D.-S., and Hille, B. (2017). Muscarinic receptor regulates extracellular signal regulated kinase by two modes of arrestin binding. Proc. Natl. Acad. Sci. *114*.

Kammermeier, P.J., and Worley, P.F. (2007). Homer 1a uncouples metabotropic glutamate receptor 5 from postsynaptic effectors. Proc. Natl. Acad. Sci. U. S. A. *104*, 6055–6060.

Kaneko, H., Zhang, S., Sekiguchi, M., Nikaido, T., Makita, K., Kurata, J., and Konno, S. (2017). Dysfunction of Nucleus Accumbens Is Associated With Psychiatric Problems in Patients With Chronic Low Back Pain. Spine (Phila. Pa. 1976). *42*, 844–853.

Kato, T., Takata, M., Kitaichi, M., Kassai, M., Inoue, M., Ishikawa, C., Hirose, W., Yoshida, K., and Shimizu, I. (2015). DSR-98776, a novel selective mGlu5 receptor negative allosteric modulator with potent antidepressant and antimanic activity. Eur. J. Pharmacol. *757*, 11–20.

Kelleher, R.J., Govindarajan, A., Jung, H.-Y., Kang, H., and Tonegawa, S. (2004). Translational control by MAPK signaling in long-term synaptic plasticity and memory. Cell *116*, 467–479.

Kelly, C.J., Huang, M., Meltzer, H., and Martina, M. (2016). Reduced Glutamatergic Currents and Dendritic Branching of Layer 5 Pyramidal Cells Contribute to Medial Prefrontal Cortex Deactivation in a Rat Model of Neuropathic Pain. Front. Cell. Neurosci. *10*, 1–12.

Khoury, E., Nikolajev, L., Simaan, M., Namkung, Y., and Laporte, S.A. (2014). Differential regulation of endosomal GPCR/β-arrestin complexes and trafficking by MAPK. J. Biol. Chem. *289*, 23302–23317.

Kim, S.H., and Chung, J.M. (1992). An experimental model for peripheral neuropathy produced by segmental spinal nerve ligation in the rat. Pain *50*, 355–363.

Kim, K.J., Yoon, Y.W., and Chung, J.M. (1997). Comparison of three rodent neuropathic pain models. Exp. Brain Res. *113*, 200–206.

Kim, S.K., Hayashi, H., Ishikawa, T., Shibata, K., Shigetomi, E., Shinozaki, Y., Inada, H., Roh, S.E., Kim, S.J., Lee, G., et al. (2016). Cortical astrocytes rewire somatosensory cortical circuits for peripheral neuropathic pain. J. Clin. Invest. *126*, 1983–1997.

King, T., Vera-Portocarrero, L., Gutierrez, T., Vanderah, T.W., Dussor, G., Lai, J., Fields, H.L., and Porreca, F. (2009). Unmasking the tonic-aversive state in neuropathic pain. Nat. Neurosci. *12*, 1364–1366.

Kolber, B.J. (2015). MGluRs head to toe in pain (Elsevier Inc.).

Kras, J. V., Dong, L., and Winkelstein, B.A. (2014). Increased Interleukin-1α and Prostaglandin E2 Expression in the Spinal Cord at 1 Day After Painful Facet Joint Injury. Spine (Phila. Pa. 1976). *39*, 207–212.

Kumar, V., Fahey, P.G., Jong, Y.-J.I., Ramanan, N., and O'Malley, K.L. (2012). Activation of Intracellular Metabotropic Glutamate Receptor 5 in Striatal Neurons Leads to Up-regulation of Genes Associated with Sustained Synaptic Transmission Including Arc/Arg3.1 Protein. J. Biol. Chem. *287*, 5412–5425.

Lee, K.-W., Westin, L., Kim, J., Chang, J.C., Oh, Y.-S., Amreen, B., Gresack, J., Flajolet, M., Kim, D., Aperia, A., et al. (2015). Alteration by p11 of mGluR5 localization regulates depression-like behaviors. Mol. Psychiatry *20*, 1546–1556.

Lei, Y., and Perez, M.A. (2017). Cortical contributions to sensory gating in the ipsilateral somatosensory cortex during voluntary activity. J. Physiol.

Leite-Almeida, H., Pinto-Ribeiro, F., and Almeida, A. (2015). Animal models for the study of comorbid pain and psychiatric disorders. Mod. Trends Pharmacopsychiatry *30*, 1–21.

Lemogne, C., Delaveau, P., Freton, M., Guionnet, S., and Fossati, P. (2012). Medial prefrontal cortex and the self in major depression. J. Affect. Disord. *136*.

Li, J.X. (2015). Pain and depression comorbidity: A preclinical perspective. Behav. Brain Res. *276*, 92–98.

Lin, F.T., Miller, W.E., Luttrell, L.M., and Lefkowitz, R.J. (1999). Feedback regulation of beta-arrestin1 function by extracellular signal-regulated kinases. J. Biol. Chem. *274*, 15971–15974.

Lindemann, L., Porter, R.H., Scharf, S.H., Kuennecke, B., Bruns, A., von Kienlin, M., Harrison, A.C., Paehler, A., Funk, C., Gloge, A., et al. (2015). Pharmacology of Basimglurant (RO4917523, RG7090), a Unique Metabotropic Glutamate Receptor 5 Negative Allosteric Modulator in Clinical Development for Depression. J. Pharmacol. Exp. Ther. *353*, 213–233.

Litaudon, P., Bouillot, C., Zimmer, L., Costes, N., and Ravel, N. (2017). Activity in the rat olfactory cortex is correlated with behavioral response to odor: a microPET study. Brain Struct. Funct. *222*, 577–586.

Lodge, D., Tidball, P., Mercier, M.S., Lucas, S.J., Hanna, L., Ceolin, L., Kritikos, M., Fitzjohn, S.M., Sherwood, J.L., Bannister, N., et al. (2013). Antagonists reversibly reverse chemical LTD induced by group I, group II and group III metabotropic glutamate receptors. Neuropharmacology *74*, 135–146.

Lüscher, C., and Huber, K.M. (2010). Group 1 mGluR-Dependent Synaptic Long-Term Depression: Mechanisms and Implications for Circuitry and Disease. Neuron *65*, 445–459.

Luttrell, L.M., Roudabush, F.L., Choy, E.W., Miller, W.E., Field, M.E., Pierce, K.L., and Lefkowitz, R.J. (2001). Activation and targeting of extracellular signal-regulated kinases by beta-arrestin scaffolds. Proc. Natl. Acad. Sci. U. S. A. *98*, 2449–2454.

Magalhaes, A.C., Dunn, H., and Ferguson, S.S.G.S. (2012). Regulation of GPCR activity, trafficking and localization by GPCR-interacting proteins.

Maihöfner, C., Forster, C., Birklein, F., Neundörfer, B., and Handwerker, H.O. (2005). Brain processing during mechanical hyperalgesia in complex regional pain syndrome: A functional MRI study. Pain *114*, 93–103.

Malherbe, P., Kratochwil, N., Knoflach, F., Zenner, M.-T., Kew, J.N.C., Kratzeisen, C., Maerki, H.P., Adam, G., and Mutel, V. (2003). Mutational analysis and molecular modeling of the allosteric binding site of a novel, selective, noncompetitive antagonist of the metabotropic glutamate 1 receptor. J. Biol. Chem. *278*, 8340–8347.

Mao, L.-M., and Wang, J.Q. (2016). Regulation of Group I Metabotropic Glutamate Receptors by MAPK/ERK in Neurons. J. Nat. Sci. *2*.

Mao, L., Yang, L., Tang, Q., Samdani, S., Zhang, G., and Wang, J.Q. (2005). The Scaffold Protein Homer1b/c Links Metabotropic Glutamate Receptor 5 to Extracellular Signal-Regulated Protein Kinase Cascades in Neurons. J. Neurosci. *25*, 2741–2752.

Marsden, W.N. (2013). Synaptic plasticity in depression: Molecular, cellular and functional correlates. Prog. Neuro-Psychopharmacology Biol. Psychiatry *43*, 168–184.

Massart, R., Dymov, S., Millecamps, M., Suderman, M., Gregoire, S., Koenigs, K., Alvarado, S., Tajerian, M., Stone, L.S., and Szyf, M. (2016). Overlapping signatures of chronic pain in the DNA methylation landscape of prefrontal cortex and peripheral T cells. Sci. Rep. *6*, 19615.

Matos, S.C., Zhang, Z., and Seguela, P. (2015). Peripheral Neuropathy Induces HCN Channel Dysfunction in Pyramidal Neurons of the Medial Prefrontal Cortex. J. Neurosci. *35*, 13244–13256.

McEwen, A.M., Burgess, D.T.A., Hanstock, C.C., Seres, P., Khalili, P., Newman, S.C., Baker, G.B., Mitchell, N.D., Khudabux-Der, J., Allen, P.S., et al. (2012). Increased Glutamate Levels in the Medial Prefrontal Cortex in Patients with Postpartum Depression. Neuropsychopharmacology *37*, 2428–2435.

Metz, A.E., Yau, H.-J., Centeno, M.V., Apkarian, A.V., and Martina, M. (2009). Morphological and functional reorganization of rat medial prefrontal cortex in neuropathic pain. Proc. Natl. Acad. Sci. U. S. A. *106*, 2423–2428.

Meye, F.J., Ramakers, G.M.J., and Adan, R.A.H. (2014). The vital role of constitutive GPCR activity in the mesolimbic dopamine system. Transl. Psychiatry *4*, e361.

Mezadri, T.J., Batista, G.M., Portes, A.C., Marino-Neto, J., and Lino-de-Oliveira, C. (2011). Repeated rat-forced swim test: Reducing the number of animals to evaluate gradual effects of antidepressants. J. Neurosci. Methods *195*, 200–205.

Min, J. (2011). Molecular Mechanism of Beta-Arrestin-dependent ERK activation Downstream of Protease-activated Receptor-2.

Minami, I., Kengaku, M., Smitt, P.S., Shigemoto, R., and Hirano, T. (2003). Long-term potentiation of mGluR1 activity by depolarization-induced Homer1a in mouse cerebellar Purkinje neurons. Eur. J. Neurosci. *17*, 1023–1032.

Newell, K.A., and Matosin, N. (2014). Rethinking metabotropic glutamate receptor 5 pathological findings in psychiatric disorders: implications for the future of novel therapeutics. BMC Psychiatry *14*, 23.

Niswender, C.M., and Conn, P.J. (2010). Metabotropic glutamate receptors: physiology, pharmacology, and disease. Annu. Rev. Pharmacol. Toxicol. *50*, 295–322.

Obara, I., Goulding, S.P., Hu, J.-H.H., Klugmann, M., Worley, P.F., and Szumlinski, K.K. (2013). Nerve injury-induced changes in Homer/glutamate receptor signaling contribute to the development and maintenance of neuropathic pain. Pain *154*, 1932–1945.

Orlando, L.R., Ayala, R., Kett, L.R., Curley, A.A., Duffner, J., Bragg, D.C., Tsai, L.-H., Dunah, A.W., and Young, A.B. (2009). Phosphorylation of the homer-binding domain of group I metabotropic glutamate receptors by cyclin-dependent kinase 5. J. Neurochem. *110*, 557–569.

Ossipov, M.H., Lai, J., Malan, T.P., and Porreca, F. (2000). Spinal and supraspinal mechanisms of neuropathic pain. Ann. N. Y. Acad. Sci. *909*, 12–24.

Osterweil, E.K., Krueger, D.D., Reinhold, K., and Bear, M.F. (2010). Hypersensitivity to mGluR5 and ERK1/2 leads to excessive protein synthesis in the hippocampus of a mouse model of fragile X syndrome. J. Neurosci. *30*, 15616–15627.

Palucha, A., and Pilc, A. (2007). Metabotropic glutamate receptor ligands as possible anxiolytic and antidepressant drugs. Pharmacol. Ther. *115*, 116–147.

Panaccione, I., King, R., Molinaro, G., Riozzi, B., Battaglia, G., Nicoletti, F., and Bashir, Z.I. (2013). Constitutively active group i mGlu receptors and PKMzeta regulate synaptic transmission in developing perirhinal cortex. Neuropharmacology *66*, 143–150.

Paradis, J.S., Ly, S., Blondel-Tepaz, É., Galan, J.A., Beautrait, A., Scott, M.G.H., Enslen, H., Marullo, S., Roux, P.P., and Bouvier, M. (2015). Receptor sequestration in response to β-arrestin-2 phosphorylation by ERK1/2 governs steady-state levels of GPCR cell-surface expression. Proc. Natl. Acad. Sci. *112*, E5160–E5168.

Park, C., Kim, J.-H., Yoon, B.-E., Choi, E.-J., Lee, C.J., and Shin, H.-S. (2010). T-type channels control the opioidergic descending analgesia at the low threshold-spiking GABAergic neurons in the periaqueductal gray. Proc. Natl. Acad. Sci. U. S. A. *107*, 14857–14862.

Park, M., Niciu, M.J., and Zarate, C.A. (2015). Novel Glutamatergic Treatments for Severe Mood Disorders. Curr. Behav. Neurosci. Reports *2*, 198–208.

Parvaz, M.A., Maloney, T., Moeller, S.J., Malaker, P., Konova, A.B., Alia-Klein, N., and Goldstein, R.Z. (2014). Multimodal evidence of regional midcingulate gray matter volume underlying conflict monitoring. NeuroImage Clin. *5*, 10–18.

Peterson, Y.K., and Luttrell, L.M. (2017). The Diverse Roles of Arrestin Scaffolds in G Protein–Coupled Receptor Signaling. Pharmacol. Rev. *69*, 256–297.

Piers, T.M., Kim, D.H., Kim, B.C., Regan, P., Whitcomb, D.J., and Cho, K. (2012). Translational Concepts of mGluR5 in Synaptic Diseases of the Brain. Front. Pharmacol. *3*, 199.

Pilc, A., Chaki, S., Nowak, G., and Witkin, J.M. (2008). Mood disorders: regulation by metabotropic glutamate receptors. Biochem. Pharmacol. *75*, 997–1006.

Price, T.J., and Inyang, K.E. (2015). Commonalities between pain and memory mechanisms and their meaning for understanding chronic pain. Prog. Mol. Biol. Transl. Sci. *131*, 409–434.

Procyk, E., Wilson, C.R.E., Stoll, F.M., Faraut, M.C.M., Petrides, M., and Amiez, C. (2014). Midcingulate Motor Map and Feedback Detection: Converging Data from Humans and Monkeys. Cereb. Cortex *26*, bhu213.

Purgert, C. a, Izumi, Y., Jong, Y.-J.I., Kumar, V., Zorumski, C.F., and O'Malley, K.L. (2014). Intracellular mGluR5 can mediate synaptic plasticity in the hippocampus. J. Neurosci. *34*, 4589–4598.

Radat, F., Margot-Duclot, a, and Attal, N. (2013). Psychiatric co-morbidities in patients with chronic peripheral neuropathic pain: a multicentre cohort study. Eur. J. Pain *17*, 1547–1557.

Ritter, S.L., and Hall, R.A. (2009). Fine-tuning of GPCR activity by receptor-interacting proteins. Nat. Rev. Mol. Cell Biol. *10*, 819–830.

Ronesi, J.A., and Huber, K.M. (2008). Homer Interactions Are Necessary for Metabotropic Glutamate Receptor-Induced Long-Term Depression and Translational Activation. J. Neurosci. *28*, 543–547.

Ronesi, J.A., Collins, K.A., Hays, S.A., Tsai, N.-P., Guo, W., Birnbaum, S.G., Hu, J.-H., Worley, P.F., Gibson, J.R., and Huber, K.M. (2012). Disrupted Homer scaffolds mediate abnormal mGluR5 function in a mouse model of fragile X syndrome. Nat. Neurosci. *15*, 431–440.

Rong, R., Ahn, J.-Y., Huang, H., Nagata, E., Kalman, D., Kapp, J.A., Tu, J., Worley, P.F., Snyder, S.H., and Ye, K. (2003). PI3 kinase enhancer-Homer complex couples mGluRI to PI3 kinase, preventing neuronal apoptosis. Nat. Neurosci. *6*, 1153–1161.

Rosenblum, K., Futter, M., Voss, K., Erent, M., Skehel, P.A., French, P., Obosi, L., Jones, M.W., and Bliss, T.V.P. (2002). The role of extracellular regulated kinases I/II in late-phase long-term potentiation. J. Neurosci. *22*, 5432–5441.

Roy, M., Shohamy, D., Daw, N., Jepma, M., Wimmer, G.E., and Wager, T.D. (2014). Representation of aversive prediction errors in the human periaqueductal gray. Nat. Neurosci. *17*, 1607–1612.

Ruscheweyh, R., Wilder-Smith, O., Drdla, R., Liu, X.G., and Sandkuhler, J. (2011). Long-term potentiation in spinal nociceptive pathways as a novel target for pain therapy. Mol Pain *7*, 20.

Ryu, H.-H., and Lee, Y.-S. (2016). Cell type-specific roles of RAS-MAPK signaling in learning and memory: Implications in neurodevelopmental disorders. Neurobiol. Learn. Mem. *135*, 13–21.

Saadé, N.E., Amin, H.A., Chalouhi, S., Baki, S.A., Jabbur, S.J., and Atweh, S.F. (2006). Spinal pathways involved in supraspinal modulation of neuropathic manifestations in rats. Pain *126*, 280–293.

Sakagami, Y., Yamamoto, K., Sugiura, S., Inokuchi, K., Hayashi, T., and Kato, N. (2005). Essential roles of Homer-1a in homeostatic regulation of pyramidal cell excitability: A possible link to clinical benefits of electroconvulsive shock. Eur. J. Neurosci. *21*, 3229–3239.

Sandkühler, J., and Gruber-Schoffnegger, D. (2012). Hyperalgesia by synaptic long-term potentiation (LTP): An update. Curr. Opin. Pharmacol. *12*, 18–27.

Schreckenberger, M., Siessmeier, T., Viertmann, A., Landvogt, C., Buchholz, H.-G., Rolke, R., Treede, R.-D., Bartenstein, P., and Birklein, F. (2005). The unpleasantness of tonic pain is encoded by the insular cortex. Neurology *64*, 1175–1183.

Schröder, H., Wu, D.F., Seifert, A., Rankovic, M., Schulz, S., H??llt, V., and Koch, T. (2009). Allosteric modulation of metabotropic glutamate receptor 5 affects

phosphorylation, internalization, and desensitization of the μ-opioid receptor. Neuropharmacology *56*, 768–778.

Schwartz, N., Temkin, P., Jurado, S., Lim, B.K., Heifets, B.D., Polepalli, J.S., and Malenka, R.C. (2014). Decreased motivation during chronic pain requires long-term depression in the nucleus accumbens. Science (80-.). *345*.

Schweinhardt, P., Fransson, P., Olson, L., Spenger, C., and Andersson, J.L.R. (2003). A template for spatial normalisation of MR images of the rat brain. J. Neurosci. Methods *129*, 105–113.

Seifert, F., and Maihöfner, C. (2009). Central mechanisms of experimental and chronic neuropathic pain: Findings from functional imaging studies. Cell. Mol. Life Sci. *66*, 375–390.

Seminowicz, D.A., Laferriere, A.L., Millecamps, M., Yu, J.S.C., Coderre, T.J., and Bushnell, M.C. (2009). MRI structural brain changes associated with sensory and emotional function in a rat model of long-term neuropathic pain. Neuroimage *47*, 1007–1014.

Sesack, S.R., Deutch, A.Y., Roth, R.H., and Bunney, B.S. (1989). Topographical organization of the efferent projections of the medial prefrontal cortex in the rat: An anterograde tract-tracing study with Phaseolus vulgaris leucoagglutinin. J. Comp. Neurol. *290*, 213–242.

Shi, M., Qi, W.J., Gao, G., Wang, J.Y., and Luo, F. (2010). Increased thermal and mechanical nociceptive thresholds in rats with depressive-like behaviors. Brain Res. *1353*, 225–233.

Shin, S., Kwon, O., Kang, J.I., Kwon, S., Oh, S., Choi, J., Kim, C.H., and Kim, D.G. (2015). mGluR5 in the nucleus accumbens is critical for promoting resilience to chronic stress. Nat. Neurosci. *18*, 1017–1024.

Shiraishi-Yamaguchi, Y., and Furuichi, T. (2007). The Homer family proteins. Genome Biol. *8*, 206.

Slattery, D. a, and Cryan, J.F. (2012). Using the rat forced swim test to assess antidepressant-like activity in rodents. Nat. Protoc. *7*, 1009–1014.

Sourdet, V., Russier, M., Daoudal, G., Ankri, N., and Debanne, D. (2003). Long-term enhancement of neuronal excitability and temporal fidelity mediated by metabotropic glutamate receptor subtype 5. J. Neurosci. *23*, 10238–10248.

Starr, C.J., Sawaki, L., Wittenberg, G.F., Burdette, J.H., Oshiro, Y., Quevedo, A.S., and Coghill, R.C. (2009). Roles of the insular cortex in the modulation of pain: insights from brain lesions. J. Neurosci. *29*, 2684–2694.

Stoppel, L.J., Auerbach, B.D., Senter, R.K., Preza, A.R., Lefkowitz, R.J., and Bear, M.F. (2017). β-Arrestin2 Couples Metabotropic Glutamate Receptor 5 to Neuronal Protein Synthesis and Is a Potential Target to Treat Fragile X. Cell Rep. *18*, 2807–

2814.

Suzuki, T., Amata, M., Sakaue, G., Nishimura, S., Inoue, T., Shibata, M., and Mashimo, T. (2007). Experimental neuropathy in mice is associated with delayed behavioral changes related to anxiety and depression. Anesth. Analg. *104*, 1570–1577.

Sweatt, J.D. (2004). Mitogen-activated protein kinases in synaptic plasticity and memory. Curr. Opin. Neurobiol. *14*, 311–317.

Szumlinski, K.K., Dehoff, M.H., Kang, S.H., Frys, K.A., Lominac, K.D., Klugmann, M., Rohrer, J., Griffin, W., Toda, S., Champtiaux, N.P., et al. (2004). Homer proteins regulate sensitivity to cocaine. Neuron *43*, 401–413.

Szumlinski, K.K., Abernathy, K.E., Oleson, E.B., Klugmann, M., Lominac, K.D., He, D.-Y., Ron, D., During, M., and Kalivas, P.W. (2006). Homer Isoforms Differentially Regulate Cocaine-Induced Neuroplasticity. Neuropsychopharmacology *31*, 768–777.

Talavera, K., Nilius, B., and Voets, T. (2008). Neuronal TRP channels: thermometers, pathfinders and life-savers. Trends Neurosci. *31*, 287–295.

Tappe, A., Klugmann, M., Luo, C., Hirlinger, D., Agarwal, N., Benrath, J., Ehrengruber, M.U., During, M.J., and Kuner, R. (2006). Synaptic scaffolding protein Homer1a protects against chronic inflammatory pain. Nat. Med. *12*, 677–681.

Tappe-Theodor, A., Fu, Y., Kuner, R., and Neugebauer, V. (2011). Homer1a Signaling in the Amygdala Counteracts Pain-Related Synaptic Plasticity, mGluR1 Function and Pain Behaviors. Mol. Pain *7*, 1744-8069-7–38.

Thompson, S.J., Millecamps, M., Aliaga, A., Seminowicz, D.A., Low, L.A., Bedell, B.J., Stone, L.S., Schweinhardt, P., and Bushnell, M.C. (2014). NeuroImage Metabolic brain activity suggestive of persistent pain in a rat model of neuropathic pain. Neuroimage *91*, 344–352.

Thomsen, A.R.B., Plouffe, B., Cahill, T.J., Shukla, A.K., Tarrasch, J.T., Dosey, A.M., Kahsai, A.W., Strachan, R.T., Pani, B., Mahoney, J.P., et al. (2016). GPCR-G Protein-β-Arrestin Super-Complex Mediates Sustained G Protein Signaling. Cell *166*, 907–919.

Ting, J.T., Daigle, T.L., Chen, Q., and Feng, G. (2014). Acute brain slice methods for adult and aging animals: application of targeted patch clamp analysis and optogenetics. Methods Mol. Biol. *1183*, 221–242.

Treadway, M.T., Waskom, M.L., Dillon, D.G., Holmes, A.J., Park, M.T.M., Chakravarty, M.M., Dutra, S.J., Polli, F.E., Iosifescu, D. V., Fava, M., et al. (2015). Illness progression, recent stress, and morphometry of hippocampal subfields and medial prefrontal cortex in major depression. Biol. Psychiatry *77*, 285–294.

Tronson, N.C., Guzman, Y.F., Guedea, A.L., Huh, K.H., Gao, C., Schwarz, M.K.,

and Radulovic, J. (2010). Metabotropic glutamate receptor 5/Homer interactions underlie stress effects on fear. Biol. Psychiatry *68*, 1007–1015.

Tu, J.C., Xiao, B., Yuan, J.P., Lanahan, A.A., Leoffert, K., Li, M., Linden, D.J., and Worley, P.F. (1998). Homer binds a novel proline-rich motif and links group 1 metabotropic glutamate receptors with IP3 receptors. Neuron *21*, 717–726.

Turk, D.C., Audette, J., Levy, R.M., Mackey, S.C., and Stanos, S. (2010). Assessment and treatment of psychosocial comorbidities in patients with neuropathic pain. Mayo Clin. Proc. *85*, S42-50.

Vachon-Presseau, E., Tétreault, P., Petre, B., Huang, L., Berger, S.E., Torbey, S., Baria, A.T., Mansour, A.R., Hashmi, J.A., Griffith, J.W., et al. (2016). Corticolimbic anatomical characteristics predetermine risk for chronic pain. Brain *139*, 1958–1970.

Vertes, R.P. (2004). Differential Projections of the Infralimbic and Prelimbic Cortex in the Rat. Synapse *51*, 32–58.

Vincent, K., Cornea, V.M., Jong, Y.-J.I., Laferrière, A., Kumar, N., Mickeviciute, A., Fung, J.S.T., Bandegi, P., Ribeiro-da-Silva, A., O'Malley, K.L., et al. (2016). Intracellular mGluR5 plays a critical role in neuropathic pain. Nat. Commun. *7*, 10604.

Vogt, B.A., and Paxinos, G. (2014). Cytoarchitecture of mouse and rat cingulate cortex with human homologies. Brain Struct. Funct. *219*, 185–192.

Wang, H., and Zhuo, M. (2012). Group I Metabotropic Glutamate Receptor-Mediated Gene Transcription and Implications for Synaptic Plasticity and Diseases. Front. Pharmacol. *3*, 189.

Wang, G.-Q., Cen, C., Li, C., Cao, S., Wang, N., Zhou, Z., Liu, X.-M., Xu, Y., Tian, N.-X., Zhang, Y., et al. (2015a). Deactivation of excitatory neurons in the prelimbic cortex via Cdk5 promotes pain sensation and anxiety. Nat. Commun. *6*, 7660.

Wang, H., Wang, B., Normoyle, K.P., Jackson, K., Spitler, K., Sharrock, M.F., Miller, C.M., Best, C., Llano, D., and Du, R. (2014). Brain temperature and its fundamental properties: a review for clinical neuroscientists. Front. Neurosci. *8*, 307.

Wang, Y., Ma, Y., Hu, J., Cheng, W., Jiang, H., Zhang, X., Li, M., Ren, J., and Li, X. (2015b). Prenatal chronic mild stress induces depression-like behavior and sex-specific changes in regional glutamate receptor expression patterns in adult rats. Neuroscience *301*, 363–374.

Wang, Y., Rao, W., Zhang, C., Zhang, C., Liu, M., Han, F., Yao, L., Han, H., Luo, P., Su, N., et al. (2015c). Scaffolding protein Homer1a protects against NMDA-induced neuronal injury. Cell Death Dis. *6*, e1843.

Wei, X., Sun, Y., and Luo, F. (2017). Impaired Spinal Glucocorticoid Receptor Signaling Contributes to the Attenuating Effect of Depression on Mechanical Allodynia and Thermal Hyperalgesia in Rats with Neuropathic Pain. Front. Cell.

Neurosci. *11*, 145.

Wessel, J.R., Danielmeier, C., Morton, J.B., and Ullsperger, M. (2012). Surprise and Error: Common Neuronal Architecture for the Processing of Errors and Novelty. J. Neurosci. *32*, 7528–7537.

Willard, S.S., and Koochekpour, S. (2013). Glutamate, glutamate receptors, and downstream signaling pathways. Int. J. Biol. Sci. *9*, 948–959.

Witkin, J.M., Marek, G.J., Johnson, B.G., and Schoepp, D.D. (2007). Metabotropic glutamate receptors in the control of mood disorders. CNS Neurol Disord Drug Targets *6*, 87–100.

Worley, P.F., Zeng, W., Huang, G., Kim, J.Y., Shin, D.M., Kim, M.S., Yuan, J.P., Kiselyov, K., and Muallem, S. (2007). Homer proteins in Ca2+ signaling by excitable and non-excitable cells. Cell Calcium *42*, 363–371.

Xiao, B., Tu, J.C., Petralia, R.S., Yuan, J.P., Doan, A., Breder, C.D., Ruggiero, A., Lanahan, A.A., Wenthold, R.J., and Worley, P.F. (1998). Homer regulates the association of group 1 metabotropic glutamate receptors with multivalent complexes of Homer-related, synaptic proteins. Neuron *21*, 707–716.

Xiao, B., Tu, J.C., and Worley, P.F. (2000). Homer: a link between neural activity and glutamate receptor function. Curr. Opin. Neurobiol. *10*, 370–374.

Yalcin, I., Barthas, F., and Barrot, M. (2014). Emotional consequences of neuropathic pain: Insight from preclinical studies. Neurosci. Biobehav. Rev. *47*, 154–164.

Yamamoto, K., Sakagami, Y., Sugiura, S., Inokuchi, K., Shimohama, S., and Kato, N. (2005). Homer 1a enhances spike-induced calcium influx via L-type calcium channels in neocortex pyramidal cells. Eur. J. Neurosci. *22*, 1338–1348.

Yanagawa, M., Yamashita, T., and Shichida, Y. (2009). Activation Switch in the Transmembrane Domain of Metabotropic Glutamate Receptor. Mol. Pharmacol. *76*.

Yang, L., Mao, L., Tang, Q., Samdani, S., Liu, Z., and Wang, J.Q. (2004). A Novel Ca2+-Independent Signaling Pathway to Extracellular Signal-Regulated Protein Kinase by Coactivation of NMDA Receptors and Metabotropic Glutamate Receptor 5 in Neurons. J. Neurosci. *24*, 10846–10857.

Young, S.R., Bianchi, R., and Wong, R.K.S. (2008). Signaling mechanisms underlying group I mGluR-induced persistent AHP suppression in CA3 hippocampal neurons. J. Neurophysiol. *99*, 1105–1118.

Young, S.R., Chuang, S.-C., Zhao, W., Wong, R.K.S., and Bianchi, R. (2013). Persistent receptor activity underlies group I mGluR-mediated cellular plasticity in CA3 neuron. J. Neurosci. *33*, 2526–2540.

Zapallow, C.M., Jacobs, M.F., Lee, K.G.H., Asmussen, M.J., Tsang, P., and Nelson,

A.J. (2013). Continuous theta-burst stimulation over the primary somatosensory cortex modulates interhemispheric inhibition. Neuroreport *24*, 394–398.

Zhang, Z., Gadotti, V.M., Chen, L., Souza, I.A., Stemkowski, P.L., and Zamponi, G.W. (2015). Role of Prelimbic GABAergic Circuits in Sensory and Emotional Aspects of Neuropathic Pain. Cell Rep. *12*, 752–759.

Zhuo, M. (2008). Cortical excitation and chronic pain. Trends Neurosci. *31*, 199–207.

Zimmerman, B., Simaan, M., Akoume, M.-Y., Houri, N., Chevallier, S., Séguéla, P., and Laporte, S.A. (2011). Role of ßarrestins in bradykinin B2 receptor-mediated signalling. Cell. Signal. *23*, 648–659.

Abstract in Korean (국문 초록)

신경병성 통증에 관한

뇌내 대사성 글루타메이트 수용체 5 관련 기전 연구

신경병성 통증은 말초 혹은 중추신경계 손상으로 인해 야기되는 병리적 통증이다. 신경병성 통증의 증상들은 잘 치료되지 않기에, 환자들은 장기간 지속되는 극심한 통증에 시달리게 되며, 우울증이나 불안증 같은 정신 증상에 쉽게 이환된다. 그러나 그 기전은 완전히 밝혀져 있지 않다.

나는 척수 신경 결찰 동물 모델, 양전자 방출 단층 촬영 (PET) 을 사용한 뇌영상 기법, 전기생리학적 기록, 약물 및 유전자 조작 기법, 동물 행동 분석 등을 사용하여 신경병성 통증의 기전을 뇌 수준에서 연구하였다. 특히 대사성 글루타메이트 수용체 5 (mGluR5) 관련 기전을 연구하였는데, 이는 이 물질이 신경 세포의 가소적 변화에 중추적인 역할을 하기 때문이다.

본 논문은 mGluR5 와 관련된 신경병성 통증 기전 연구 세 가지를 설명하는 부분과, mGluR5 의 활성 상태에 관해 고찰하는 부분으로 구성되어 있다. 제 1 장에서는 내측 전전두엽 피질 부위의 mGluR5 수치가 신경병성 통증 상태에서 증가함을 보이고, 이러한 증가가 불쾌감과 부정적 기분을 증폭시키는 원인이 됨을 밝힌다. 제 2 장에서는 신경병성

통증 행동의 정도를 나타내는 뇌내 mGluR5 발현 패턴을 다룬다. PET 영상에서 나타나는 이러한 패턴을 이용하여 신경병성 통증을 객관적으로 평가할 수 있는 방법을 개발하였기에 소개한다. 제 3 장에서는 수도관 주위 회색질 (PAG) 내의 mGluR5 활성도에 초점을 맞춘다. PAG 내의 mGluR5 가 정상상태에서는 지속적인 활성 상태에 있으며, 이를 비활성화시킬 경우 만성 통증을 유발한다는 것을 발견하였다. 제 4 장에서는 mGluR5 가 지속적인 활성 상태를 유지하는 분자적 기전에 대해 고찰한다.

종합적으로, 본 논문은 통증이 어떻게 만성화되는지, 그리고 왜 잘 낫지 않는지 보여 준다. 신경병성 통증 상태에서의 뇌 변화를 조사하고 그 기전을 mGluR5 에 초점을 맞추어 밝힌다. 기전에 기반하여, 각 뇌 영역들에 있는 mGluR5 를 만성 신경병성 통증을 치료하기 위한 치료 표적으로 확인한다. 또한, 신경병성 통증을 이환 중인 개별적인 대상의 상태를 해석하는 방법을 설명한다. 이 방법은 뇌내 mGluR5 패턴 정보를 사용하여 통증 상태를 객관적으로 평가하기에, 임상에서 진단 목적으로 적용될 수 있을 것이다. 본 논문은 신경병성 통증 상태의 뇌가 보이는 특성에 대한 새로운 통찰을 제공하고, 생리학적 및 병리학적 조건에서 mGluR5 활성 상태가 유지되는 현상에 대한 새로운 관점을 제시한다.

Keywords: 신경병성 통증, 대사성 글루타메이트 수용체 5, 내측 전전두엽, 수도관 주위 회색질